Report Prepared by:

Brandon S. Berke and
Alberto A. Sagüés

UPDATE ON CONDITION OF REINFORCED EARTHWALL STRAPS

Contract No. BD544-32

Final Report to Florida Department of Transportation

A. A. Sagüés
Principal Investigator
Department of Civil and Environmental Engineering

UNIVERSITY OF SOUTH FLORIDA
Tampa, FL 33620
March 31, 2009

Technical Report Documentation Page

1. Report No.	2. Government Accession No.	3. Recipient's Catalog No.
BD544 - 32		

4. Title and Subtitle	5. Report Date
UPDATE ON CONDITION OF REINFORCED EARTHWALL STRAPS	March 31, 2009
	6. Performing Organization Code

7. Author(s)	8. Performing Organization Report No.
Brandon S. Berke and A. A. Sagüés	

9. Performing Organization Name and Address	10. Work Unit No. (TRAIS)
Department of Civil and Environmental Engineering University of South Florida Tampa, FL 33620	11. Contract or Grant No. BD544 - 32

12. Sponsoring Agency Name and Address	13. Type of Report and Period Covered
Florida Department of Transportation 605 Suwannee St. MS 30 Tallahassee, Florida 32399 (850)414-4615	Final Report 05/01/2006 - 3/31/2009
	14. Sponsoring Agency Code

15. Supplementary Notes

Prepared in cooperation with the USDOT and FHWA

16. Abstract

Mechanically stabilized earth (MSE) walls are in widespread use but durability is a concern. Corrosion of reinforcement in walls using metallic components is a potentially important limitation as strips are often thin (e.g. only 4 mm). A 1994-8 FDOT investigation of 10 MSE structures determined that corrosion rates were low as expected for soils meeting specifications. At that time the walls were instrumented for future corrosion measurements and non-destructive monitoring. The walls had accumulated another decade of service by the start of the present survey, conducted to provide an indication of corrosion-related aging and improve long term performance projections. Surface appearance of coupons extracted from actual reinforcement elements in five of the walls showed little evidence of distress. Metallographic examination showed only moderate wastage of the galvanized layer, corresponding to low corrosion rates (~0.2 to ~1.1 μm/y). An extended series of linear polarization resistance (LPR) measurements yielded galvanized reinforcement apparent corrosion rates (ACR) that were also low and (average ~0.7 μm/y) and in agreement with those estimated metallographically. Similar analysis of results from the earlier survey yielded ~0.9 μm/y. Average ACR values for ~11 years old embedded plain steel elements were ~6 μm/y. Similar plain steel elements of average age ~0.5 year had ACR ~8 μm/y. The drop in average ACR values with time was in the order of that expected for buried components. Corrosion macrocell current measurements showed interactions that corresponded to an appreciable fraction of the overall corrosion rate. This information was used to apply a localized corrosion multiplier in the damage projections. A statistical model that takes into account the estimated galvanized steel and plain steel corrosion rates and their variability was applied to project the evolution of corrosion damage in a generic Florida MSE wall, using data developed in the present and previous surveys. Consistent with the very small ACR values obtained for the galvanized layers, both inputs result in projections of minimum damage : <5% and <1% elements failed (lost half the thickness of the base steel) at age 100 years, and for about one half of elements failed after 200 years. The findings indicate that corrosion deterioration so far has been mild in the structures investigated, and a good prognosis for adequate corrosion performance in future decades barring unusual circumstances such as extensive backfill contamination. Periodic continuation surveys should be conducted for verification.

17. Key Words	18. Distribution Statement
Reinforced earth walls, galvanized strips, corrosion, soil, durability forecasting, modeling.	No Restriction This report is available to the public through the NTIS, Springfield, VA 22161

19. Security Classif. (of this report)	20. Security Classif. (of this page)	21. No. of Pages	22. Price
Unclassified	Unclassified	118	

DISCLAIMER

The opinions, findings, and conclusions expressed in this publication are those of the authors and not necessarily those of the State of Florida Department of Transportation.

SI* (MODERN METRIC) CONVERSION FACTORS

APPROXIMATE CONVERSIONS TO SI UNITS

Symbol	When You Know	Multiply By	To Find	Symbol
		LENGTH		
in	inches	25.4	millimeters	mm
ft	feet	0.305	meters	m
yd	yards	0.914	meters	m
mi	miles	1.61	kilometers	km
		AREA		
in^2	square inches	645.2	square millimeters	mm^2
ft^2	square feet	0.093	square meters	m^2
yd^2	square yard	0.836	square meters	m^2
ac	acres	0.405	hectares	ha
mi^2	square miles	2.59	square kilometers	km^2
		VOLUME		
fl oz	fluid ounces	29.57	milliliters	mL
gal	gallons	3.785	liters	L
ft^3	cubic feet	0.028	cubic meters	m^3
yd^3	cubic yards	0.765	cubic meters	m^3
		NOTE: volumes greater than 1000 L shall be shown in m^3		
		MASS		
oz	ounces	28.35	grams	g
lb	pounds	0.454	kilograms	kg
T	short tons (2000 lb)	0.907	megagrams (or "metric ton")	Mg (or "t")
		TEMPERATURE (exact degrees)		
°F	Fahrenheit	5 (F-32)/9 or (F-32)/1.8	Celsius	°C
		ILLUMINATION		
fc	foot-candles	10.76	lux	lx
fl	foot-Lamberts	3.426	$candela/m^2$	cd/m^2
		FORCE and PRESSURE or STRESS		
lbf	poundforce	4.45	newtons	N
lbf/in^2	poundforce per square inch	6.89	kilopascals	kPa

APPROXIMATE CONVERSIONS FROM SI UNITS

Symbol	When You Know	Multiply By	To Find	Symbol
		LENGTH		
mm	millimeters	0.039	inches	in
m	meters	3.28	feet	ft
m	meters	1.09	yards	yd
km	kilometers	0.621	miles	mi
		AREA		
mm^2	square millimeters	0.0016	square inches	in^2
m^2	square meters	10.764	square feet	ft^2
m^2	square meters	1.195	square yards	yd^2
ha	hectares	2.47	acres	ac
km^2	square kilometers	0.386	square miles	mi^2
		VOLUME		
mL	milliliters	0.034	fluid ounces	fl oz
L	liters	0.264	gallons	gal
m^3	cubic meters	35.314	cubic feet	ft^3
m^3	cubic meters	1.307	cubic yards	yd^3
		MASS		
g	grams	0.035	ounces	oz
kg	kilograms	2.202	pounds	lb
Mg (or "t")	megagrams (or "metric ton")	1.103	short tons (2000 lb)	T
		TEMPERATURE (exact degrees)		
°C	Celsius	1.8C+32	Fahrenheit	°F
		ILLUMINATION		
lx	lux	0.0929	foot-candles	fc
cd/m^2	$candela/m^2$	0.2919	foot-Lamberts	fl
		FORCE and PRESSURE or STRESS		
N	newtons	0.225	poundforce	lbf
kPa	kilopascals	0.145	poundforce per square inch	lbf/in^2

*SI is the symbol for the International System of Units. Appropriate rounding should be made to comply with Section 4 of ASTM E380.

EXECUTIVE SUMMARY

Widespread use of mechanically stabilized earth (MSE) walls arose across the United States since 1971, and approximately 40,000 are in use nationally at present. Durability is a concern as target service life often exceeds 75 years. Corrosion of reinforcement in walls using metallic components is a potentially important durability limitation given the relatively thin (e.g. only 4 mm) strips used.

A 1994-98 FDOT investigation of 10 MSE structures determined that corrosion rates were in all structures as low as expected for soils meeting specifications. Only minor deterioration was observed at one location with partial chloride contamination. During that investigation the walls were instrumented for corrosion measurements and the test location connections remained in place for future non-destructive monitoring. Most of those structures were relatively young at the time of testing but had already accumulated another decade of service by the start of the present survey. Assessment of present condition, together with the detailed information available for the same structures one decade earlier, was conducted in this project to provide an indication of corrosion-related aging of MSE walls in FDOT service. That information was used to improve the accuracy of a durability prediction model for long term corrosion damage projection. The findings of this follow up investigation are presented next.

Surface appearance of coupons extracted from actual reinforcement elements in five of the walls showed little evidence of distress. There was no external evidence of any earth reinforcement corrosion in any of the walls. Analysis of extracted backfill revealed no unusual contamination. Metallographic examination of the reinforcement coupons showed only moderate wastage of the galvanized layer, corresponding to low corrosion rates, estimated to range from ~0.2 to ~1.1 μm/y.

An extended series of linear polarization resistance (LPR) measurements yielded galvanized reinforcement apparent corrosion rates (ACR) that were also low and (average ~0.7 μm/y) and in general agreement with those estimated metallographically. Similar analysis of results from the earlier survey yielded ~0.9 μm/y. These values are at the low end of the range commonly anticipated for galvanized steel reinforcement in MSE walls. LPR tests produced average ACR ~6 μm/y values for ~11 years old embedded plain steel elements in the same walls. The average ACR for measurements conducted for the same or similar elements at average age ~0.5 year was ~8 μm/y. These values are within the anticipated range for buried steel in similar conditions. The fractional drop in average ACR values between both surveys, although subject to uncertainty due to variability in the data and subject to future confirmation, was in the order of that expected for buried components. The approximate accuracy and the electrochemical ACR estimates for galvanized steel was supported by agreement

with direct metallographic examination, while internal consistency was established for both galvanized and plain steel ACR measurements by comparison with the results of independent electrochemical impedance spectroscopy tests in the field.

Corrosion macrocell current measurements at one of the test sites showed interactions between the front and back portions of the reinforcement that corresponded to an appreciable fraction of the overall corrosion rate. This information was used to apply a localized corrosion multiplier in the damage projection model described next.

A statistical model that takes into account the estimated galvanized steel and plain steel corrosion rates and their variability was applied to project the evolution of corrosion related damage in a generic Florida MSE wall, using the data developed in the present and previous surveys. Consistent with the very small ACR values obtained for the galvanized layers, both inputs result in projections of minimum damage : <5% and <1% elements failed (lost half the thickness of the base steel) at age 100 years, and for about one half of elements failed after 200 years. The overall observations indicate that corrosion deterioration so far has been mild in the structures investigated, and that there is a good prognosis for adequate corrosion performance in future decades barring unusual circumstances such as extensive backfill contamination. Periodic continuation surveys should be conducted for verification.

TABLE OF CONTENTS

ACKNOWLEDGEMENT

The assistance with field inspections of collaborators at the FDOT State Materials Office and from Concorr Florida, Inc. is greatly appreciated.

1 INTRODUCTION AND OBJECTIVES

1.1 Introduction

As widespread use of mechanically stabilized earth (MSE) walls, arose across the United States since 1971[1, 2], investigations were conducted to determine durability of the structures as around 40,000 are in use nationally. Major durability studies for MSE walls are currently ongoing nationally by the Federal Highway Administration, and individual state studies in New York, Kentucky, Georgia, North Carolina, South Dakota, California, and Florida.

MSE is an old technology that became further developed in the past century. The process was an ancient practice in China in which branches were inserted into dirt mounds as a strengthening method. The practice was found to be used in 18th century France as well. Currently the process is executed by taking metallic strips or meshes anchored by concrete medallions. Layers of backfill soil are compacted while placing layers of reinforcement like a sandwich. The concrete medallions are typically made out of tessellating patterns [3].

Corrosion of reinforcing strips in an MSE wall results from the oxidizing environment in soils. Various groups evaluated buried steel and galvanized steel to make empirical data of corrosion wastage in various soil environments [4, 5]. Corrosion of zinc is of particular interest since galvanizing the reinforcement strips is a standard method for corrosion protection of MSE wall reinforcements. Wastage information gathered from Stuttgart University's analysis of NBS data linear wastage approximations, and backfill material in MSE walls (Table 1.1) was used to make design guidelines. [1] American Association of State Highway and Transportation Officials (AASHTO) created design standards based upon the aforementioned data as to what type of corrosion wastage rates to expect in MSE structures.(Table 1.2). Note that Table 1.1 only applies to soils with a resistivity of less than 5,000 Ω•cm [4,5].

Table 1.1 AASHTO backfill guidelines for MSE walls. [5]

Parameter	Limit or Range
pH	5-10
Chlorides	<100 ppm
Sulfates	<200 ppm
Resistivity	>3,000 Ω•cm
Organic Content	<1%

Table 1.2 AASHTO corrosion rate guidelines for galvanized steel in MSE walls. [5]

Material Layer	Age (years)	Corrosion Rate (μm/y)
Zinc	0 - 2	15
	2 - time of depletion	4
Base Steel	zinc depletion - 75 years	12
	>75 years after zinc depletion	7

Galvanizing provides corrosion resistance first by the intrinsically low corrosion rate of zinc in most natural soil environments. When the zinc layer wastage eventually exposes some of the base steel, it is protected from rapid corrosion by galvanic coupling with the remaining zinc layer. The latter has typically a highly negative corrosion potential that polarizes the steel towards the immune regime. Galvanizing of MSE strips is achieved by hot dipping steel into a molten zinc bath, mutually fusing the zinc and iron and creating a series of intermetallics there as noted in Figure 1. [5] In MSE reinforcements, the hot dipping is rather robust (strong in adhesion, and toughness) as coatings are on the order of 100 μm thick [3].

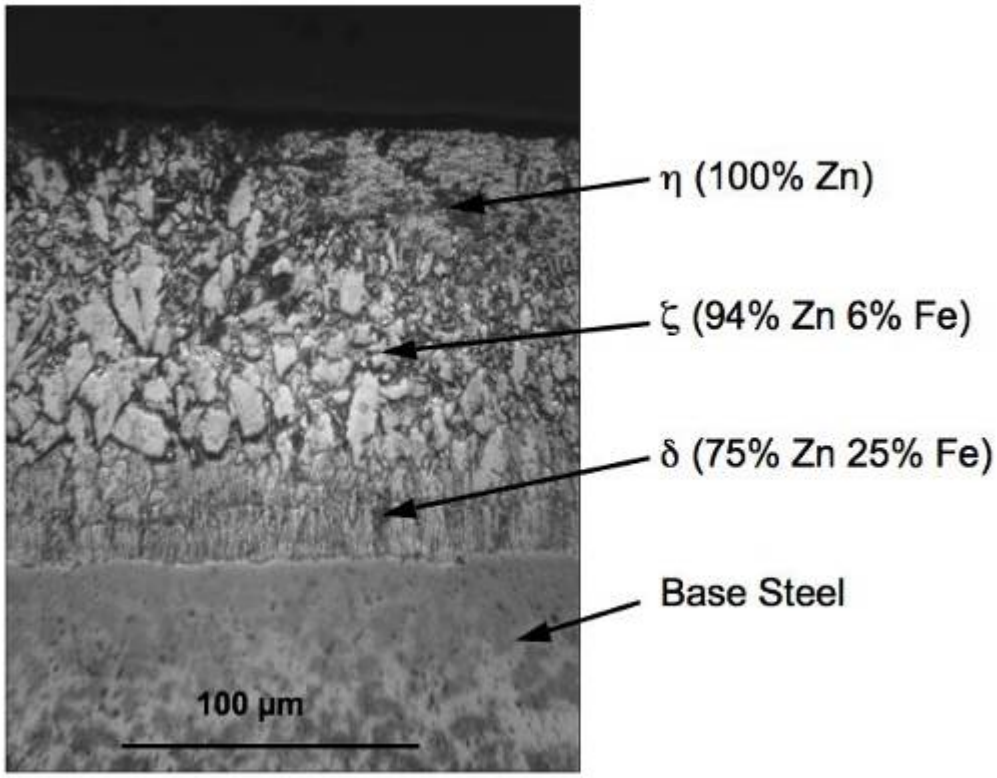

Figure 1 - Microstructure of galvanized steel from an unexposed archival MSE strip, and identification of layers and compositions. [6]

Corrosion performance of MSE reinforcement has been the subject of various investigations, highlights of which are noted in the following. In initial investigations during the 1980s, the Federal Highway Administration (FHWA) evaluated the durability of MSE walls by extracting strips from field sites and measuring metal loss by comparison with assumed initial dimensions and mechanical tests of yield strength of strips [1]. Currently nondestructive testing (NDT) is often performed involving at least half-cell potential measurements typically with a $Cu/CuSO_4$ electrode (CSE). Linear polarization resistance, LPR, is also frequently measured to evaluate quantitative corrosion rates. LPR measurements yield polarization resistances, which are related to a corrosion currents leading to apparent corrosion rates, ACR [1].

A 2005 FHWA study reviewed some national and international practices that may lead to severe reinforcement corrosion and in some instances failure of the walls [1]. Failures were found to be mainly the result of corrosive agents in the backfill materials. Aggressive backfill conditions included high chloride concentrations in the soil (~5000 ppm), low soil pH (less than pH 5), and high concentrations of organic compounds. One notable failure resulted from an accident in which a tanker in Spain crashed into a wall, spilling corrosive chemicals into the backfill [1].

The New York State Department of Transportation (NYSDOT) established a yearly monitoring reporting program for their MSE walls, starting in 1999 and still in practice. NYSDOT co-developed computerized equipment to measure LPR of the metal reinforcements in MSE walls [7, 8].

The Kentucky Transportation Center (KTC) only instrumented 4 of the 129 MSE walls in the state in 2003. KTC also inserted corrosion coupons and found the galvanizing of the coupons to still be present after two years. KTC's evaluation on backfill from Kentucky MSE walls led to an addition to the AASHTO standard, requiring organic backfill content to be less than 1%. The KTC created a statewide database of all of the MSE walls in Kentucky [9].

The Georgia Department of Transportation (GDOT) tested 13 walls of which three experienced high corrosion rates. In one location aggressive conditions resulted from contaminated water from a nearby polluted creek and clay clumping in the backfill [10]. The most notable failure, in which strips were corroded through in places, was observed in a wall built with reinforcements made of an aluminum-magnesium alloy. The aluminum alloy failed to passivate in the soil, which was inundated with chlorides and iron, and thus corroded much faster than expected [10].

The North Carolina Department of Transportation (NCDOT) was cited nationally in 2006 by Gladstone et al for its good practice in monitoring North Carolina's MSE walls [1]. NCDOT inserted coupons of galvanized and plain

steel, which were instrumented for making half-cell measurements. This enabled an NCDOT MSE wall inspector to find out when the zinc became depleted on the coupons and presumably the MSE wall strips [11]. The NCDOT found corrosion rates to be very low (average of 1.3 μm/y) in the five MSE walls. Installation of more monitoring stations at MSE walls throughout North Carolina was considered [11].

The South Dakota Department of Transportation (SDDOT) evaluated an MSE wall while it was being replaced. This replacement enabled visual inspection of the conditions of the mesh reinforcement grids in the wall. Though deformation due to settling was observed, severe corrosion didn't occur because the backfill didn't allow strong deicing chemicals to penetrate. Additionally, SDDOT inserted 36 in. reinforcement strips of different types (galvanized, epoxy coated, and black steel). Evaluations showed that in areas of elevated sulfate concentrations and lower soil resistivities severe corrosion covered the plain steel strips; zinc reaction products were observed on the galvanized strips, and the epoxy remained intact. The study concluded that epoxy-coating reinforcing strips was a good protection method against aggressive environments whenever backfill conditions can't be controlled [12].

The California Department of Transportation, Caltrans, makes evaluations emphasizing direct examination of the strips. The method involves pulling out entire reinforcement strips and evaluating these elements. Evaluations of the strips entail measuring amounts of pitting observed and residual tensile strength of the strips. Caltrans experienced problems with corrosion at some locations thought to have resulted because AASHTO standards for backfill were not followed [13]. Additionally, in some of these sites, the reinforcement strips were not galvanized [13]. Furthermore there were suspicions that the water used to stop the dusting during the construction was contaminated with corrosion inducing chemicals [13].

An FDOT investigation completed in 1998 [14] determined from testing conducted from 1994 to 1998 that corrosion rates were in all structures examined as low as expected for soils meeting AASHTO specifications. Only minor deterioration was observed at one location with partial chloride contamination. The results were used as baseline data to formulate a quantitative durability model [14, 15] that projected that, in the absence of disrupting events, corrosion performance predicted a period of ~ 50 years with negligible reinforcement failure, and only ~5% failure after 100 years. However, laboratory experiments indicated that severe contamination as it may occur during a hurricane-induced saltwater flood could dramatically reduce corrosion-related service life. For a wall with a saltwater flood at year zero, the model projected failure development 10 times earlier than in the absence of the flooding event.

During the 1994-98 investigation 10 MSE structures were instrumented at 8 different Florida sites for corrosion measurements; and soil and metal samples

were retrieved from several of the sites to evaluate the electrochemical properties of the backfill and to assess the condition of the galvanized coating after several years of exposure. The test location connections remained in place for future non-destructive monitoring. Most of those structures were relatively young at the time of testing but are still in service and have now accumulated another decade of service. Therefore present age is a significant fraction of a typical (e.g. 75-year) design service life. Assessment of present condition, together with the detailed information available for the same structures one decade earlier, can provide a highly useful indication of corrosion-related aging of MSE's in FDOT service. That information can then be used to improve the accuracy of the durability prediction model to benefit future design and maintenance planning for these structures. The present investigation was conducted accordingly.

1.2 Objectives and approach

The objective of this investigation is to extend the baseline of FDOT MSE corrosion performance to reveal long term trends, and thus improve the reliability of durability model projections.

The approach to achieve those objectives is to:

(1) Assess the present condition of existing sites evaluated in the 1994-1997 surveys by nondestructive measurements and by extracting soil and reinforcement samples.

(2) Evaluate field samples in the laboratory including experiments with simulated systems for comparison as needed.

(3) Operate and expand as needed predictive models to predict future evolution of corrosion damage in existing and future FDOT MSE sites.

The activities and findings conducted toward achieving the objective are detailed in the following sections.

2 METHODOLOGY

2.1 Field Sites and Instrumentation Details

The following terminology applies to these descriptions:

Site: An overall locale (e.g. Howard Frankland Bridge).

Structure: One or more structural components associated with the Site (e.g. Tampa-end causeway of the Howard Frankland Bridge).

Wall: One of the MSE walls in the Structure.

Location: A place at the Wall where one or more test clusters have been implemented.

Test Cluster: A group of neighboring buried metallic components that have been instrumented for testing and/or exposed and sampled for direct metallic component and/or soil assessment. A cluster may include carbon steel rods embedded in the soil at the time of an earlier field visit. Metallic components in a cluster may be all associated with a single wall concrete panel (sometimes referred to as a medallion) or involve components of two medallions immediately above each other.

Test Points: Permanent external electric contacts to instrumented metallic components and openings for reference electrode placement.

In the past survey from 1994-98, ten walls were instrumented to allow for electrochemical measurements on the buried elements in the MSEWs [14,15]. The sites/structures were chosen to represent the diversity of MSE walls found across Florida. The site list and rationale for each site is compiled in Table 2.1 and geographic locations in Florida are shown in Figure 2. The same sites as available were revisited in the present study.

Table 2.1 Structure details for each site.

Site # and Code	Structure and Wall	Regime and Rationale for Testing	Year Built	Age (Years)†	# of Test Clusters*
1A - BRN	Brickell Ave. Bridge NW Wall, Miami	Coastal, Possible inundation	1995	10	2
1B - BRS	Brickell Ave. Bridge SE Wall, Miami	Coastal, Possible inundation	1995	10	2
2 - HFB	Howard Frankland Bridge, Tampa	Coastal, Possible inundation	1992	13	6ˇ
3 - PAV	Pensacola Ave., Tallahassee	Land, oldest in FL 10 years ago	1979	N/A**	4
4A - PCE	Palm City Bridge NE Wall, Stuart	Coastal, Possible inundation	1991	15	4
4B - PCW	Palm City Bridge NW Wall, Palm City	Coastal, Tidal Saltwater Aggressive Regime	1991	15	2
5 - PSL	Port St. Lucie Blvd., Port St. Lucie	Coastal, Tidal Saltwater Aggressive Regime	1992	14	2
6 - OCA	State Rd. 200, Ocala	Land, Old, Long Term Baseline	1984	23	2
7 - ABJ	Acosta Bridge, Jacksonville	Coastal, Non-Spec. Backfill	1990	17	2
8 - VET	Veteran's Expressway, Tampa	Land, Representative of Present Practice	1995	12	2

*Set of reinforcements instrumented for electrical contacts
†Age of the structure when visited during the current survey.
ˇ4 Original clusters and two new ones from 2006
** Demolished before second survey.
Site codes are same as structure codes except for BR designating BRN/BRS and PC designating PCE/PCW.

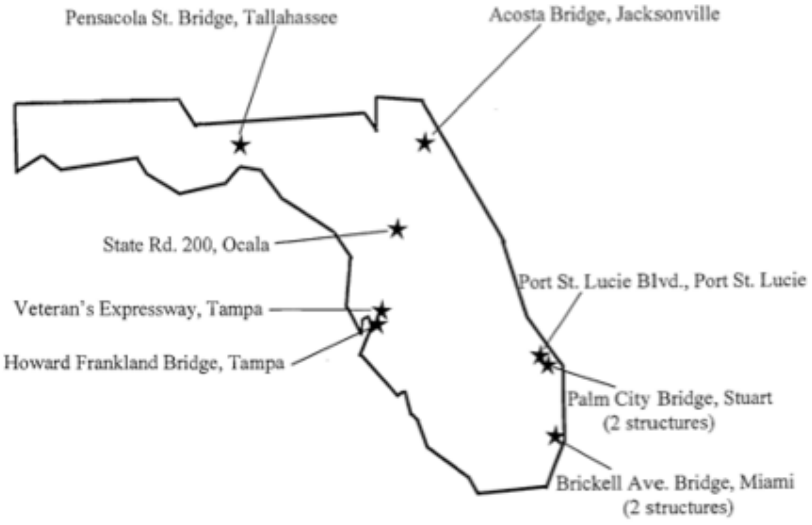

Figure 2 - Locations of MSE walls chosen for instrumentation throughout the state of Florida. Reproduced from Ref. [15]

Initial site, structure wall and location details of the panels were presented by Sagüés et al [15]. Those details are reproduced in Appendix 1 amended and updated to account for the actual condition of the sites, new buried components, accurate test point cluster information, and noting any damaged test points.

All geographic coordinates given for a site (or structure/wall if differentiated within a site) in the following are simplified to one second resolution. The coordinates correspond to a point located centrally to the instrumented wall locations. Additional directions and descriptions are given to facilitate accessing a site.

Specific details on sites and subcategories including test points and reinforcing element surface areas are found also in Appendix 1. Details on how permanent external connections to buried metallic elements were made are given by Sagüés et al [15]. During field visits alligator clips attached to the external contact enabled interfacing the field equipment.

2.1.1 Brickell Ave., Miami, BR Site

The BR site includes two structures on opposite sides (North and South) of the drawbridge that crosses the Miami River in downtown Miami. Test locations were implemented in walls at the Northwest and Southeast portions of the corresponding structures. Each location consisted of two test clusters, one near ground level and the other elevated. The Northwest wall location and its test clusters and points are accessible through a gate on 64 SE 4th St. for a car to drive to the site. There are City of Miami offices (with which it may be required to coordinate access operations) at the Knight Center, which is nearby on SE 4th Street.

The Southeast wall locations and cluster test points were at the time of the visits adjacent to a construction site, yet a DOT access road exists which is the first left turn available southbound after crossing the bridge, extending to the South side of the bridge and running along the MSE wall.

The coordinates of are 25°46’13”N x 80°11’25”W and 25°46’10”N x 80°11’23”W for the Northwest and Southeast wall locations respectively. The electric test points for each cluster are fitted in either one or two 4” diameter capped PVC ports.

2.1.2 Howard Frankland Bridge, Tampa Bay, HFB Site

The HFB site has one Wall located on the Tampa-end causeway of the Howard Frankland Bridge on southbound I-275. The Wall can be reached by a DOT service road, which emerges beyond the breakdown lane. The coordinates

are 27°56’25”N x 82°33’10”W. There were 4 locations (each at one panel, R7, R11, R15 and R17) instrumented in the 1994-8 survey.

In August 2006, two additional panels were instrumented (R9 and R21). The instrumentation of the two panels utilized similar methods to those used in the first survey, by attaching stainless steel rods to the galvanized meshes and other added electrodes.
While instrumenting the new panels, coupons in the form of ~4” segments were cut out from the galvanized mesh wire for examination. See Table XX Appendix 3 for additional information on extraction points and coupons. Furthermore, for each panel that didn’t previously have a plain steel rebar (R7, R9 R15, and R21), 2.4m long No. 4 (4/8 in. - 1.77 cm diameter) rebar was inserted at positions indicated in Appendix 1. Moreover, extra 1-in diameter holes were drilled into the panels and covered with PVC fittings to allow future insertion of other electrodes.

Electrical connections to panels R7 and R15 were no longer working as evidenced in resistivity measurements between the meshes to other buried elements. See Reference 14 for details.

2.1.3 Pensacola Ave., Tallahassee , PAV Site

The site was demolished before the present project started in 2006. The location of the site was on the Florida State University campus at the coordinates of 30°26'24"N x 84°18'24"W.

2.1.4 Palm City Bridge, Stuart/Palm City, PC Site

The PC site consists of one structure containing two walls on the Northeast (PCE) and Northwest (PCW), on the bridge on Florida State Road 714 that crosses the South fork of the St. Lucie River. The PCE wall’s coordinates are 27°10’32”N x 80°15’49”W, and is currently (2009) across from a Marine Max yacht dealership. The PCE wall contains 4 locations with test clusters at panel rows, R1, R5, R14, and R28.

The PCW wall was the most complicated wall to reach in this investigation as the access point is in a tidal zone. To get to PCW, one makes the first left turn on the Southwest side of the bridge to park under the bridge’s West side just past its causeway. The PCW contains 2 locations with test clusters at rows R3W and R5W. The coordinates for PCW are 27°10’24”N x 80°15’30”W.

The reference electrode connection was damaged at the PCW Panel R3W and was initially repaired by inserting a stainless steel screw into the wire stump.

The repair was not effective, so a CSE temporarily inserted in the soil hole of the panel was used instead as a reference electrode for the polarization measurements At PCE, the Panel R1 connection stainless steel rod to the bottom strip was broken were it emerged at the concrete surface, making electrical connections with alligator clips difficult but still feasible.

2.1.5 Port St. Lucie Blvd., Port St. Lucie, PSL Site

The PSL site is on Florida State Road 716 on the Southeast corner of the bridge that crosses the Northern fork of the St. Lucie River. The coordinates are 27°16’21”N x 80°19’5”W. The Wall is located in the flood plane of the river so over the course of time flooding brought dirt to the site. This added dirt caused panel R7’s bottom strip connection to be buried, and the area became covered in overgrowth. Additionally, when the site was instrumented, the stainless steel rods for test points were not thoroughly cleaned when the concrete patch was made to fill in the access hole made for inserting the rebar and reference, so further filing may be necessary to ensure good electrical contacts. The wall has two locations with test clusters, R3 and R7.

The area adjacent to the wall was cleared to remove the overgrown brush. Additionally a shovel was needed to uncover the bottom galvanized strip connection in panel R7.

2.1.6 State Rd. 200 Bridge, Ocala, OCA Site

The OCA site is on Florida State Road 200 where it crosses the CSX railroad tracks. The wall is adjacent to the newly created Thompson Bowl Park of Ocala.. The OCA site coordinates are 29°10'45”N x 82° 8'42"W. Access to the site is achieved by turning North from State Rd 200 onto Southwest 10th Ave. and turning east onto Southwest 9th St. The wall has two locations with test clusters, R6 and R25.

2.1.7 Acosta Bridge, Jacksonville, ABJ Site

The ABJ site’s wall is the westernmost MSE wall on the Acosta Bridge with coordinates 30°19'9"N x 81°39'46"W. Driving to the MSE wall requires going westbound on Prudential Dr. and turning North at the railroad tracks but not crossing them. After driving parallel to the tracks about 100 m, one can park the vehicle some 20 m away from the MSE wall. The wall has two locations with test clusters, R9 and R21.

2.1.8 Veterans Expressway Overpass, Tampa, VET Site

This site is located on the NW part of the overpass of the Veterans Expressway (Florida State Toll Road 589) as it crosses Gunn Highway (Hillsborough County Road 587) at coordinates 28° 3'59"N x 82°34'2"W. There

are two locations, R16 and R23, with test clusters. The steel rod connection to the buried rebar in R16 was modified in July, 2007 to enable a banana plug wire connector tip to fit directly into the steel rod instead of using an alligator clip, creating a more secure electrical contact.

2.2 Field Evaluation Procedure

During a field visit, a battery of non destructive tests was conducted to evaluate corrosion behavior of the reinforcements and added rebars. In addition, at some sites the panels were cored through so actual coupons of reinforcing strips or meshes could be examined. Soil samples were extracted from selected sites. A summary description is given in the following; further procedure details are given by Sagüés et al [14,15].

2.2.1 Half-cell Potential

At each site a copper/copper sulfate electrode (CSE) was placed in both soil through a hole in the panel and against a freshly chipped sample of panel concrete. The potential of each metallic element was measured against the reference electrode using a high impedance voltmeter. To verify measurements, mutual metal to metal potentials were obtained and contrasted with the regular measurements for consistence.

2.2.2 Macrocell Current

At the Brickell Ave. MSE walls, additional galvanized strips and rebars were placed in two pieces. Each piece was set up as a front (closest to the external panel) and back piece. The two pieces would act as a long strip or rebar when they were electrically shorted together. By opening the jumper connection between front and back and inserting an ammeter of ≤5 Ω resistance, a macrocell current was measured. The current direction and magnitude enabled determination of which end of the strip behaved as a net anode/cathode and the extent of corrosion macrocell action.

2.2.3 Mutual Resistance

Using a Nilsson model 400 AC soil resistance meter (Nilsson Electrical Laboratory Inc., Jersey City, NJ) in the two-point setting (coupling connectors C1 and P1 and C2 and P2 with jumpers; C and P denote current and potential terminals respectively), resistances were measured between each pair of elements in the same cluster. This method allows determining if broken or shorted connections exist. The Nilsson meter uses a square wave at 97Hz so as to avoid interference from power line stray currents.

2.2.4 Solution Resistance

The Nilsson model 400 meter was used in a three-point configuration to obtain the solution resistance for the IR compensation of the linear polarization resistance measurements. The current and potential terminal at one end (C2-P2) was coupled with a jumper. The current terminal at the other end (C1) was connected to the working electrode (the chosen strip, mesh, or steel). The corresponding potential terminal (P1) was connected to the reference electrode, and C2-P2 were connected to the counter electrodes (the opposite strip or mesh).

2.2.5 Linear Polarization Resistance

In the Linear Polarization Resistance (LPR) method, a potentiostat connected to a computer (either a Gamry™ Reference 600 with a laptop computer or Gamry™ PCI4-300 with a built in computer (Gamry, Westchester, PA)) records current response to an applied potential ramp in the cathodic direction. Figure 3 shows the Gamry™ PCI4-300 being used in the field.

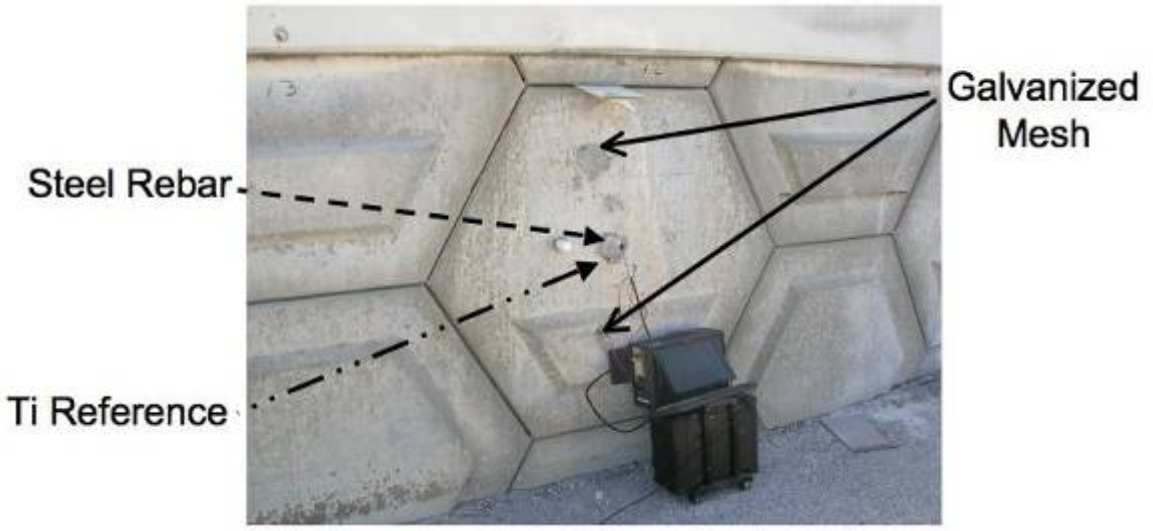

Figure 3 - An LPR test using the Gamry™ potentiostat shows the machine configured with the added rebar as a working electrode, the activated titanium as the reference electrode, and the bottom mesh as the counter electrode.

The polarization scan started from the open circuit potential (OCP) which is the initial undisturbed potential between the working electrode and the reference electrode. The potential was scanned from the OCP to 10mV below the OCP at a ~100μV/s scan rate; potential and current data were acquired typically at ~0.1 mV steps. The working, reference and counter electrode configurations were same as those used for the solution resistance measurement

arrangements. The Working and Working Sense tips of the Gamry™ devices were coupled together to connect to the working electrode, the reference electrode tip was connected to the reference electrode, and the counter electrode tip was connected to the counter electrode.

When performing the first field investigations the standard software script for LPR was used in the Gamry™ Framework software. However it became apparent in many applications that the E-I curve showed a current step causing data reliability issues. The step appeared to originate from current range switching problems related to the large apparent interfacial capacitance of the buried elements. Gamry engineer, Dr. Bob Rodgers created a customized script named, "_USF Polarization Resistance Ver 4.exp" that limited the lowest current range to 300nA and increased the stability settings. The script also required sample times greater than one second and minimized the common mode voltage on the I/E converter. This script was then upgraded for use with the Gamry™ 600, which was first taken to the field for the Jacksonville Site inspection and then used since (August 2007). The new script was called "Concrete polarization resistance.exp". In addition to adding compatibility to the new Framework software this script also uses 10 points from the initial voltage scan to calculate a sample period. Some minor anomalies still remained but the updated procedures yielded generally adequate results, confirmed with test measurements with dummy cells using discrete components.

The equipment created a .dta file from each field test. The data were imported into a Microsoft™ Excel™ spreadsheet. The columns of 'Vf' and 'Im' were copied into a new worksheet and the data was plotted against the open circuit potential, OCP, so a column of Vf-Vo (Vo=OCP) was made.

From the plot a 2nd order polynomial fit was applied to the graph and the equation was used to find the slope of the E-I curve at the terminal potential value 10 mV below the OCP. The trend line polynomial fit generally had very good fit quality, with R^2 >0.95 in most cases. The reported polarization resistance (Rp) is the difference of the terminal slope value and the solution resistance value obtained per Item 2.2.4.

An alternative simplified galvanostatic method to evaluate Rp was used in selected reinforcement strips of VET and PCW, where interference of unknown origin introduced intermittent artifacts in the computer controlled tests. In the alternative method a nearly constant current of ~100 μA was impressed, by means of a 9V battery and a high value resistor, between counter and working electrodes while monitoring the working electrode-reference electrode potential with a 0.1 mV resolution high impedance voltmeter. The current level was adjusted to obtain <10 mV cathodic potential excursion after 180 s of current application. The ratio of potential excursion at 180 s to the impressed current, minus the value of Rs obtained per Item 2.2.4, was reported as the value of Rp. Comparison with Rp values with the computerized system under normal

operating conditions showed typical better than 20% agreement between both methods. Details of the alternative method will be published elsewhere [16].

2.2.6 Electrochemical Impedance Spectroscopy

The Electrochemical Impedance Spectroscopy (EIS) tests were conducted for selected elements in the frequency range from 5 mHz to 5 kHz with 3 points per decade resolution. The Gamry™ potentiostats indicated above were used for these measurements as well.

2.2.7 Other Tests

Reinforcement coupons were collected at selected locations listed in Table 2.2 at cored holes indicated in Appendix1. Cutting out samples of the reinforcement was achieved by using a small power saw that could be operated through a 5" diameter cored hole through the panel. Soil samples were obtained at selected locations through core holes used for extracting coupons, as indicated in Appendix 1.

Table 2.2 Extracted Samples

Wall	Sample /Panel	Elevation (m)*	Soil Extracted†
HFB	Top Mesh / R9	1.3	√
	Top Mesh Hook / R9	1.3	√
	Top Mesh/ R21	1.4	X
	Bottom Mesh/ 21	0.7	X
PCW	Top Right Strip / R2W	0.4	√
	Top Left Strip / R4W	0.4	√
PSL	Top Left Strip / R8	0.3	√
OCA	Bottom Right Strip / R5 A and B	0.2	√
	Top Right Strip / R24	0.5	√
ABJ	Top Right Strip / R20	0.5	√

†Indicates a 10 liter bucket of soil was removed from the panel row location
*Elevations are with respect to ground or designated reference level per Appendix 1.

2.3 Laboratory Evaluations

2.3.1 Soil Tests

Soil tests were performed using FDOT methods [17] for soil resistivity, pH[A], chloride concentration and sulfate concentration. Resistivity and pH determinations were made at times ranging from 1-4 weeks of sample extraction.

[A] Determinations using pH paper, not available for HFB.

Chloride and sulfate analyses were conducted after sample storage periods ranging from 3-20 months after extraction, possibly affecting the results as noted later on.

2.3.2 Metallography

The reinforcement coupons were cleaned of any loose debris or loose corrosion products and the overall coating plus remaining deposit thickness was measured with a magnetic coating thickness gauge (Mikrotest III, ElektroPhysik, Arlington Heights, IL) at multiple sampling points. Small portions of the coupons were cut out with a slow speed diamond saw (Isomet, Beuhler, Lake Bluff, IL) with non-aqueous lubricant (Isocut Fluid, Buehler, Lake Bluff, IL) and then cold mounted in a metallographic epoxy compound which promotes edge retention (Epoxicure, Buehler, Lake Bluff, IL). The metallographic preparation was conducted with water free grinding and polishing to prevent oxidation of the zinc. The polished samples were etched to provide contrast between the base steel and zinc layers with a 1% nitric acid solution in denatured ethyl alcohol. A metallographic microscope was used to measure the thickness of the corrosion wastage and remaining zinc at multiple locations around the sample perimeter.

3 RESULTS

3.1 Field Data

This section presents some results in summary form. A comprehensive listing of the corresponding detailed primary field data appears in Appendix 2.

3.1.1 Visual Appearance of Wall and Extracted Reinforcement

Results are summarized in Table 3.1. Figure 4 shows metallographs demonstrating both high and low corrosion.

Table 3.1 Visual Appearance of Wall and Extracted Reinforcement

Wall	Location - Panel	Coating Condition Rating[1]	Red Rust[2]	External Wall Condition
BRN	-	-	-	No apparent distress
BRS	-	-	-	One concrete spall
HFB	9 Top Mesh	VG	NP	Numerous small concrete spalls reflecting estuary chloride exposure and low rebar cover.
	9 Top Hook	VG	NP	
	21 Top Mesh	VG	NP	
	21 Bot. Mesh	VG	NP	
PCE	-	-	-	No apparent distress
PCW	2W	VG	<5%	Scale on panels from tidal exposure
	4W	VG	NP	
PSL	8	VG	<5%	No apparent distress
OCA	5	G	<10%	Covered in ivy, otherwise no apparent distress
	24	VG	<5%	
ABJ	20	G	<10%	No apparent distress
VET	-	-	-	No apparent distress

1. VG = Very Good, red rust < 5%, G=Good, red rust between 5-20%. Rating reflects percentage of rust on entire specimen surface.
2. NP = No red rust present.

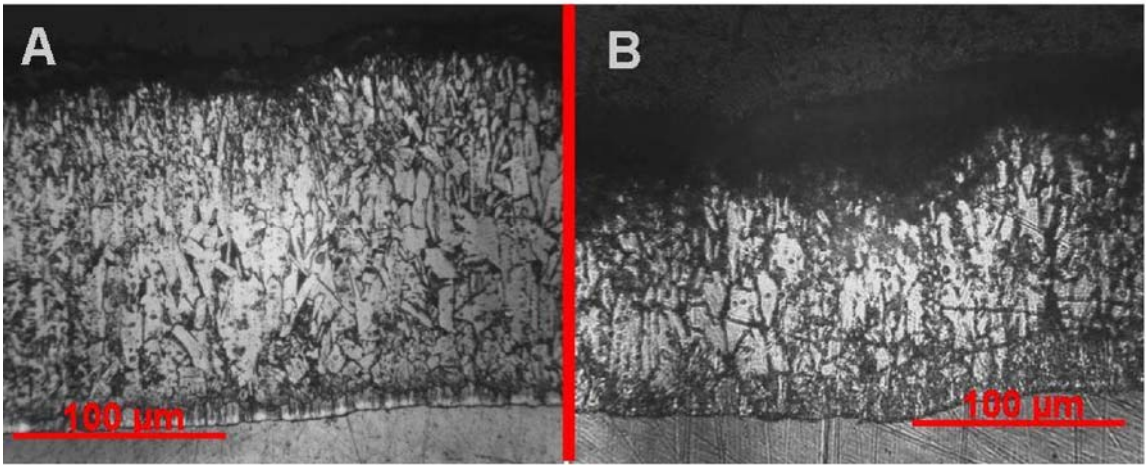

Figure 4 - Examples of metallographic cross sections showing low (A) and high corrosion wastage (B). The base metal is at the bottom.

3.1.2 Solution Resistance, Polarization Resistance, Apparent Corrosion Rates From LPR and Half-cell Potential Values

Solution resistance (Rs), polarization resistance (Rp), and apparent corrosion rate (ACR) results for individual tests are given in Tables A2-1 to A2-7 of Appendix 2 for both the 1994-98 and the present survey. Averaged ACR results of multiple tests of each element for each field visit and corresponding half-cell potentials for both surveys are presented in Table 3.2.

Table 3.2 Summary of electrochemical field observations for instrumented structures. (continued on next page)

Structure #	Site and Location	Environment	Panel Set	Element[1]	Internal Connection[2]	Electrochemical Testing																			
						Potential vs. CSE (V)										Corrosion Rates (μm/y)[3]									
						First Survey						Second Survey				First Survey						Second Survey			
						Visit 1	Visit 2	Visit 3	Visit 4	Visit 5	Visit 6	Visit 1	Visit 2	Visit 3	Visit 4	Visit 1	Visit 2	Visit 3	Visit 4	Visit 5	Visit 6	Visit 1	Visit 2	Visit 3	Visit 4
						2/9/95	9/26/95	1/26/96	3/18/96	8/29/97	11/26/97	10/16/06	12/26/06	4/5/07	6/3/08	2/9/95	9/26/95	1/26/96	3/18/96	8/29/97	11/26/97	10/16/06	12/26/06	4/5/07	6/3/08
1A	Brickell Ave.; Northwest (NW) wall Miami	Coastal	NW top	GL	GSC	-	-0.543	-	-	-	-0.841	-	-	-	-0.841	-	0.71	-	-	-	-	-	-	-	0.21
				GR	GSC	-	-0.691	-	-	-	-0.862	-	-	-	-0.862	-	0.74	-	-	-	-	-	-	-	0.49
				GB+GF	GSC	-	-0.689	-	-	-	-0.805	-	-	-	-0.805	-	0.69	-	-	-	-	-	-	-	0.17
				SB+SF	SSR	-	-0.471	-	-	-	-0.583	-	-	-	-0.583	-	12	-	-	-	-	-	-	-	13
			NW bottom	GL	GSC	-	-0.347	-0.554	-0.558	-0.716	-0.708	-	-0.732	-0.719	-0.708	-	0.71	-	1.2	-	-	-	0.34	0.34	0.45
				GR	GSC	-	-0.216	-0.368	-0.334	-0.445	-0.543	-	-0.520	-0.508	-0.543	-	1.4	-	2.3	-	-	-	2.3	2.3	2.1
				GB+GF	GSC	-	-0.369	-0.581	-0.555	-0.730	-0.741	-	-0.805	-0.787	-0.741	-	0.66	-	1.2	0.51	-	-	0.31	0.29	0.39
				SB+SF	SSR	-	-0.440	-0.250	-0.211	-0.367	-0.124	-	-0.397	-0.383	-0.124	-	15	-	25	0.58	-	-	10.0	8.8	13
1B	Brickell Ave.; Southeast (SE) wall Miami	Coastal	SE top	L	GSC	-	-0.460	-	-	-	-	-0.543	-	-	-0.617	-	0.64	-	-	-	-	0.52	-	-	0.48
				R	GSC	-	-0.475	-	-	-	-	-0.628	-	-	-0.590	-	0.64	-	-	-	-	0.54	-	-	0.45
				F+B	GSC	-	-0.455	-	-	-	-	-0.567	-	-	-0.571	-	0.74	-	-	-	-	0.51	-	-	0.30
			SE bottom	L	GSC	-0.504	-0.492	-0.470	-0.384	-0.656	-0.681	-0.631	-	-	-0.541	0.84	1.3	-	2.3	1.9	-	0.68	-	-	0.65
				R	GSC	-0.529	-0.577	-0.585	-0.483	-0.712	-0.710	-0.610	-	-	-0.608	0.69	1.2	-	2.1	0.89	-	0.62	-	-	0.59
				F+B	GSC	-0.508	-0.517	-0.546	-0.435	-0.696	-0.689	-0.573	-	-	-0.558	0.71	0.43	-	4.1	0.91	-	0.40	0.40	-	0.39
						11/15/95	12/13/95	2/8/96	4/22/96	7/2/96	6/20/97	8/16/06	2/22/07			11/15/95	12/13/95	2/8/96	4/22/96	7/2/96	6/20/97	8/16/06	2/22/07		
2	Howard Frankland, Tampa	Coastal	R7	top G	ZAC	-0.747	-0.793	-0.786	-0.882	-0.841	-0.699	-0.542	-0.476			0.74	0.10	0.56	0.66	-	-	-	-		
				bot. G	ZAC	-0.752	-0.797	-0.782	-0.837	-0.778	-0.644	-0.305	-0.315			0.64	-	0.51	0.53	-	-	-	-		
				S	SSR	-	-	-	-	-	-	-0.562	-0.358			-	-	-	-	-	-	7.8	2.4		
			R9	top G	ZAC	-	-	-	-	-	-	-0.702	-0.641			-	-	-	-	-	-	0.70	0.32		
				bot. G	ZAC	-	-	-	-	-	-	-0.702	-0.579			-	-	-	-	-	-	0.56	0.50		
				S	SSR	-	-	-	-	-	-	-0.580	-0.357			-	-	-	-	-	-	11	2.6		
			R11	top G	ZAC	-	-0.749	-0.751	-0.929	-0.960	-0.637	-0.641	-0.641			-	0.69	1.1	0.51	-	-	0.75	0.39		
				bot. G	ZAC	-	-0.723	-0.734	-0.909	-0.882	-0.605	-0.587	-0.596			-	0.53	0.64	0.48	-	-	0.67	0.41		
				S	SSR	-	-0.471	-0.476	-0.585	-0.572	-0.363	-0.333	-0.319			-	0.48	5.2	5.2	-	-	1.5	1.4		
			R15	top G	ZAC	-0.766	-0.823	-0.853	-0.999	-	-0.670	-0.667	-0.589			0.71	-	0.69	0.69	-	-	-	-		
				bot. G	ZAC	-0.772	-0.842	-0.837	-0.995	-	-0.645	-0.137	-0.398			0.58	-	0.58	0.58	-	-	-	-		
				S	SSR	-	-	-	-	-	-	-0.520	-0.303			-	-	-	-	-	-	4.9	-		
			R17	top G	ZAC	-	-0.861	-0.699	-0.784	-0.805	-0.599	-0.591	-0.580			-	-	0.30	0.53	-	-	0.46	0.28		
				bot. G	ZAC	-	-0.695	-0.707	-0.770	-0.786	-0.626	-0.577	-0.598			-	-	0.23	0.46	-	-	0.52	0.30		
				S	SSR	-	-0.414	-0.417	-0.450	-0.469	-0.346	-0.321	-0.335			-	-	0.76	2.7	-	-	2.4	1.6		
			R21	top G	ZAC	-	-	-	-	-	-	-0.620	-0.522			-	-	-	-	-	-	0.55	0.30		
				bot. G	ZAC	-	-	-	-	-	-	-0.607	-0.622			-	-	-	-	-	-	0.46	0.26		
				S	SSR	-	-	-	-	-	-	-0.500	-0.372			-	-	-	-	-	-	2.3	1.2		

Table 3.2 (cont.) Summary of electrochemical field observations for instrumented structures.

Structure #	Site and Location	Environment	Panel Set	Element[1]	Internal Connection[2]	Electrochemical Testing																			
						Potential vs. CSE (V)										Corrosion Rates (μm/y)[3]									
						First Survey						Second Survey				First Survey						Second Survey			
						Visit 1	Visit 2	Visit 3	Visit 4	Visit 5	Visit 6	Visit 1	Visit 2	Visit 3	Visit 4	Visit 1	Visit 2	Visit 3	Visit 4	Visit 5	Visit 6	Visit 1	Visit 2	Visit 3	Visit 4
3	Pensacola St.; Tallahassee	Land	N/A	N/A	N/A	N/A	N/A	N/A	N/A	N/A	N/A					N/A	N/A	N/A	N/A	N/A	N/A				
						5/3/96	7/30/96	9/25/96	11/14/97			8/24/07				5/3/96	7/30/96	9/25/96	11/14/97			8/24/07			
4A	Palm City Northeast Wall Stuart	Coastal	R1	top G	SSC	-0.620	-0.718	-0.579	-0.631			-0.599				0.33	0.76	0.53	0.33			0.54			
				bot. G	SSC	-0.660	-0.759	-0.633	-0.651			-0.568				0.43	0.56	0.53	0.43			-			
				S	SSR	-0.370	-0.409	-0.302	-0.386			-0.398				7.3	3.1	2.6	1.5			4.1			
			R5	top G	SSC	-0.601	-0.623	-	-0.585			-0.558				0.74	1.0	-	0.64			0.94			
				bot. G	SSC	-0.581	-0.609	-	-0.569			-0.544				0.56	-	-	0.53			0.74			
			R14	top G	SSC	-0.648	-0.720	-	-			-0.649				0.53	0.79	-	-			0.30			
				bot. G	SSC	-0.605	-0.638	-	-			-0.565				0.38	0.79	-	-			0.88			
				S	SSR	-0.474	-0.372	-	-			-0.309				2.3	2.4	-	-			0.93			
			R28	top G	SSC	-	-0.641	-	-			-0.690				0.48	1.1	-	-			0.29			
				bot. G	SSC	-	-0.648	-	-			-0.651				0.53	0.38	-	-			0.29			
						7/31/96	9/26/96	11/20/96	11/14/97			1/1/08	1/26/09			7/31/96	9/26/96	11/20/96	11/14/97			1/1/08	1/26/09		
4B	Palm City Northwest Wall Stuart	Coastal; Tidal saltwater	R3W	top G	GSC	-0.673	-0.812	-0.830	-0.838			-0.747	-0.741			-	0.99	0.25	0.66			-	0.65		
				bot. G	GSC	-	-0.750	-0.874	-0.733			-0.696	-0.610			-	1.3	2.4	1.8			-	0.27		
				S	SSR	-	-0.647	-0.74	-0.631			-0.579	-0.539			-	24	20	60			-	9.3		
			R5W	top G	GSC	-0.711	-0.776	-0.814	-0.780			-0.614	-0.625			-	0.64	0.48	0.58			-	0.46		
				bot. G	GSC	-	-0.942	-0.865	-0.749			-0.659	-0.603			-	2.7	-	2.1			-	1.4		
				S	SSR	-0.516	-0.442	-0.539	-0.464			-0.324	-0.321			-	0.74	17	5.9			-	7.6		
						11/19/96	11/14/97					1/3/08	9/10/08			11/19/96	11/14/97					1/3/08	9/10/08		
5	Port Saint Lucie Blvd.: Port Saint Lucie	Coastal; Tidal saltwater	R3	top G	GSC	-0.799	-0.782					-0.695	-0.716			1.7	1.9					-	0.20		
				bot. G	GSC	-0.782	-0.781					-0.733	-0.774			2.4	1.9					-	0.39		
				S	SSR	-0.631	-0.533					-0.512	-0.525			62	8.3					7.6	6.5		
			R7	top G	GSC	-0.785	-0.765					-0.757	-0.726			2.8	1.2					0.65	0.83		
				bot. G	GSC	-0.801	-0.754					-	-0.728			4.1	2.2					-	0.64		
				S	SSR	-0.735	-0.621					-0.618	-0.572			51	2.2					1.1	1.4		

Table 3.2 (cont.) Summary of electrochemical field observations for instrumented structures.

Structure #	Site and Location	Environment	Panel Set	Element[1]	Internal Connection[2]	Electrochemical Testing																			
						Potential vs. CSE (V)										Corrosion Rates (μm/y)[3]									
						First Survey						Second Survey				First Survey						Second Survey			
						Visit 1	Visit 2	Visit 3	Visit 4	Visit 5	Visit 6	Visit 1	Visit 2	Visit 3	Visit 4	Visit 1	Visit 2	Visit 3	Visit 4	Visit 5	Visit 6	Visit 1	Visit 2	Visit 3	Visit 4
6	State Rd. 200; Ocala	Land				1/15/97	4/9/97	9/26/97				6/6/07	12/28/07			1/15/97	4/9/97	9/26/97				6/6/07	12/28/07		
			R6	top G	GSC	-0.628	-0.663	-0.606				-0.642	-0.618			0.20	0.23	0.25				0.26	0.19		
				bot. G	GSC	-0.638	-0.577	-0.578				-0.620	-0.594			0.28	0.30	0.36				0.88	1.1		
				S	SSR	-0.497	-0.340	-0.293				-0.310	-0.292			9.8	4.5	3.3				3.8	3.0		
			R25	top G	GSC	-0.560	-0.527	-0.591				-0.525	-0.550			0.56	0.64	-				0.72	0.7		
				bot. G	GSC	-0.565	-0.522	-0.593				-0.527	-0.542			0.84	0.84	-				1.8	-		
				S	SSR	-0.558	-0.251	-0.243				-0.257	-0.272			4.6	4.3	-				-	1.7		
7	Acosta Bridge; Jacksonville	Coastal				4/8/97	9/25/97					8/15/07	12/27/07			4/8/97	9/25/97					8/15/07	12/27/07		
			R9	top G	GSC	-0.505	-0.427					-0.445	-0.426			15	0.58					0.61	0.26		
				bot. G	GSC	-0.496	-0.420					-0.454	-0.426			21	0.66					0.98	0.34		
				Zn-Al	Zn-Al	-0.895	-0.649					-0.571	-0.552			79	0.56					2.1	-		
				S	SSR	-0.470	-0.403					-0.440	-0.420			470	-					18	15		
			R21	top G	GSC	-0.610	-0.561					-0.540	-0.525			20	0.69					0.78	0.31		
				bot. G	GSC	-0.523	-0.512					-0.526	-0.507			23	0.91					0.92	0.50		
				S	SSR	-0.432	-0.233					-0.291	-0.290			37	2.7					1.4	-		
8	Vetaran's Expressway ; Tampa	Land				5/31/07	7/19/07					5/31/07	7/19/07	1/22/09		6/4/97	1/16/98					5/31/07	7/19/07	1/22/09	
			R16	top G	GSC	-0.484	-0.512					-0.651	-	-0.473		1.4	0.99					1.02	-	0.89	
				bot. G	GSC	-0.466	-0.480					-0.592	-	-0.421		1.5	1.0					0.83	-	0.80	
				Zn-Al	Zn-Al	-0.840	-0.290					-0.868	-	-0.707		2.2	0.71					-	-	-	
				S	SSR	-0.458	-0.823					-0.434	-	-0.279		6.9	5.5					-	5.4	5.70	
			R23	top G	GSC	-0.578	-0.580					-0.656	-	-0.562		1.3	0.81					2.0	-	0.82	
				bot. G	GSC	-0.572	-0.566					-0.623	-	-0.541		1.3	0.97					2.0	-	0.88	
				Zn-Al	Zn-Al	-0.785	-0.869					-0.875	-	-0.731		4.2	0.76					1.9	-	1.80	

1. L=left; R=right; F=front; B=back; bot.=bottom; S=stainless steel; G=galvanaized steel; Zn-Al=85-15% Zn-Al strip.
2. GSC=galvanized steel clamp; SSR=stainless steel rod; SSC=stainless steel clamp; ZAC=Zn alloy clamp.
3. Corrosion rates for the steel rods are an average of two measurements, using the top and bottom galvanized strips as counter electrodes.

3.1.3 Electrochemical Impedance Spectroscopy

Comparison of polarization resistance values obtained by LPR and EIS are shown in Figure 5 and Figure 6. Detailed listing of EIS parameters obtained for each EIS test of the present survey, as well as the corresponding ACR values is presented in Tables A2-8 to A2-14 of Appendix 2.

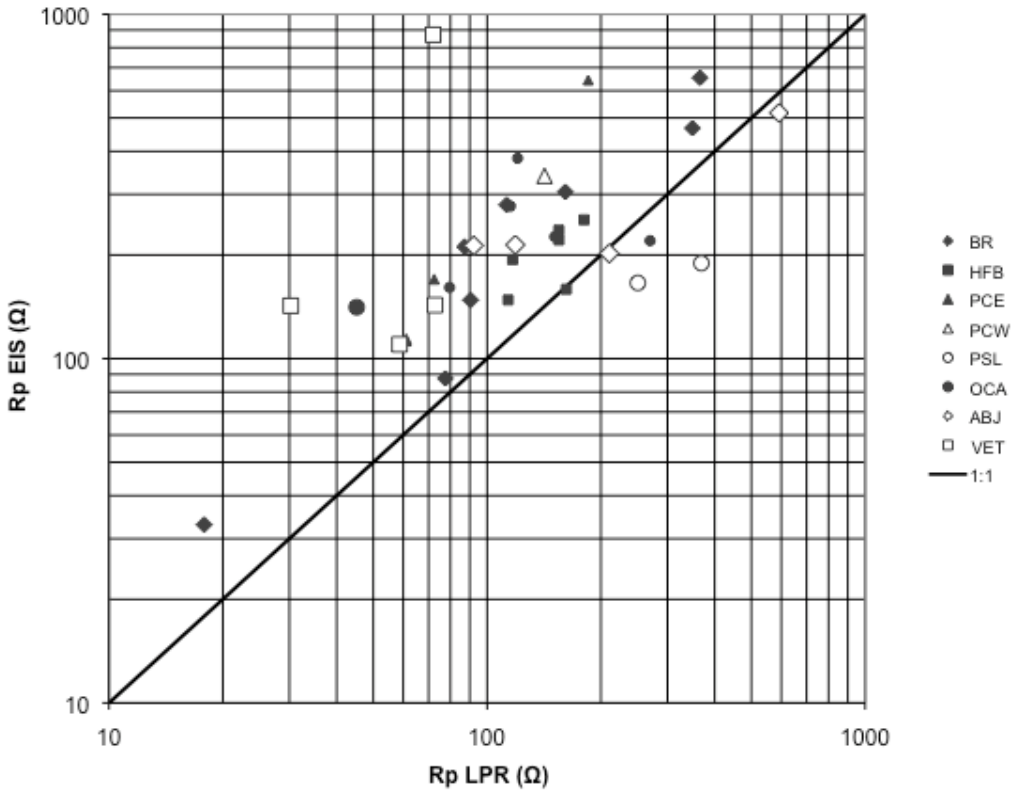

Figure 5 - Comparison of Rp values obtained by LPR and EIS for the same galvanized steel elements and during the same field visit for the indicated walls. The diagonal line corresponds to an ideal 1:1 correlation.

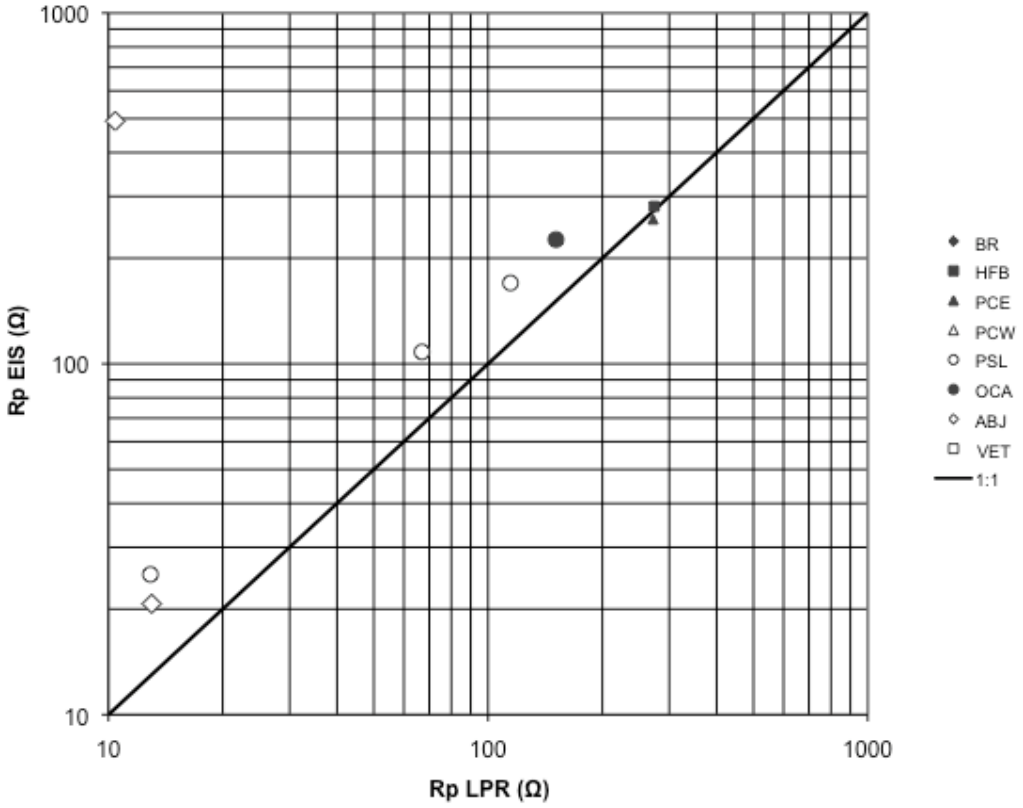

Figure 6 - Comparison of Rp values obtained by LPR and EIS for the same plain steel elements and during the same field visit for the indicated walls. The diagonal line corresponds to an ideal 1:1 correlation.

3.1.4 Macrocell Current Values

These data could only be reliable obtained during the June, 2008 visit to the BR site. Results are shown in Table 3.3.

Table 3.3 Macrocell currents for the Brickell Ave. Bridge site from June 2008.

Connection	(+) / (-)	Time (s)	BRN	BRS
			(mA)	
Top	Back Galv / Front Galv	5	-0.01	0.07
		10	-0.01	0.06
		60	-0.01	0.07
	Back Steel / Front Steel	1	0.105	-
		10	0.10	
		60	0.105	
Bottom	Back Galv / Front Galv	5	-0.09	0.00*
		10	-0.09	0.00*
		60	-0.09	≤0.004**
	Back Steel / Front Steel	1	0.07	-
		10	0.075	
		60	0.075	

*Partial data indicates negligible macrocell activity
**Value taken at higher resolution setting
Positive values indicate the element denoted by (+) is the net cathode.

3.2 Laboratory Data

3.2.1 Soil Tests Data

Soil properties obtained in the present survey are displayed in Table 3.4.

Table 3.4 Averaged‡ soil properties measured in the 1994-98 and 2006-09 surveys.

Wall	Cl^- (ppm)		SO_4^{2-} (ppm)		Resistivity (kΩ•cm)		pH	
	'94-98	'06-09	'94-98	'06-09	'94-98	'06-09	'94-98	'06-09
BRN	13	-	30	-	42	-	9.1	-
BRS	5.3	-	9.0	-	34	-	9.1	-
HFB	22	ND	0.70	5.0	16	16	8.3	-
PCE	2.5	-	ND	-	40	-	9.1	-
PCW	160**	ND	67**	11	1.2**	13	-	8
PSL	20	ND	7.5	15	7.5	9.3	8.3	7.8
OCA	8.3	ND	3.0	4.0	37	24	7.3	6.5
ABJ	4.7	ND	0.75	3.5	29	16	8.4	7
VET	2.3	-	7.3	-	21	-	5.5	-

‡Detailed measurements are found in Appendix 4: Soil Properties. Resistivity average reported as inverse of average conductivity if multiple samples existed.
*ND indicates below detection limit
** 94-98 survey showed high variability of composition for PCW

3.2.2 Metallographic and Magnetic Gage Measurements

Except for HFB, all samples extracted came from the lowest elevations possible per core drill placement. Figure 4 shows metallographs illustrating instances of low corrosion (nearly complete galvanized layer) and high corrosion (including a thick corrosion product layer). Table 3.5 shows averages of thickness measurements for each wall and for a coupon from a control regular production MSE strip retained from experiments performed during the 1994-98 investigation.

Table 3.5 Summary of Metallographic and Magnetic Gage Thickness Measurements (μm)

Wall	Age at time of Coupon Extraction (y)	Number of Coupons	Metallographic				Magnetic Gage
			Remaining Galvanized Layer	Corrosion Product Layer	Total Thickness	ACR (μm/y) MET	Total Thickness
BRN	-	-	-	-	-	-	-
BRS	-	-	-	-	-	-	-
HFB	13.8	3	107	55	161	4.0	210
PCE	-	-	-	-	-		-
PCW	17.8	2	56	50	106	2.8	145
PSL	11.9	1	139	22	161	1.8	189
OCA	24.6	3	119	15	135	0.61	150
ABJ	17.7	1	75	15	90	0.85	104
VET	-	-	-	-	-		-
Control	-	-	151	-	151		140

(Average of measurements for all coupons of each wall)

4 DISCUSSION

4.1 Direct assessment results

Visual appearance of the walls examined (Table 3.1) did not reveal any outward signs of distress related to corrosion of the earth reinforcement or any other obvious structural distress. The numerous small spalls present in HFB were examined separately from this investigation and found to be consistent with instances of very small (e.g. 6 mm) concrete cover over the medallion's rebar. The small cover likely permitted rapid penetration of chloride from the concrete surface (the wall is placed ~ 5m from the shore of the causeway facing estuarial waters containing in the order of 10,000 ppm Cl-) with consequent initiation and propagation of corrosion of the rebar. BRS had one spall which was similar in rational to the spalls in HFB, except the BRS wall was also painted.

Chloride content of the soil extracted from core holes (Table 3.4) was non detectable. This result may reflect the long storage period before the analyses were conducted, possibly promoting conversion of the chloride into evasive species [18] or forms non detectable by the method used. Thus, the chloride analysis results from the present survey will not be considered to be relevant by themselves. Sulfate contents and pH were in the general range of those obtained in the earlier survey, suggesting that, if no artifact from long term storage affected those analyses, no adverse evolution of that parameter in the intervening period. Unlike the soil chemical composition analysis, most pH and resistivity measurements were conducted shortly after sample extraction and thus considered to be reliable, an expectation supported by the results being generally close to those obtained in the 1994-98 survey. The resistivity values were amply above the 3,000 ohm-cm design minimum, consistent with the interpretation that no recent adverse soil contamination took place in the structures from which soil samples were taken.

Visual examination of reinforcement coupons showed little indication of distress with condition description ranging from good to very good, and only small regions of incipient rust. The rating of the galvanizing was based upon the amounts of red rust visible with Very Good and Good ratings corresponding to less than 5%, 20%, and 50% of the surface area respectively. These observations are consistent with results from examination of strip holding hardware and visual inspection at cored locations conducted in the 1994-98 survey and further indicative of no severe aging deterioration since. Yet the more exhaustive metallographic examination of coupons conducted in the present survey showed however distinct indications of wastage of the galvanized layer in progress as documented in Table 3.5, where corrosion product layers are on average a sizable fraction of the remaining galvanized layer. As a confirmation of the metallographic measurements, in Figure 7 shows general consistency

between the metallographic total thickness results and the magnetic gage measurements. Quantitative analysis of the results to estimate integrated corrosion rates and comparison with results from electrochemical measurements is presented later on.

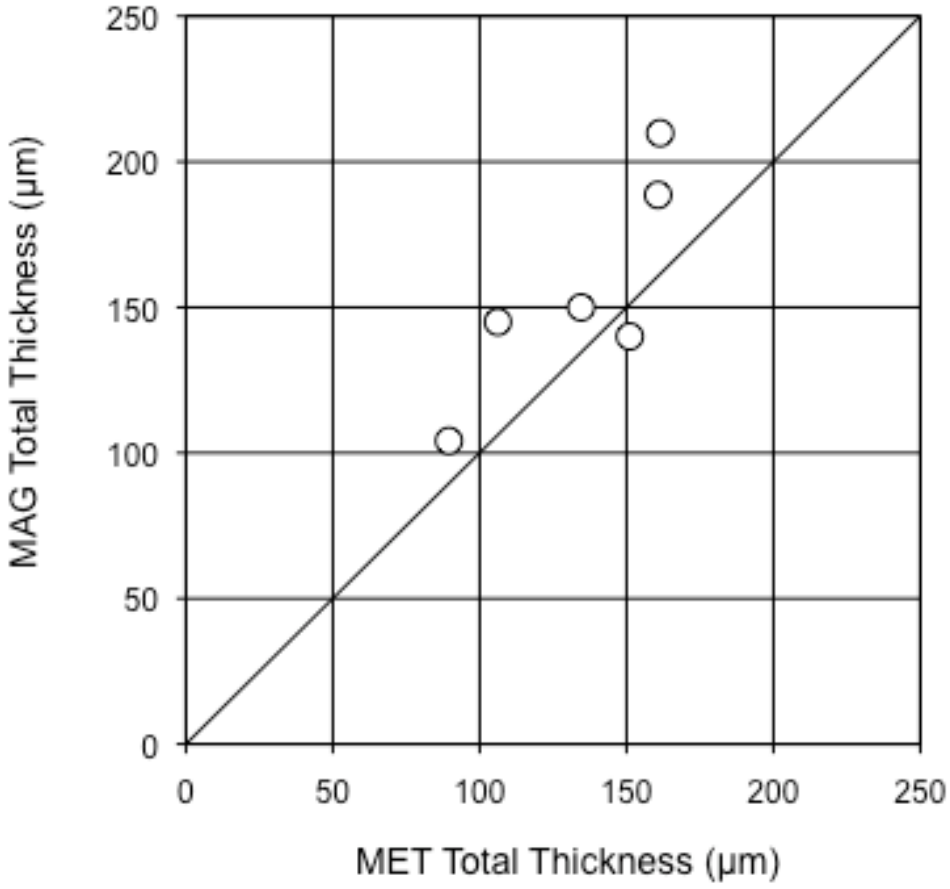

Figure 7 - Comparison of galvanized layer plus corrosion product thickness from metallographic measurements (MET Total Thickness) with total film thickness determined with a magnetic thickness gage (MAG), averaged for coupons extracted n the present survey from each Wall. The diagonal line corresponds to an ideal 1:1 correlation. Data from Table 3.5.

4.2 Electrochemical estimates of corrosion wastage

The corrosion rates estimated from electrochemical measurements (obtained from the LPR method unless indicated otherwise) are the result of calculations based on numerous assumptions [19] which can be only be partially fulfilled in any given system. Those values are considered therefore as an approximation of the actual corrosion rate at the time of the measurement and will be reported in the following as apparent corrosion rates (ACR), expressed in μm/y.

The information from Table 3.2 was used to obtain ACR averages for each galvanized reinforcing element over all visits in the present survey. The highest and lowest element ACR averages for each wall (except for BR where the two walls at that site were treated as one) were noted. Those element averages were in turn averaged for each wall. The results including high and low values are displayed in Figure 8, along with similar results for the 1994-98 survey, indicating the structure age range spanned in each survey.

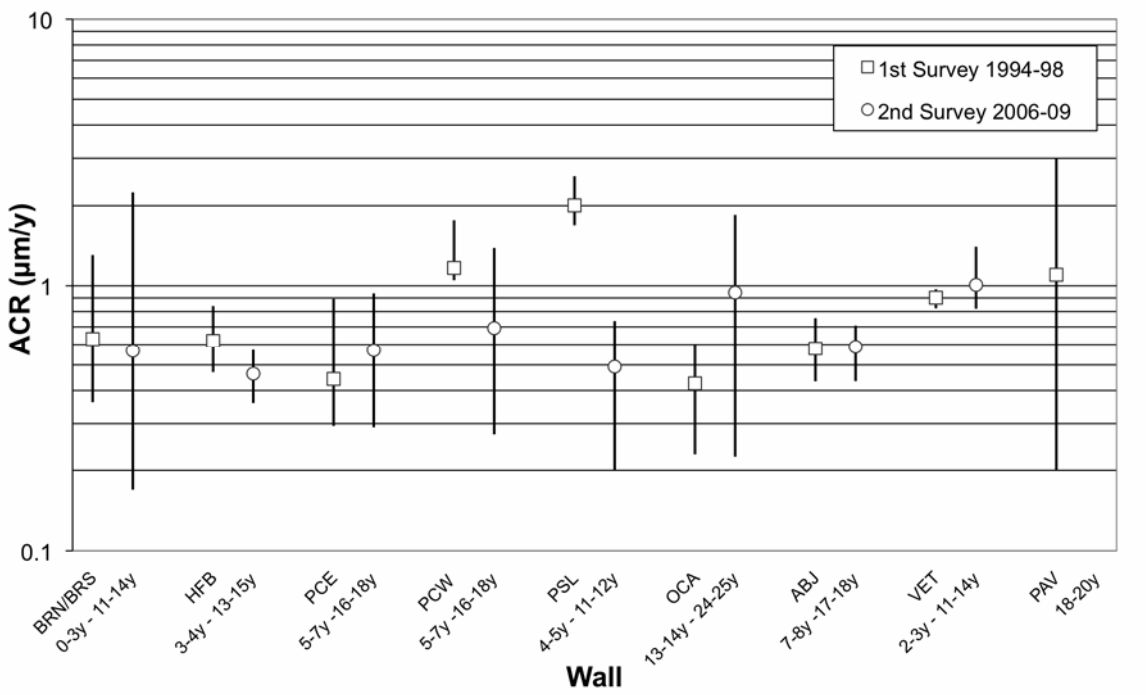

Figure 8 - Wall averaged galvanized steel ACR values for the present and previous surveys.

The averaged ACR results for galvanized steel at each wall were generally of the same order for both surveys, with a very small value of<1μm/y in most cases. This value is, encouragingly, at the low end of the range commonly anticipated for buried galvanized steel [5]. With one exception (PSL) individual wall survey-to-survey differences in average ACR were markedly smaller than the range spanned by the results of individual measurements in a given wall,

thus obscuring any effect of interim aging on ACR. To assist in revealing overall trends, the results were graphically summarized in Figure 9, which shows cumulative distributions of ACR for both surveys.

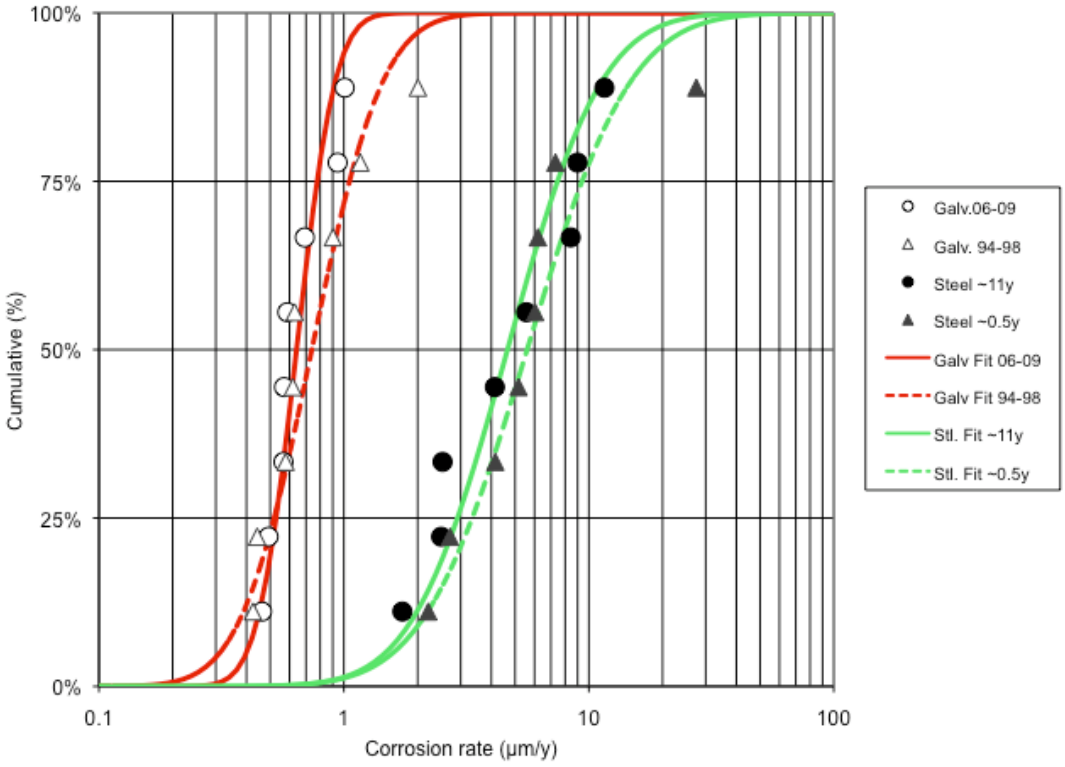

Figure 9 - Cumulative distributions of ACR averaged for each wall from the 1994-98 and 2006-09 surveys, fitted with cumulative lognormal distributions. Results for Galvanized steel are grouped per survey. Results for plain steel rods are grouped per element age group as indicated in the text.

The galvanized steel ACR cumulative distributions from the 1994-98 and 2006-09 surveys nearly overlap so a more detailed analysis was implemented to elucidate possible underlying trends. The distributions are markedly skewed when displayed in a linear plot but become more symmetric in a logarithmic plot as in Figure 9. Following the presentation by Sagüés et al [14], the data were fit with ideal lognormal distributions with resulting parameters summarized in Table 4.1. As shown in the table and consistent with visual appearance in Figure 9, the median and average ACR values for the earlier survey are somewhat higher (by 15% and 27% respectively) than those found in the current survey. Such change would be in the expected direction (corrosion rates decreasing with time of burial [3, 4]) but statistical significance of these figures is however limited in view of the large variability of results. The lognormal standard deviations, when expressed as ratios from the value one lognormal standard deviation above median to that of median, are high (1.7 and 1.3 for the earlier and present

surveys respectively, or 70% and 30% variations). In an ideal lognormal distribution the standard deviation of the median of the 8-value sample considered would be ~3 times smaller than the overall standard deviation. If that were to apply to the current case, then the calculated decrease in median (and average) ACR values from the previous to the current surveys may be considered to be only marginally significant.

Table 4.1 Analysis of wall-averaged ACR results.

Elements	Galvanized		Plain Steel	
Survey	1994-98	2006-09	1994-98*	2006-09*
Average Age (y)	5.9	16.0	0.5	10.6
Average ln(ACR) (μm/y)	-0.30	-0.45	1.72	1.54
Std. Dev. ln(ACR) (μm/y)	0.53	0.29	0.77	0.70
Lognormal Std. Dev. expressed as ratio	1.7	1.3	2.1	2.0
Median per Lognormal Dist. (μm/y)	0.74	0.64	5.60	4.65
Average (μm/y)	0.85	0.67	7.65	5.68
ACR Early/Aged Ratio-Median	1.15		1.20	
ACR Early/Aged Ratio-Avge.	1.27		1.35	
n based on median ACR	0.59		0.94	
n based on average ACR	0.76		0.90	

*Steel elements newly placed in HFB grouped with those of the 1994-98 survey.

A similar treatment was applied to ACR data in Table 3.2 for the plain steel bars, with the results seen in Figure 9 and Table 4.1. With the exception of BR the steel bars were buried after the walls had been in place for some time, and in the case of HFB half of the steel bars were buried during the first survey and half during the second. Therefore, the plain steel ACR data are grouped by age at the time of testing, with one group for average age ~11y (buried during the first survey and tested during the second) and the other group for average age ~0.5y (for all bars buried and tested during the first survey plus the 4 bars buried at HFB during the second survey). The plain steel ACR values in both surveys

were, with little statistical uncertainty, much higher (average ~ 6 μm/y) than those for the galvanized elements. On the other hand, as in the galvanized steel case the cumulative distributions for the early and late age data are quite close to each other. Other parallels with the galvanized steel case are noted in the following. The plain steel ACR data are better approximated by a lognormal distribution than by a linear one. The lognormal fit values are shown in Table 3.2. The median and average plain steel ACR values for the earlier ~0.5y tests are higher (by 20% and 35% respectively) than those in the ~11 year tests, but the wall to wall variability indicated by the standard deviation (corresponding to ~100% in the upward direction, ~50% downward) is even greater that in the case of the galvanized steel elements. Thus, even accounting for lesser uncertainty in the value of the median (and average) on account of the multiple sample size the calculated overall decrease with time in the ACR of plain steel is also marginally statistically significant. Regardless of the time dependence question, it is noted that the ~6 μm/y average corrosion rates found for steel in the relatively long term ~11y tests are well within the range of those reported in the literature for similar buried conditions [4, 5].

While recognizing the uncertainty in the time dependence indicated above, it is instructive to determine how those trends would compare with general observation of corrosion wastage in buried metals. As found in the investigations by Romanoff and others [4, 5] corrosion metal loss x tends to follow a dependence with time t given by

$$x = k\, t^{n} \qquad \text{Eq. (1)}$$

where k is a proportionality constant and n a parameter with value between 0 and 1. The corresponding corrosion rate time dependence is therefore

$$dx/dt = k\, n\, t^{\,n-1} \qquad \text{Eq. (2)}$$

Rearranging Eq.(2) to solve for n and using the median and average ACR values from Table 4.1 yields nominal n values displayed further below on the same Table. For galvanized steel the nominal n values computed using either the median or the average ACR values were near 0.7, which is in agreement with values often reported in the literature for buried galvanized steel as summarized in Table 4.2 [4, 5]. In contrast, the nominal n values computed for plain steel were closer to unity, denoting a corrosion rate that decreases relatively slowly with time. That trend also approximates results with reported values of n between for plain steel that are somewhat higher than those for galvanized steel. Due to the variability and associated uncertainty in time trends noted above, later measurements over a wider time baseline may be needed to better resolve time dependence of corrosion rate in these structures.

Table 4.2 Time dependence parameter n from sources reported in References [4] and [5].

Study	Galvanized	Plain Steel
NBS* Avg. [3]	0.65	0.80
NBS* Max. [3]	0.65	0.80
France** Low [4]	0.60	0.65
France** High [4]	0.60	1.00

* National Bureau of Standards
** French soil box investigations.

4.3 Accuracy and consistency of electrochemical corrosion measurements

A validation check of the accuracy of the ACR determinations was conducted for galvanized steel elements by comparison with integrated wastage estimates from the metallographic examinations. The corrosion products were assumed to have a zinc content (66 wt%) and density (3.05 gcm^{-3}) similar to those of solid $Zn(OH)_2$, a common composition for zinc corrosion products [20]. The average corrosion product thickness for each structure per Table 3.5 was converted accordingly to the equivalent thickness of solid zinc as an estimate of galvanized layer wastage. The wastage thickness was divided by the age of the wall at the time of coupon extraction to obtain a metallographically estimated corrosion rate (MET CR) reflecting the average corrosion rate experienced during the entire exposure period. Results are shown in Figure 10, where the diagonal line represents ideal agreement between LPR ACR and MET CR results. There is order-of-magnitude agreement between metallographic and electrochemical corrosion assessments for individual walls based on either survey, and significantly better correlation when the average of all walls is considered (filled symbols). It is emphasized that the metallographic method result reflects metal wastage rate averaged over the entire exposure period, while the electrochemical measurement determine instantaneous corrosion rate. Thus the value of a direct comparison is limited by variability in corrosion rates both long term (as in the expected gradual decrease of rate with time while the galvanized layer is in place) and short term reflecting seasonal and tidal influences. Further limitation is due to the small amount and size of reinforcement coupons available, and that the coupons were always from one region of the wall, closest to the outer surface thus introducing a sample bias that may not reflect conditions further in. In contrast, the electrochemical measurements involve the entire buried element length. Keeping in mind these factors and the typical method uncertainty and actual variability in corrosion distribution, the metallographic results generally support the validity of the electrochemical LPR measurements.

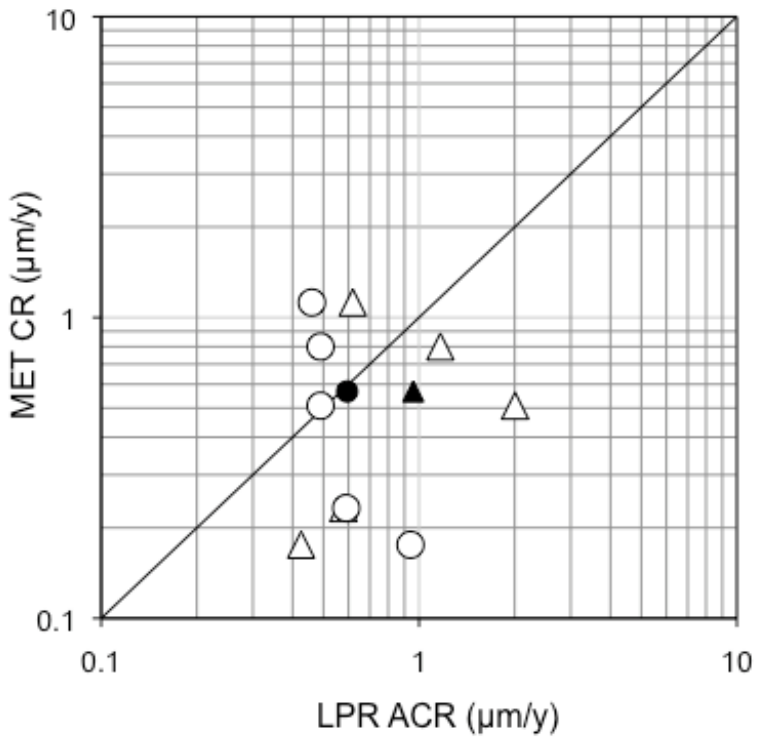

Figure 10 - Comparison of integrated corrosion rates evaluated from metallographic measurements (MET) of coupons extracted from five walls in the present survey, averaged for coupons from each wall, with corresponding average ACR values from LPR measurements. The calculations assumed that the corrosion products behaved as solid $Zn(OH)_2$. Triangles: 1994-98 survey. Circles: 2006-09 survey. Open symbols: results from individual walls. Filled symbols: average of all values in each survey. The diagonal line corresponds to an ideal 1:1 correlation.

Although the approximate validity of the LPR estimates of corrosion rate for galvanized steel was supported by the direct metallographic observations, it is important to examine to what extent the ACR values may vary when alternative electrochemical techniques are used. Consequently, the internal consistency of the electrochemical ACR determinations was examined by contrasting LPR results with those from independent EIS measurements performed from time to time at selected elements, as detailed in Appendix 2. Analysis of the results was performed by fitting the EIS data with the analog circuit shown in Figure 11, restricting the analysis to the frequency range 0.01 Hz to 0.8Hz. That procedure yields values for the polarization resistance, Rp EIS, which can be compared with those obtained by the LPR method. EIS analysis reliability was limited by uncertainty inherent to the generally low values of the frequency dispersion coefficient observed in soil systems [15], especially for cases where the value of Rp was high [21].

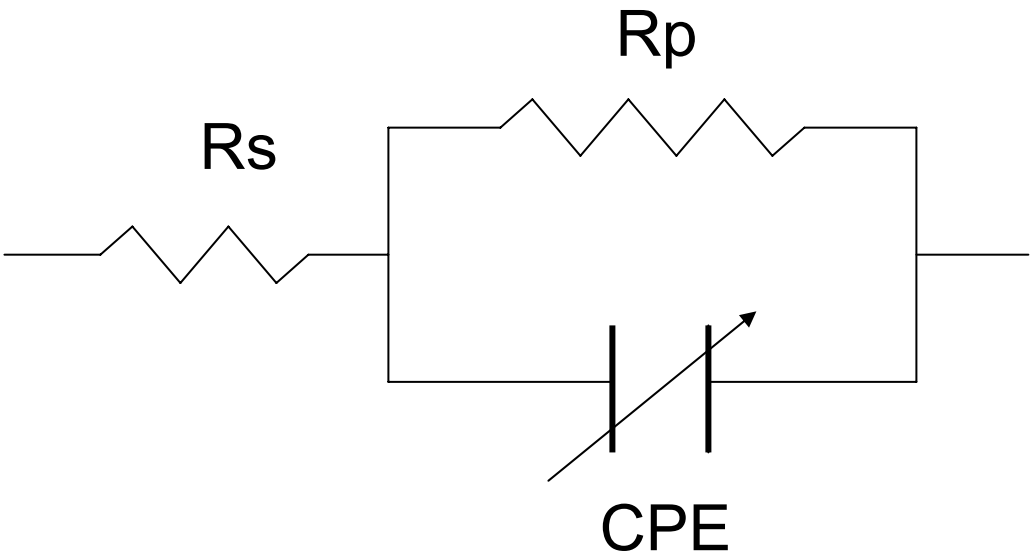

Figure 11 - Analog circuit used to analyze the EIS data. The constant phase angle element (CPE) has parameters Yo ($S \bullet s^n$) and n.

Consequently only analyses for which Rp EIS <1kohm were contrasted with the LPR polarization resistance (Rp LPR) determinations. The comparison results are shown in Figures 5 and 6 for tests with galvanized and plain steel elements respectively. With the exception of one Rp EIS value at the high end of the range in both cases, there is approximate correlation between both methods over a wide range of values. Superimposed on a moderate amount of scatter there is also an overall offset of ~1.5:1 for the observed Rp EIS / Rp LPR, which is not surprising given the many working assumptions and consequent model uncertainty involved in the interpretation of these types of data [18, 20]. This comparison supports concluding that a reasonable degree of internal consistency exists for the electrochemical ACR determinations. The systematic offset between results of alternative test methods underscores the importance of using consistent electrochemical measurement and analysis methodology from survey to survey.

Another independent indication of corrosion activity is provided by the macrocell current measurements, for which the BR walls have been instrumented. Table 3.3 shows that significant macrocell action was taking place in five of the six instrumented elements, with macrocell currents in the 10 to 130 μA range. In three of those the cases (one galvanized and two steel divided elements), the cathode was the half of the element further away from the external surface indicating that corrosion was greater at the front. The elements with the opposite polarity were both part of divided galvanized strips. When translated into a current density and corresponding average enhanced corrosion rate at the anode, the effect is in the order of a fraction of 1 μm/y. Although small in absolute terms, it must be recalled that the typical ACR values are also of the

same order, so corrosion macrocells could easily double the local corrosion rate at the net anode. Any further localization of the macrocell current could likewise multiply the metal loss in small regions, possibly leading to a substantial decrease of cross section there.

The half cell potentials observed in the present survey (Table 3.2) had values comparable to those in the 1994-98 survey, as shown in the summary of average values in Table 4.3. As observed in the previous survey, these potentials are only roughly informative of corrosion condition. More detailed analysis of the results did not reveal a clear correlation between ACR and the half cell potential. It is possible however that a correlation may be observed in the future as consumption of the galvanized layer begins to expose some of the more Fe-rich lower layers of the film and eventually the base steel itself. This consumption would results in potentials between those of galvanized steel and plain steel.

Table 4.3 Average galvanized steel half-cell potentials (V) vs. a CSE in contact with soil for the present and previous surveys.

Wall	2006-09	1994-98
BRN	-0.750	*-0.480*
BRS	-0.586	*-0.532*
HFB	-0.569	-0.744
PCE	-0.603	-0.643
PCW	-0.662	-0.742
PSL	-0.733	-0.781
OCA	-0.577	-0.587
ABJ	-0.481	-0.507
VET	-0.565	-0.530

4.4 Predictive Model

The predictive model used is the same as described previously [14, 15], operated to reflect the corrosion distributions obtained in the present as well as the previous surveys. A generic Florida condition is considered, so as a working estimate the lognormal distribution parameters based on those given in Table 4.1 are used and assumed to reflect the distribution of corrosion rates over the strips in a given structure. The corrosion rates are considered to be time-invariant as opposed to time dependent as discussed previously for simplicity and conservativeness. Separate calculations are conducted using the 1994-98 and the 2006-09 distributions to reveal sensitivity to the parameter choices and to examine the implications of the added data developed in the present investigations.

As the model is detailed in those previous publications [14, 15], only salient points are addressed, following the treatment by Sagüés et al [14]. The following modeling assumptions apply: The corrosion rates actually used for the calculations are those per the Table 4.1 distributions but multiplied by 2 to account for corrosion localization per the discussion in the previous section. Except for that multiplier, corrosion is treated as uniform along the strips. Corrosion at the strip edges is ignored. Element failure is declared upon the base steel reaching one half of its original thickness (one quarter loss of thickness on each side), since when that condition is reached stresses on the strip are likely to have grossly exceed the original design value. The average strip is considered to have a steel thickness s = 4mm and a galvanized layer thickness g = 150μm.

Per the above assumptions and as indicated in [14] the time to failure of a galvanized strip is given by

$$t_f = \frac{g}{v_g} + \frac{s}{4v_s} \qquad \text{Eq. (3)}$$

where v_g and v_s are the corrosion rates of the galvanized and the plain steel (after it is exposed) for a given element. Each element has its own galvanized and plain steel corrosion rate values assigned per the assumed distributions. Calling $C_g(v_g)$ and $C_s(v_s)$ the cumulative distribution of ACR values for the galvanized layer and base steel respectively , and calling $P_g(v_g)$ the probability distribution for the galvanized layer ACR:

$$P_g(v_g) = \frac{d\left(C_g(v_g)\right)}{dv_g} \qquad \text{Eq. (4)}$$

the derivation by Sagüés et al [14] shows that

$$\mathrm{Ff}(t) = \int_{v_g = g/t}^{\infty} P_g(v_g)\left(1 - C_s\left[\tfrac{s}{4}\left(t - \tfrac{g}{v_g}\right)\right]\right) dv_g \qquad \text{Eq. (5)}$$

where Ff(t) is the fraction of elements in the wall that failed by time t.

Though the corrosion rates are conservatively assumed to be time-invariant; this simplification may be relaxed in future model implementations as more reliable time dependence data are developed over a longer period of time.

Figure 12 shows the projections based on Eq. (7) and the parameters abstracted from the previous and the present surveys. Consistent with the very small ACR values obtained for the galvanized layers, both inputs result in projections of minimum damage (<5% elements failed) at age 100 years, and for reaching one half of elements damaged after 200 years. The results from the present survey yield a moderately more optimistic outlook due to the fractional decrease in ACR values with respect to the first survey discussed earlier. Given

the sustained character of the trends confirmed by the present survey, no further model expansion was deemed necessary at this time.

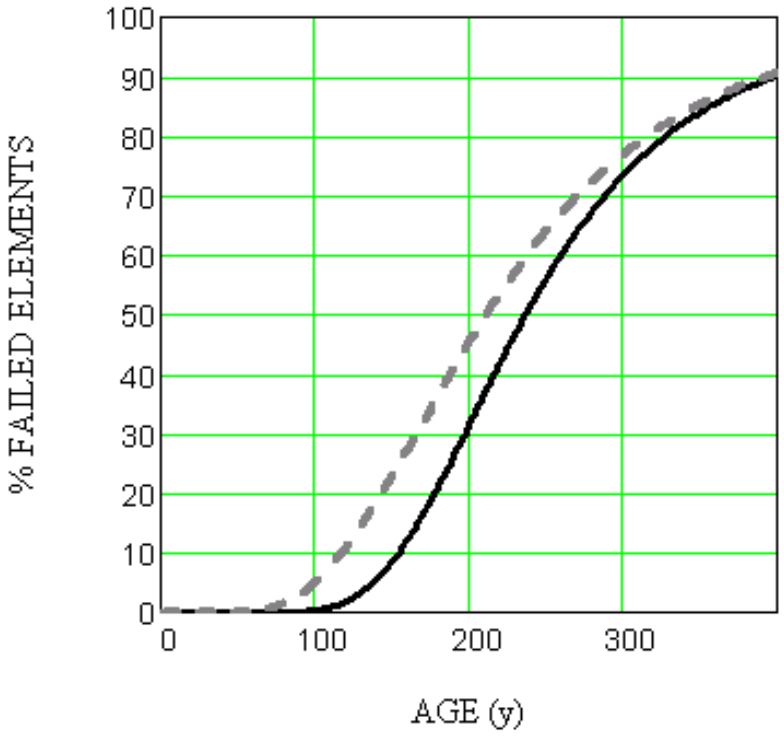

Figure 12 - Model projections of percentage of damage elements in a generic MSE wall as function of wall age. The projections are based on the lognormal distribution parameters in Table 4.1. The dashed and solid lines correspond to the parameters abstracted from the 1994-98 and the 2006-09 survey data respectively.

It is emphasized that the model projections are based on sweeping assumptions as well as on apparent corrosion rate values only approximately validated by direct observation. Consequently, the projections are subject to considerable uncertainty and should be treated with caution. Nevertheless, the overall observations indicate that corrosion deterioration so far has been mild in the structures investigated, and that there is a good prognosis for adequate corrosion performance in future decades barring unusual circumstances such as extensive backfill contamination. Periodic continuation surveys should nevertheless be conducted for verification. The low apparent corrosion rates observed appear to reflect successful control of backfill composition to avoid corrosive agents. Events such as saltwater inundation (addressed by Sagüés et al [15]) or aggressive chemical spills could dramatically degrade corrosion performance and in such circumstances the corrosion condition of the affected structure should be promptly assessed in detail.

5 CONCLUSIONS

1. Nine reinforced mechanically stabilized earth (MSE) walls (average age 16 years) in seven Florida sites representing a variety of service conditions were evaluated as a follow up to a previous survey conducted a decade earlier. Surface appearance of coupons extracted from actual reinforcement elements in five of the walls showed in general little evidence of distress. There was no external evidence of any earth reinforcement corrosion in any of the walls. Chemical analysis and resistivity measurements of extracted backfill revealed no unusual contamination.

2. Metallographic examination of the reinforcement coupons showed only moderate wastage of the galvanized layer, corresponding to low corrosion rates, estimated to range from ~0.2 to ~1.1 μm/y.

3. An extended series of linear polarization resistance (LPR) measurements yielded galvanized reinforcement apparent corrosion rates (ACR) that were also low (average ~0.7 μm/y) and in general agreement with those estimated metallographically. Similar analysis of results from the earlier survey yielded ~0.9 μm/y. These values are at the low end of the range commonly anticipated for galvanized steel reinforcement in MSE walls.

4. LPR tests produced average ACR ~6 μm/y values for ~11 years old embedded plain steel elements in the same walls. The average ACR for measurements conducted for the same or similar elements at average age ~0.5 year was ~8 μm/y. These values are within the anticipated range for buried steel in similar conditions.

5. The fractional drop in average ACR values between both surveys, although subject to uncertainty due to variability in the data and subject to future confirmation, was in the order of that expected for buried components.

6. The approximate accuracy and the electrochemical ACR estimates for galvanized steel was supported by agreement with direct metallographic examination, while internal consistency was established for both galvanized and plain steel ACR measurements by comparison with the results of independent electrochemical impedance spectroscopy tests in the field.

7. Corrosion macrocell current measurements at one of the test sites showed interactions between the front and back portions of the reinforcement that corresponded to an appreciable fraction of the overall corrosion rate. This information was used to apply a localized corrosion multiplier in the damage prediction model.

8. A statistical model that takes into account the estimated galvanized steel and plain steel corrosion rates and their variability was applied to project the evolution of corrosion related damage in a generic Florida MSE wall, using the data developed in the present and previous surveys. Consistent with the very small ACR values obtained for the galvanized layers, both inputs result in projections of minimum damage (<5% and <1% elements failed for the earlier and present survey) at age 100 years, and for about one half of elements experiencing damage after 200 years.

9. The overall observations indicate that corrosion deterioration so far has been mild in the structures investigated, and that there is a good prognosis for adequate corrosion performance in future decades barring unusual circumstances such as extensive backfill contamination. Periodic continuation surveys should be conducted for verification.

10. The low apparent corrosion rates observed appear to reflect successful control of backfill composition to avoid corrosive agents.

6 REFERENCES

1. Gladstone, R., Anderson, P., Fishman, K., Withiam, J., "Durability of Galvanized Soil Reinforcement: 30+ Years of Experience with MSE," presented at the 85th Annual Meeting of TRB, Washington, D.C., 2006.

2. "The performance of buried galvanized steel earth reinforcements after 20 years or service", P. Anderson and J. Sankey, in Landmarks in Earth Reinforcement, Ochlai et al (eds), Swets & Zeitlinger, ISBN 90 2651 863 3, 2001.

3. Elias, V., Christopher, B., Berg, R., "Mechanically Stabilized Earth Walls and Reinforced Soil Slope Design and Construction Guidelines," Rep. No. FHWA-NH1-00-043, National Highway Institute, Federal Highway Administration, Washington D.C., 2001.

4. Romanoff, M., "Underground Corrosion," NBS Circular 579, U.S. Dept. of Commerce, Washington, 1957.

5. Elias, V., "Durability/Corrosion of Soil Reinforced Structures," Report No. FHWA-RD-89-186, NTIS, Springfield, VA, December 1990.

6. Coating Properties, Galvanized Rebar Resource Center, 22 Aug. 2008, <http://www.galvanizedrebar.com/coating_properties.htm>

7. Wheeler, J., "MSES Corrosion Evaluation Program, End of the Year Report for 1998," New York State Department of Transportation Geotechnical Engineering Bureau, Albany, 1999.

8. Wheeler, J., "MSES Corrosion Evaluation Program, End of the Year Report for 2001," New York State Department of Transportation Geotechnical Engineering Bureau, Albany, 2001.

9. Beckham, T., Sun, L., Hopkins, T., "Corrosion Evaluation of Mechanically Stabilized Earth Walls," Rep. No. KTC-05-28/SPR-239-02-1F, Kentucky Transportation Center, Lexington, KY, 2005.

10. McGee, P., "Reinforced Earth Wall Strip Serviceability Study," Final Report: Study No. 8405, Georgia Department of Transportation, Atlanta, GA,1985.

11. Medford, W.M., "Monitoring the Corrosion of Galvanized Earth Wall Reinforcement," North Carolina Department of Transportation Field Investigation, presented at 78th Annual Meeting of TRB, Washington, D.C., January 13, 1999, (preprint).

12. Johnston, D., “Corrosion Monitoring of Hot Springs VSL Mechanically Stabilized Earth Wall,” Rep. No. SD2004-02-F, South Dakota Department of Transportation Office of Research, 2005.

13. Coats, D., Castanon, D., Parks, D., “Needs Assessment for a Maintenance Monitoring Program For Mechanically Stabilized Embankment Structures,” State of California Department of Transportation, Sacramento, CA, 2003.

14. Sagüés, A., Scott, R., Rossi, J., Peña, J., Powers, R., Corrosion of Galvanized Strips in Florida, Reinforced Earth Walls, Journal of Materials in Civil Engineering, August 2000, pp. 220-227, 2000.

15. Sagüés, A., Rossi, J., Scott, R., Peña, J.A., Simmons, T. “Influence of Corrosive Inundation on the Corrosion Rates of Galvanized Tie Strips In Mechanically Stabilized Earth Walls”, Rep. No. WPI0510686, Florida Department of Transportation Research Center, Tallahassee, FL, 1998.

16 Sagüés, A., Berke, B., To Be Published, 2009.

17 Florida Department of Transportation, Florida Test Methods, FM 5-550, 551, 552, and 553, FDOT State Materials Office, www.dot.state.fl.us

18 Oeberg, G., “Chloride and Organic Chlorine in Soil”, Acta Hydrochim, Hydrobiol. 26, pp. 137-144, 1998.

19 Sagüés, A,, Kranc, S. and Moreno, E., “"An Improved Method for Polarization Resistance from Small Amplitude Potentiodynamic Scans in Concrete", Corrosion, Vol. 54, p.20, 1998.

20 Zhang, X.G., "Corrosion and electrochemistry of Zinc", Plenum Press, New York, 1996

21 Sagüés, A,, Kranc, S. and Moreno, E., "Time Domain Response of a Corroding System with Constant Phase Angle Interfacial Component: Application to Steel in Concrete", Corrosion Science, Vol.37, p.1097, 1995.

APPENDIX 1: SITE INSTRUMENTATION DIAGRAMS

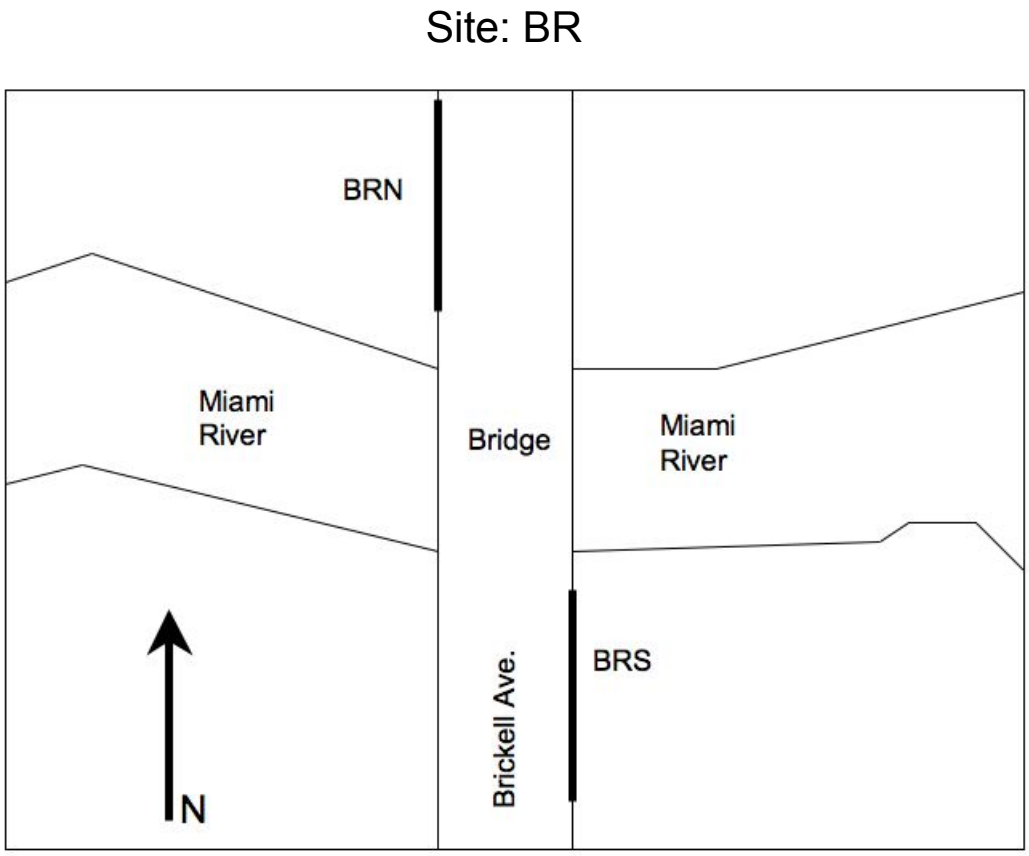

Figure 13 - Site diagram of the Brickell Ave. Site.

Appendix 1: Site Instrumentation Diagrams (Continued)

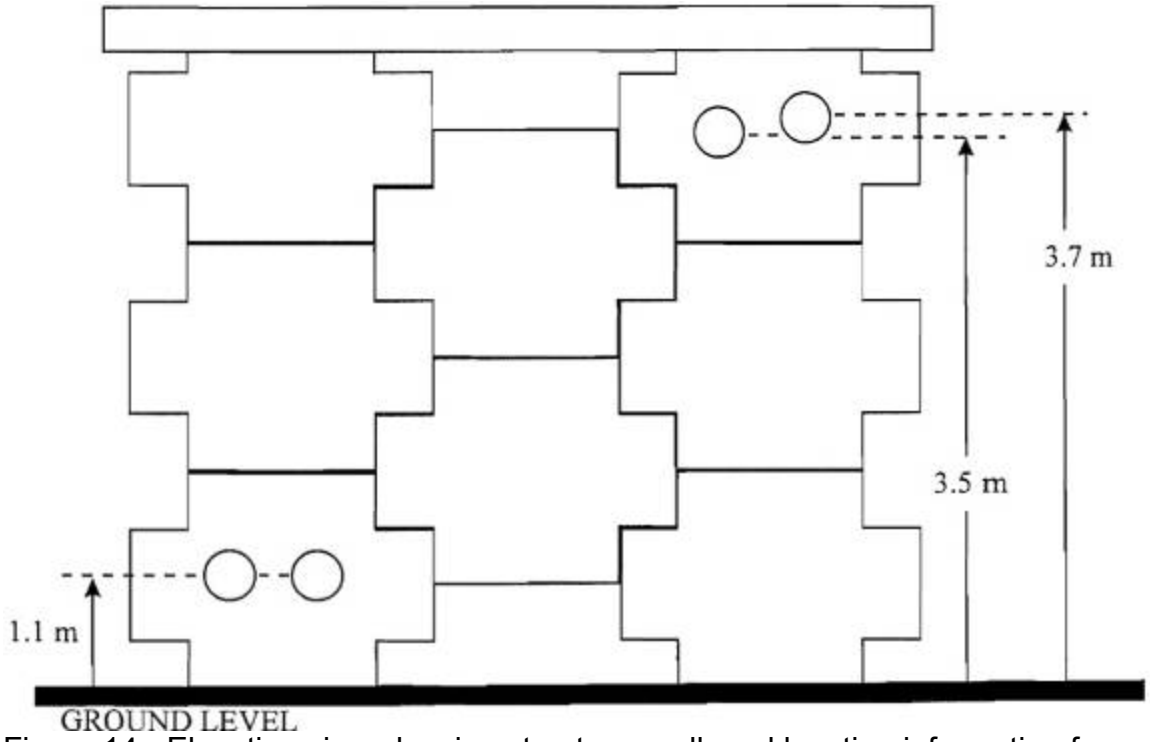

Figure 14 - Elevation view showing structure, wall, and location information for BRN [15].

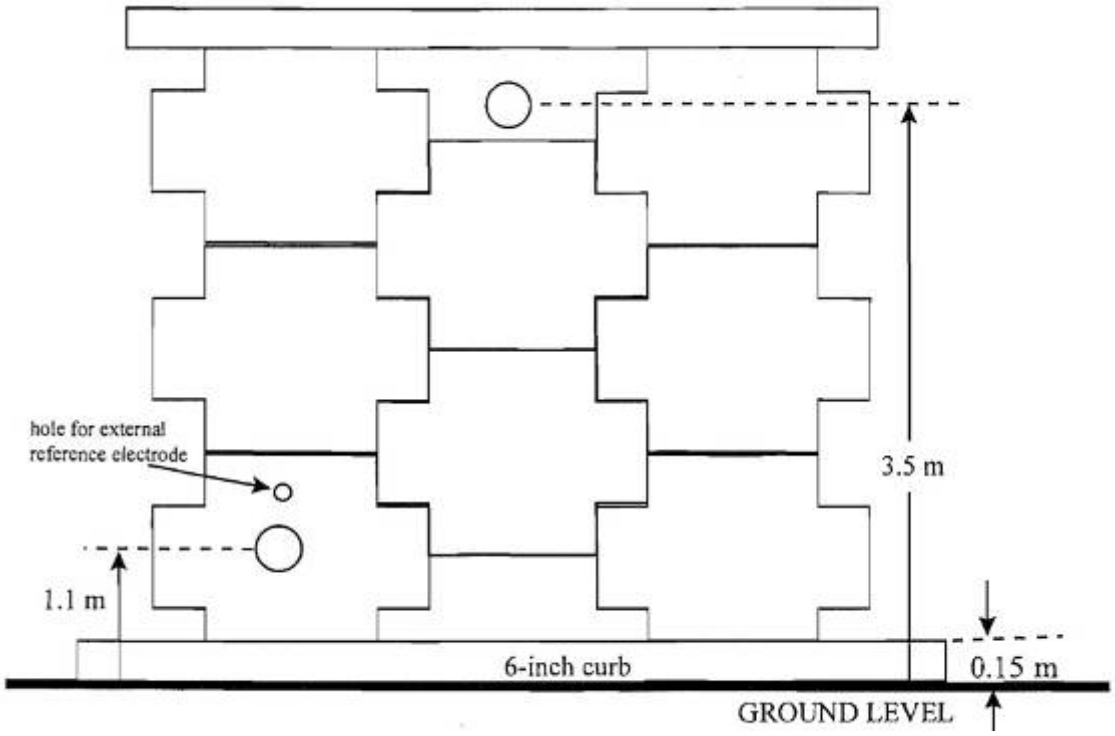

Figure 15 - Elevation view showing structure, wall, and location information for BRS [15].

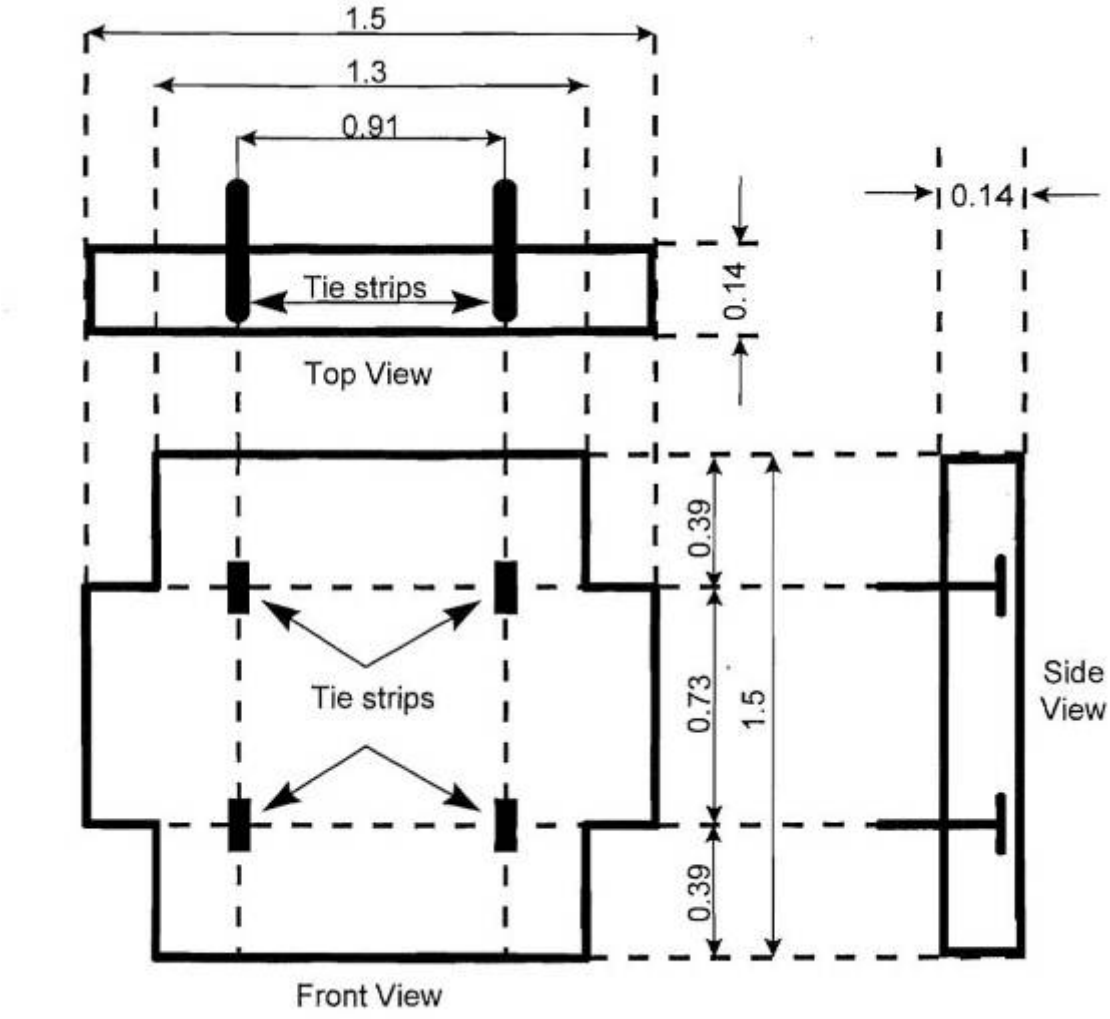

Figure 16 - Dimensions of typical concrete panels and tie strip locations for the BR. site. All dimensions are in meters [15].

Appendix 1: Site Instrumentation Diagrams (Continued)

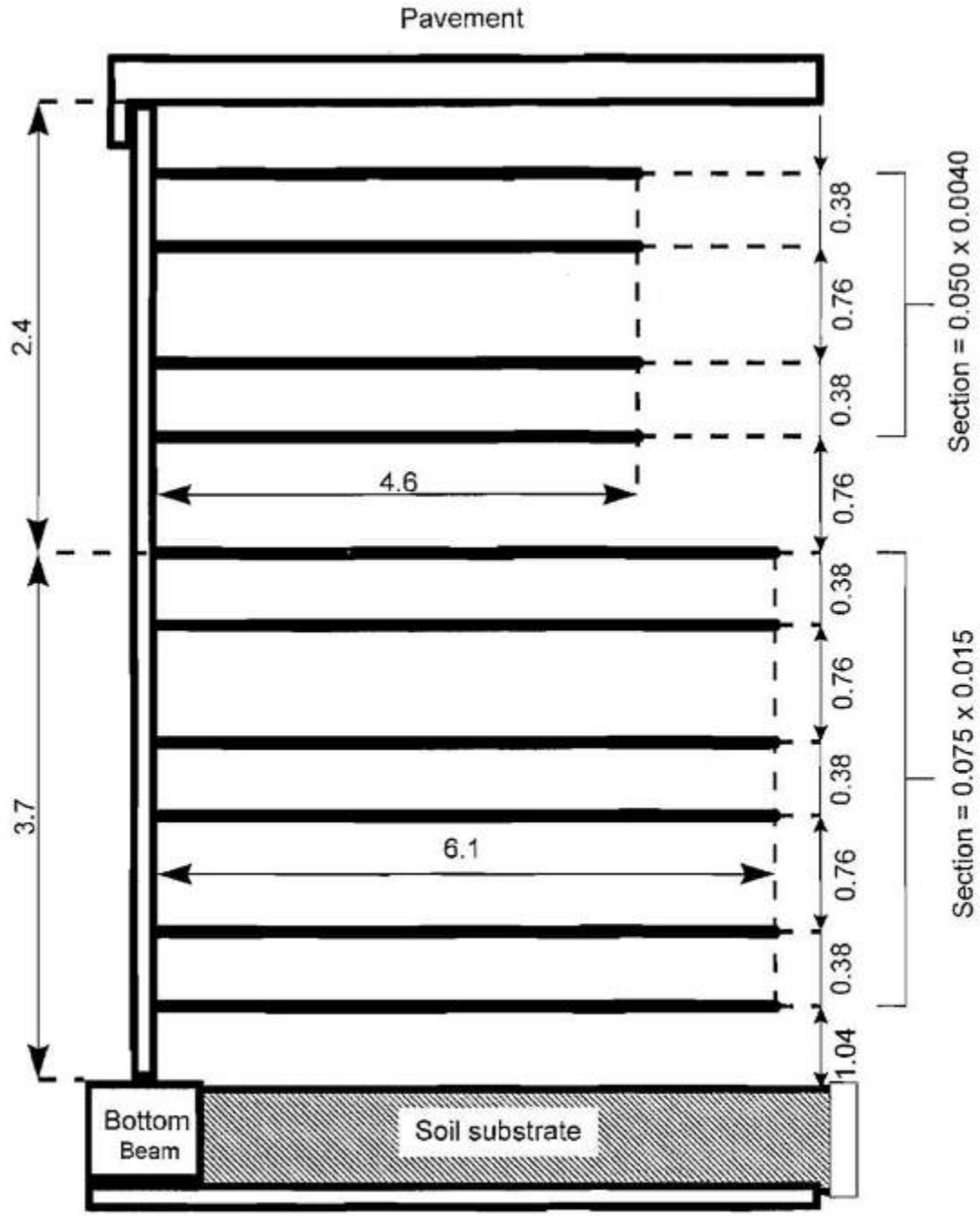

Figure 17 - Reinforcement placement in BR site MSE walls. All dimensions are in meters [15].

Appendix 1: Site Instrumentation Diagrams (Continued)

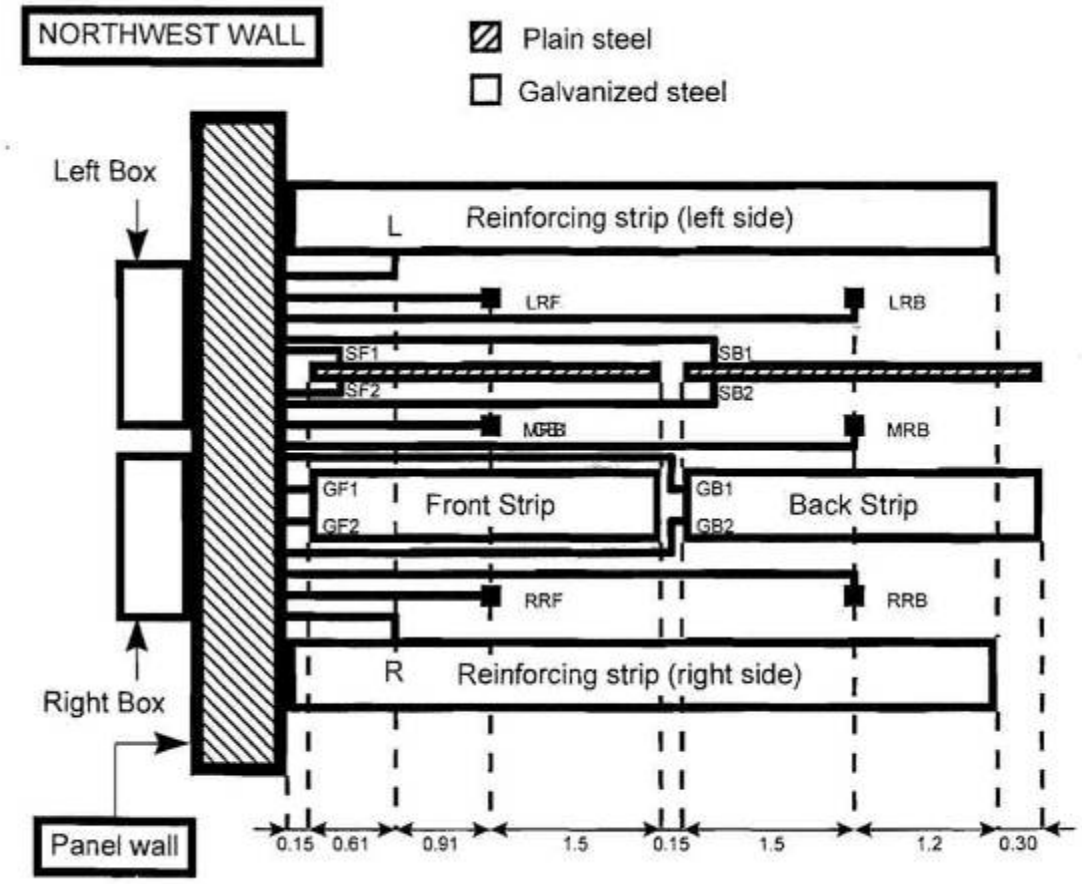

Figure 18 - Cluster diagram showing layout of elements in BRN. All dimensions are in meters [15].

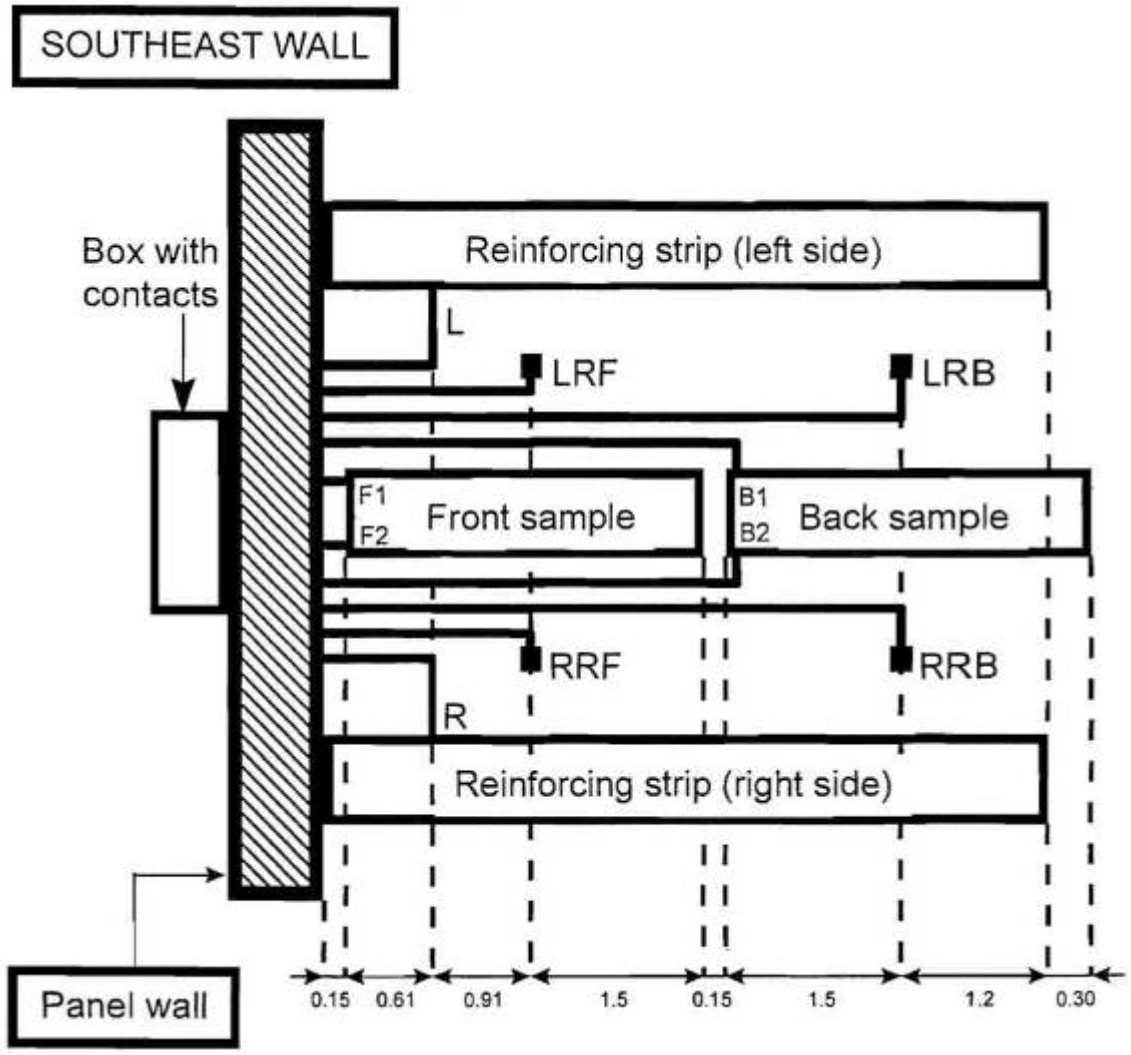

Figure 19 - Cluster diagram showing layout of elements in BRS. All dimensions are in meters [15].

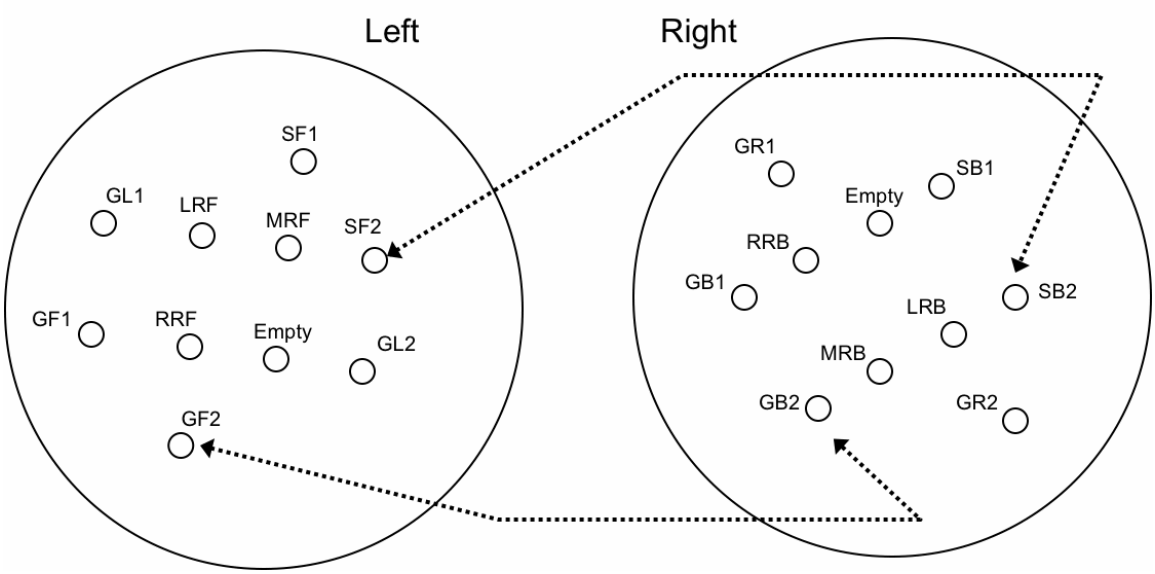

Figure 20 - Test points BRN, bottom layer. Normally connected jumpers shown.

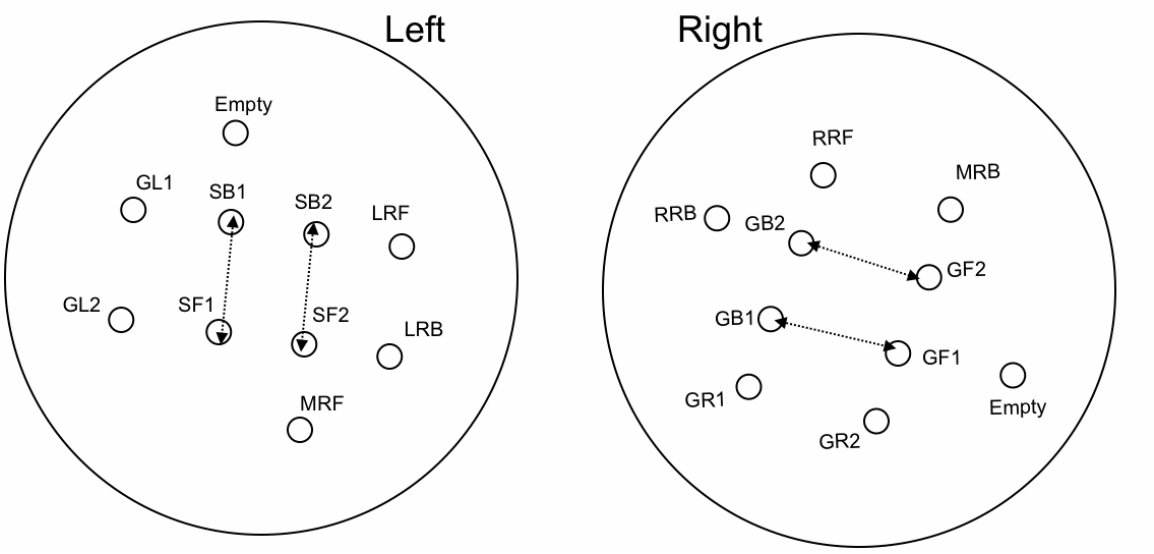

Figure 21 - Test points BRN, top layer. Normally connected jumpers shown.

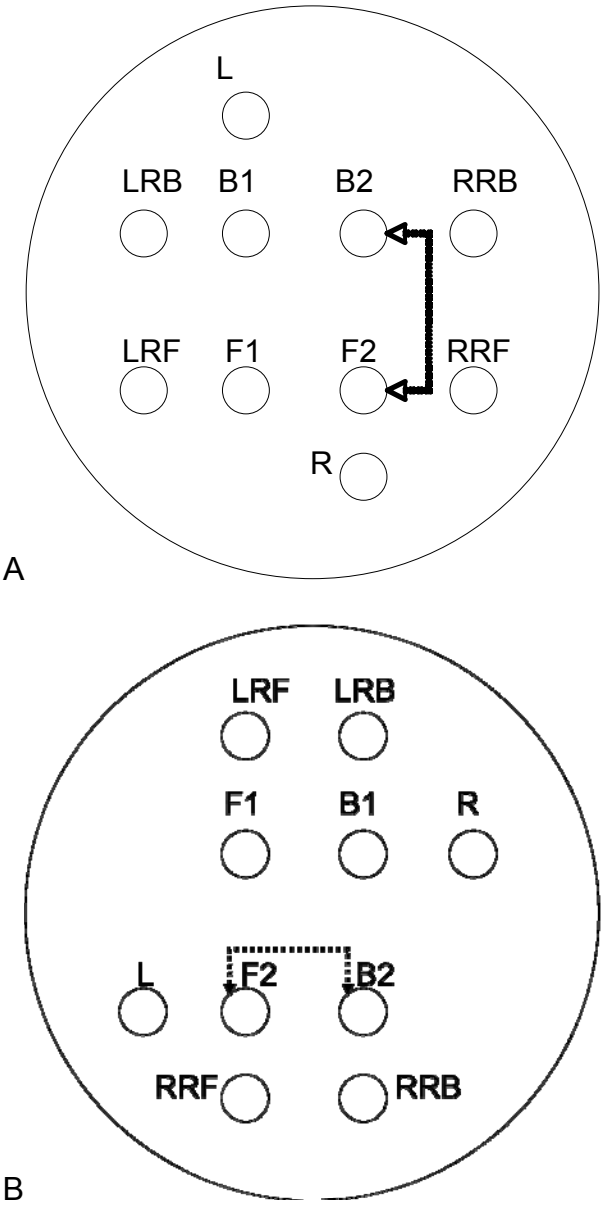

Figure 22 - Test points BRS top (A) and bottom (B) layers. Normally connected jumpers shown.

Site: HFB

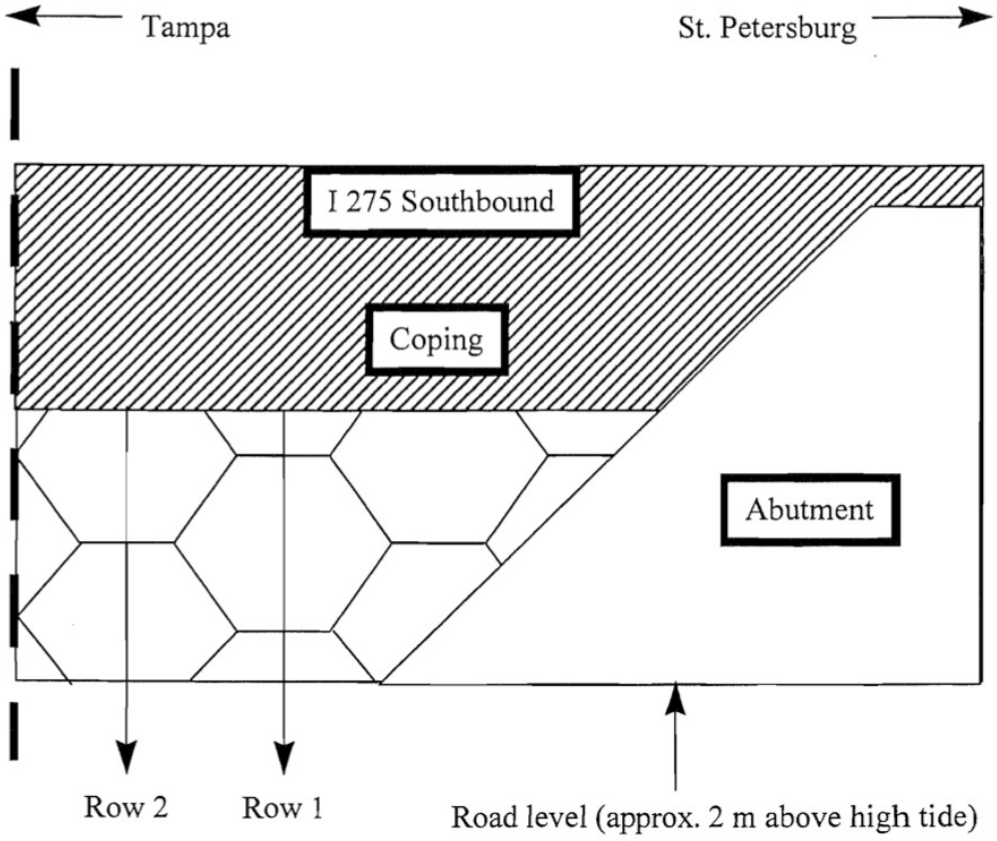

Figure 23 - Elevation view of HFB MSE wall showing panel nomenclature [15].

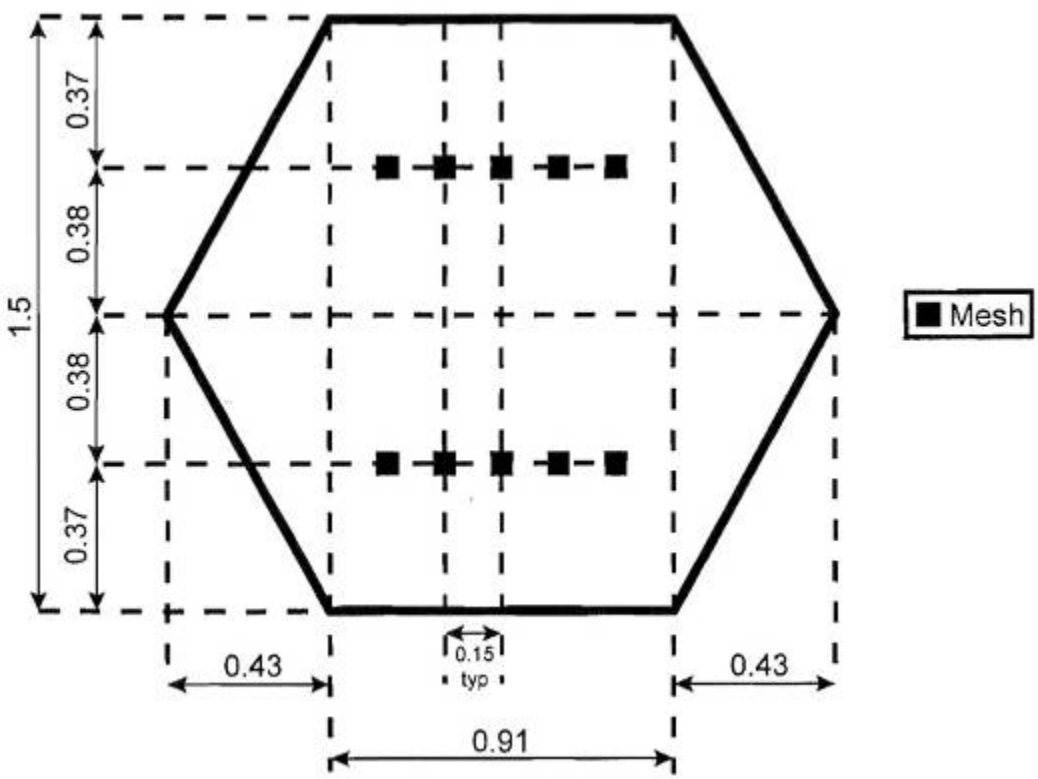

Figure 24 - Dimensions of typical concrete panels and tie strip locations for the HFB site. All dimensions are in meters [15].

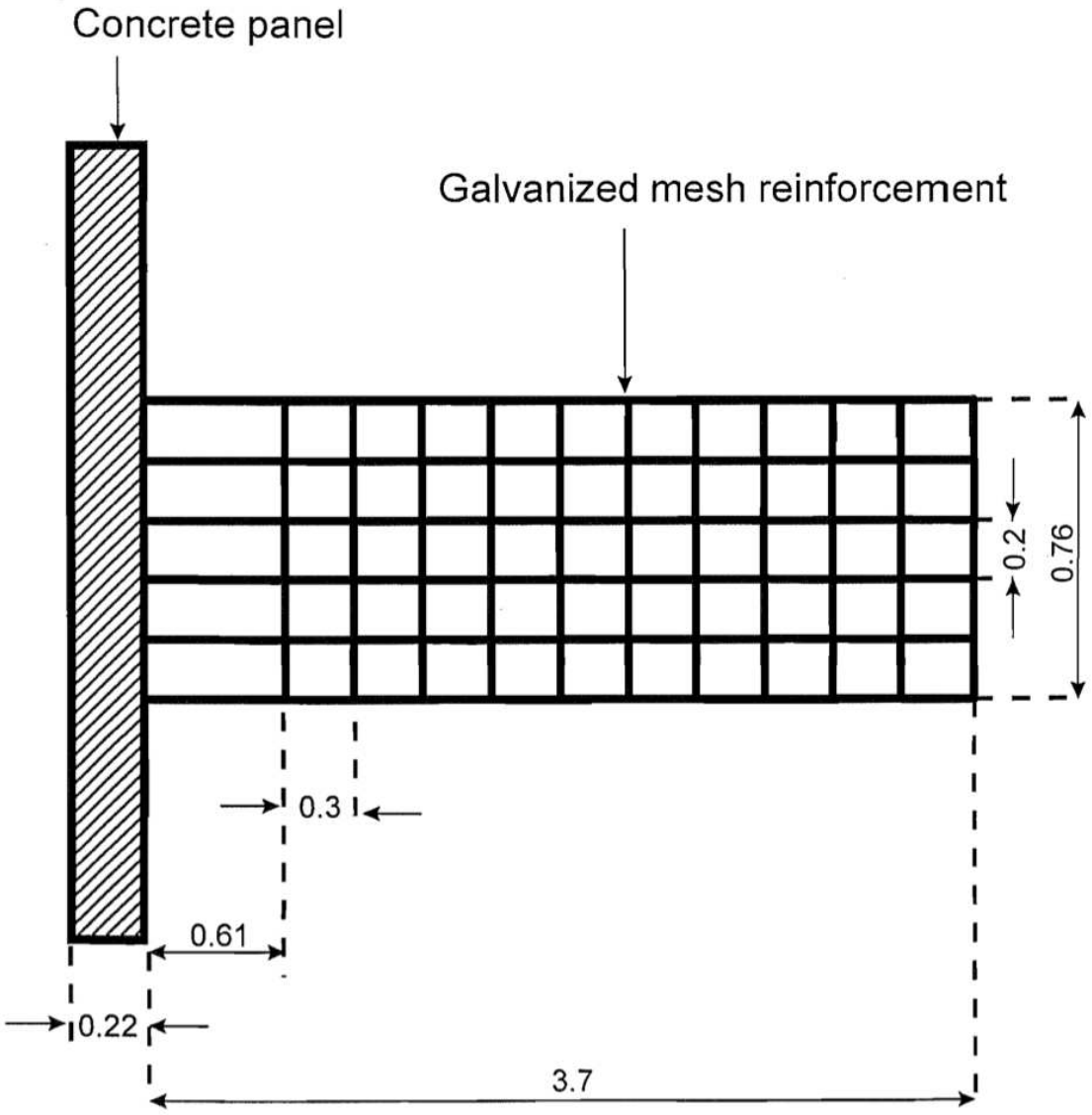

Figure 25 - Top view of a mesh and panel at HFB. All dimensions are in meters and not to scale [15].

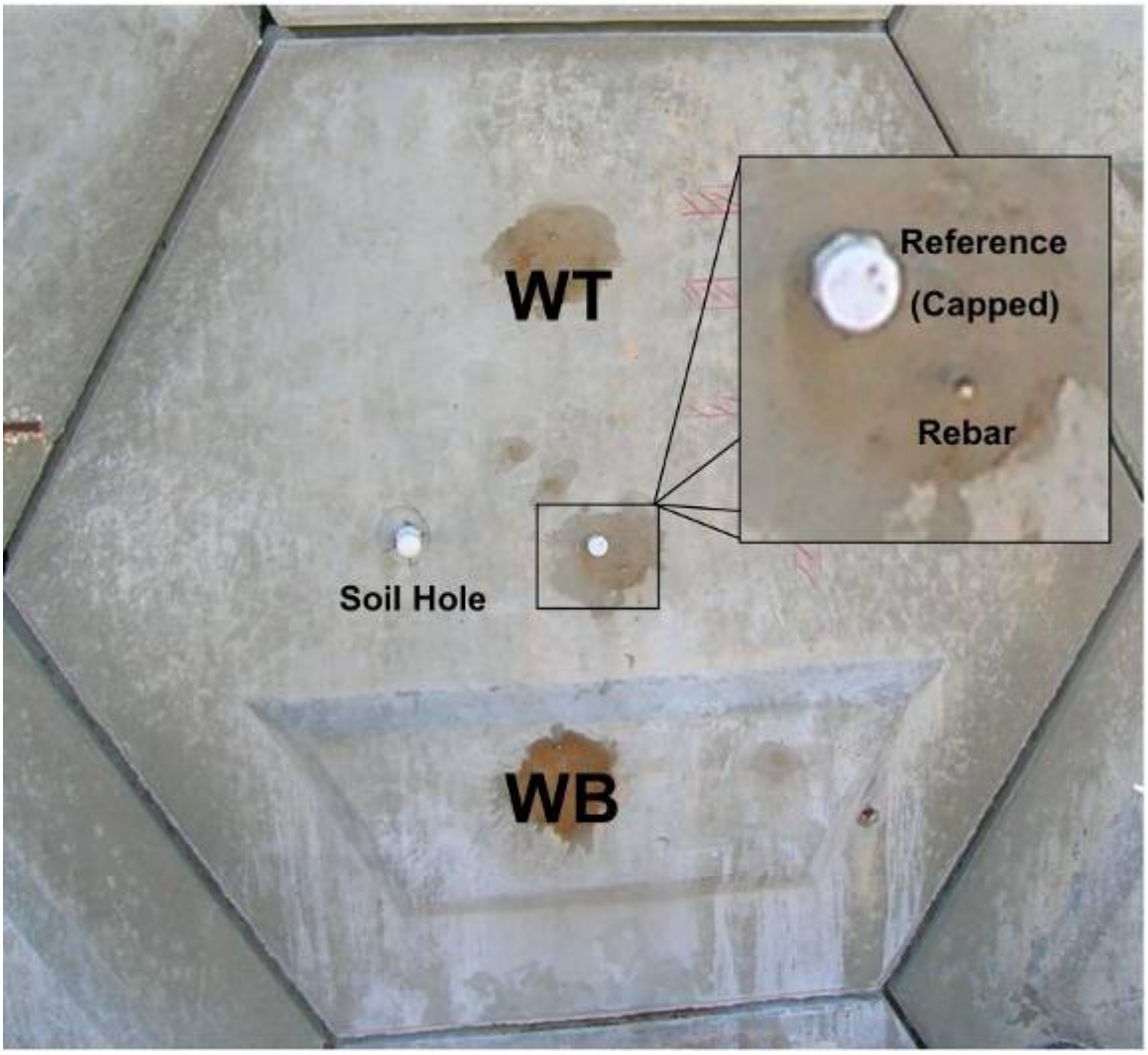

Figure 26 - Panel layout for HFB panels R7, R9, R15, and R21. Panel R9 is shown in this figure. Panels R7 and R15 do not have PVC caps over their reference electrode covers. WT and WB refer to the top and bottom mesh connectors respectively.

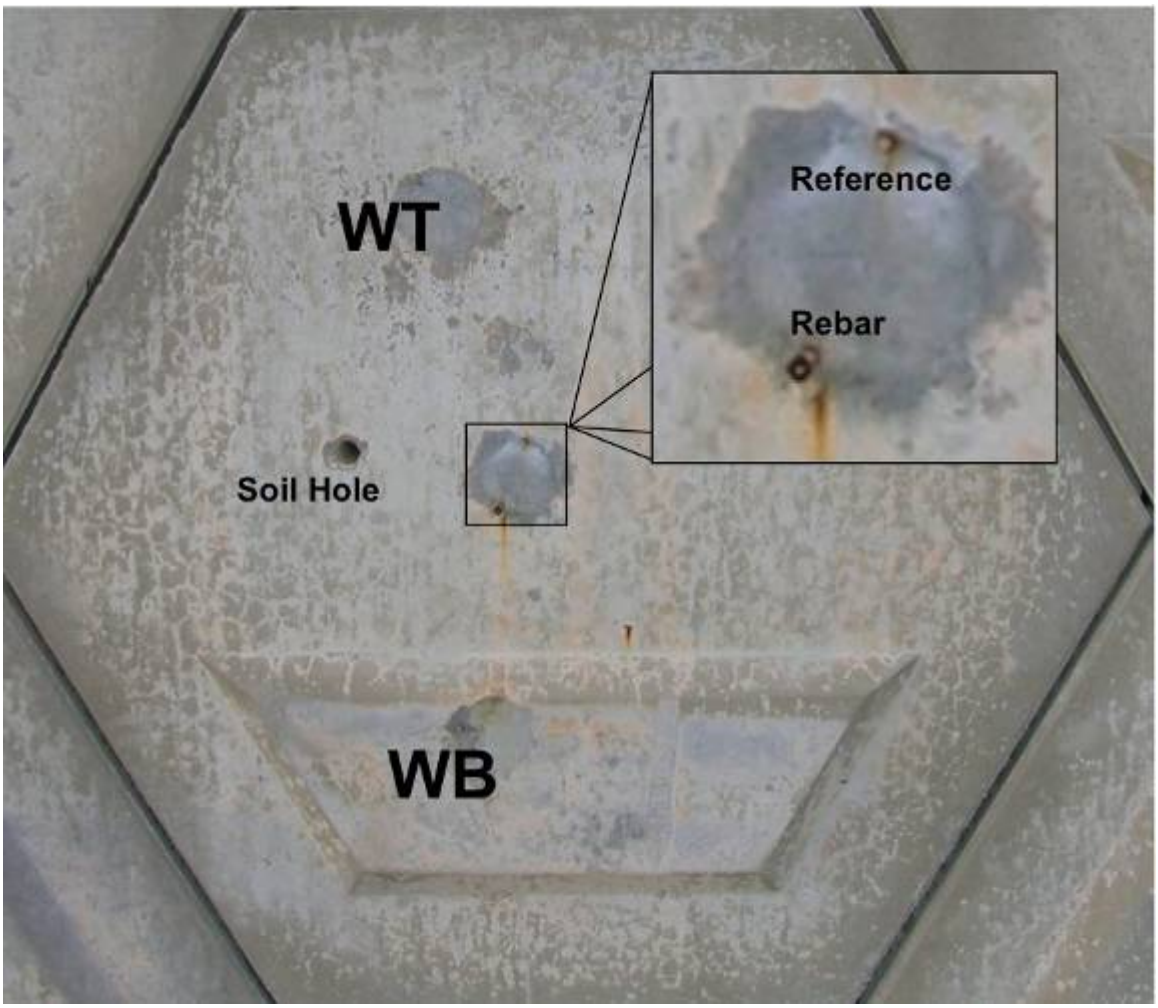

Figure 27 - Panel layout for HFB panel R11. WT and WB refer to the top and bottom mesh connectors respectively.

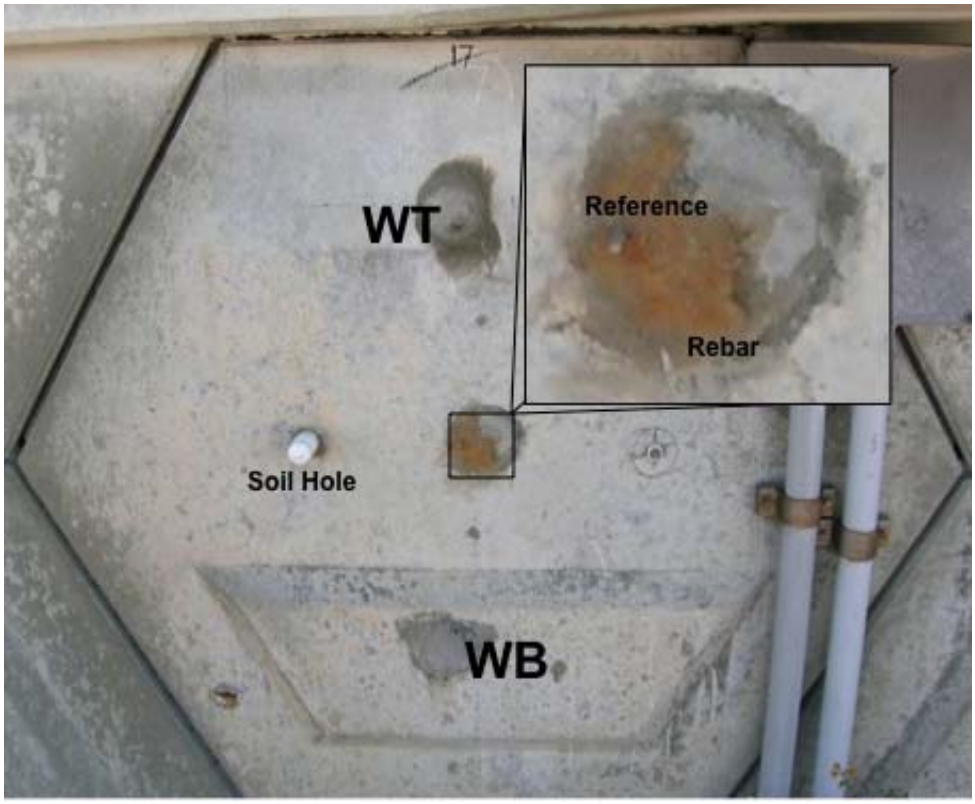

Figure 28 - Panel layout for HFB panel R17. WT and WB refer to the top and bottom mesh connectors respectively.

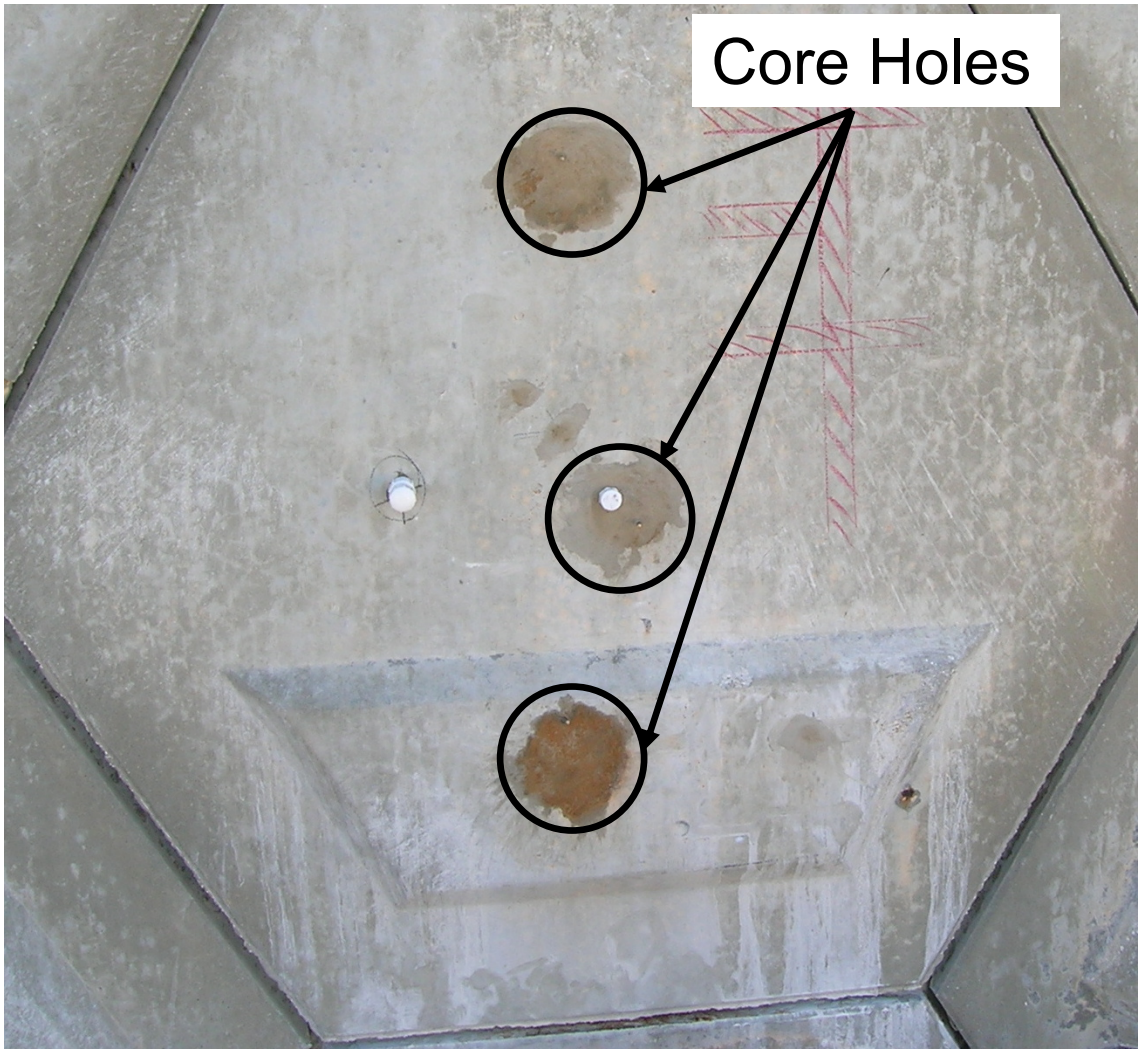

Figure 29 - Core hole locations in HFB panel R9. Soil samples were extracted from each hole. Metal reinforcement coupons (a piece of mesh and the connector hook) were only removed from the top hole.

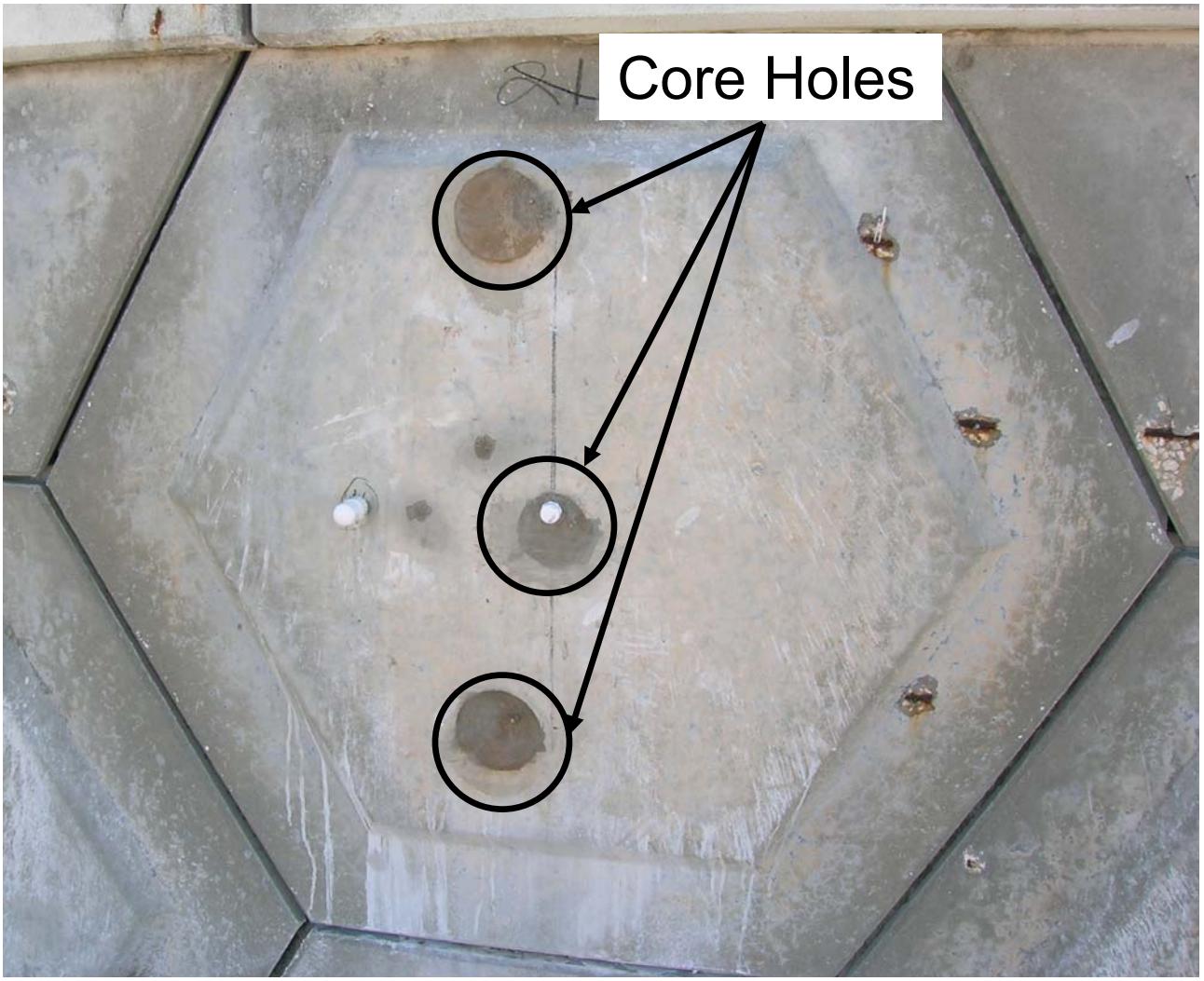

Figure 30 - Core hole locations in HFB panel R21. Metal reinforcement coupons were only removed from the top and bottom holes. Small spalls, caused by panel concrete reinforcing steel corrosion at points of low concrete cover, are visible.

Appendix 1: Site Instrumentation Diagrams (Continued)

Site: PC

PCE Wall

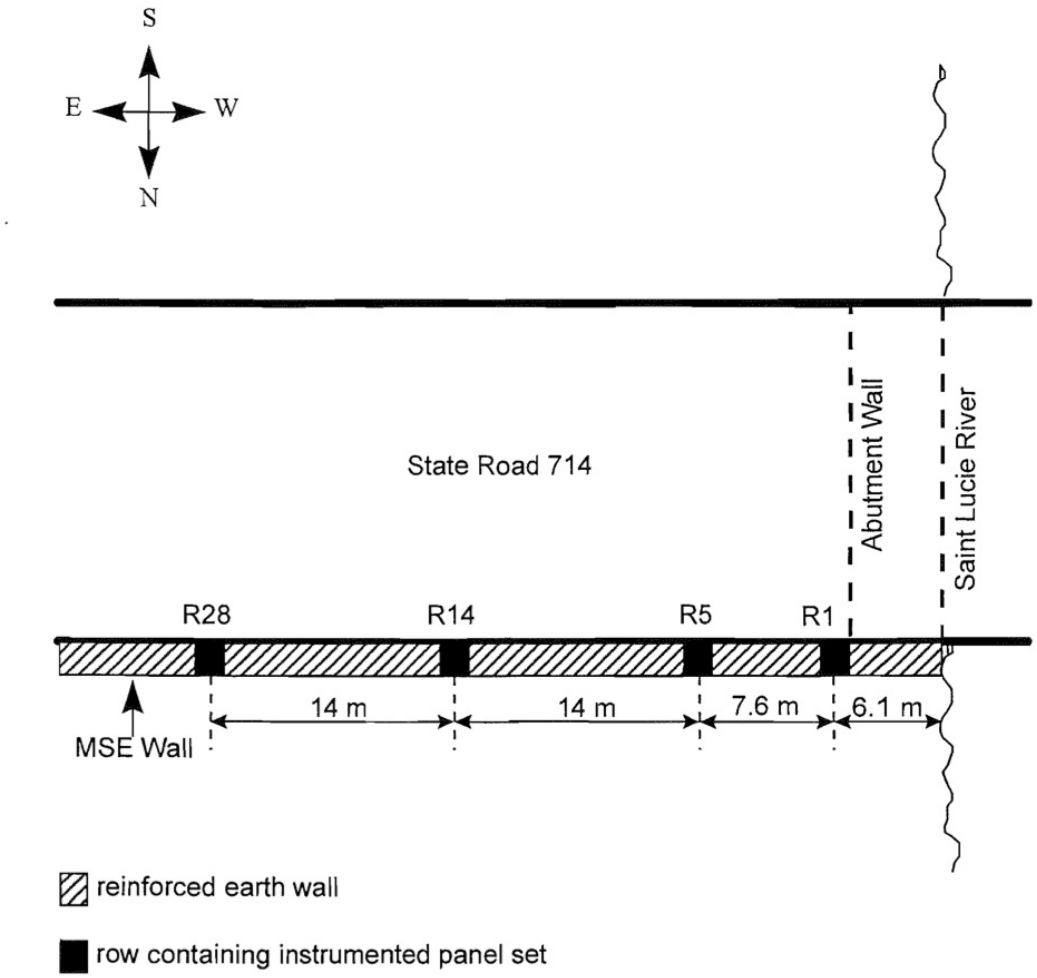

Figure 31 - Plan view of PCE showing panels with instrument clusters. Dimensions are not to scale [15].

Appendix 1: Site Instrumentation Diagrams (Continued)

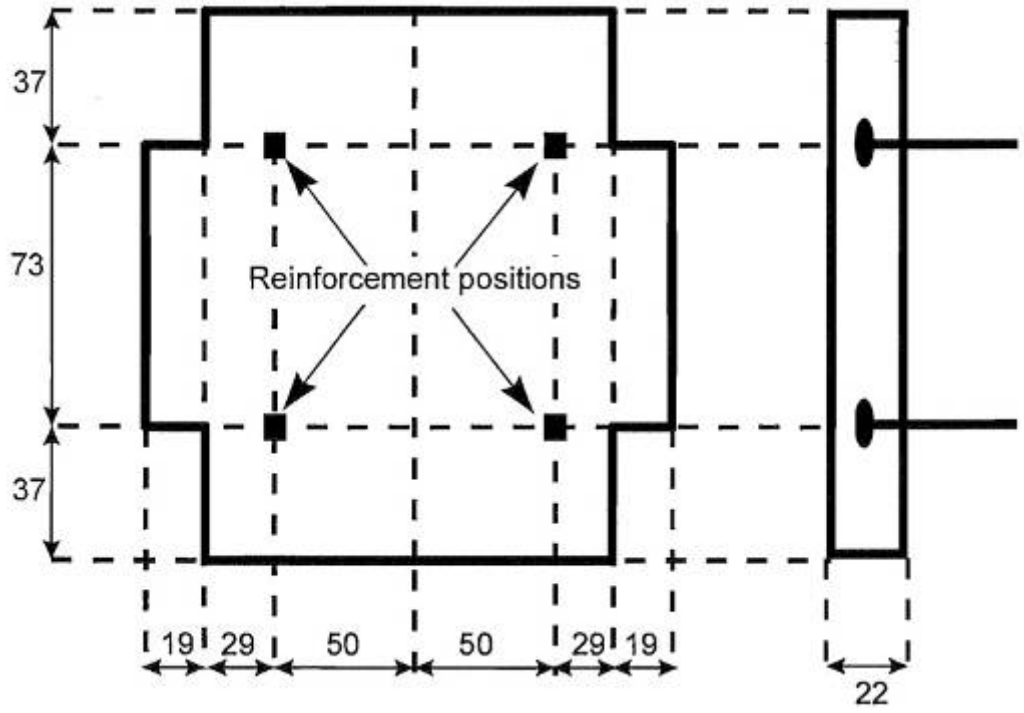

Figure 32 - Dimensions of typical concrete panels and tie strip locations for PCE. All dimensions are in meters [15].

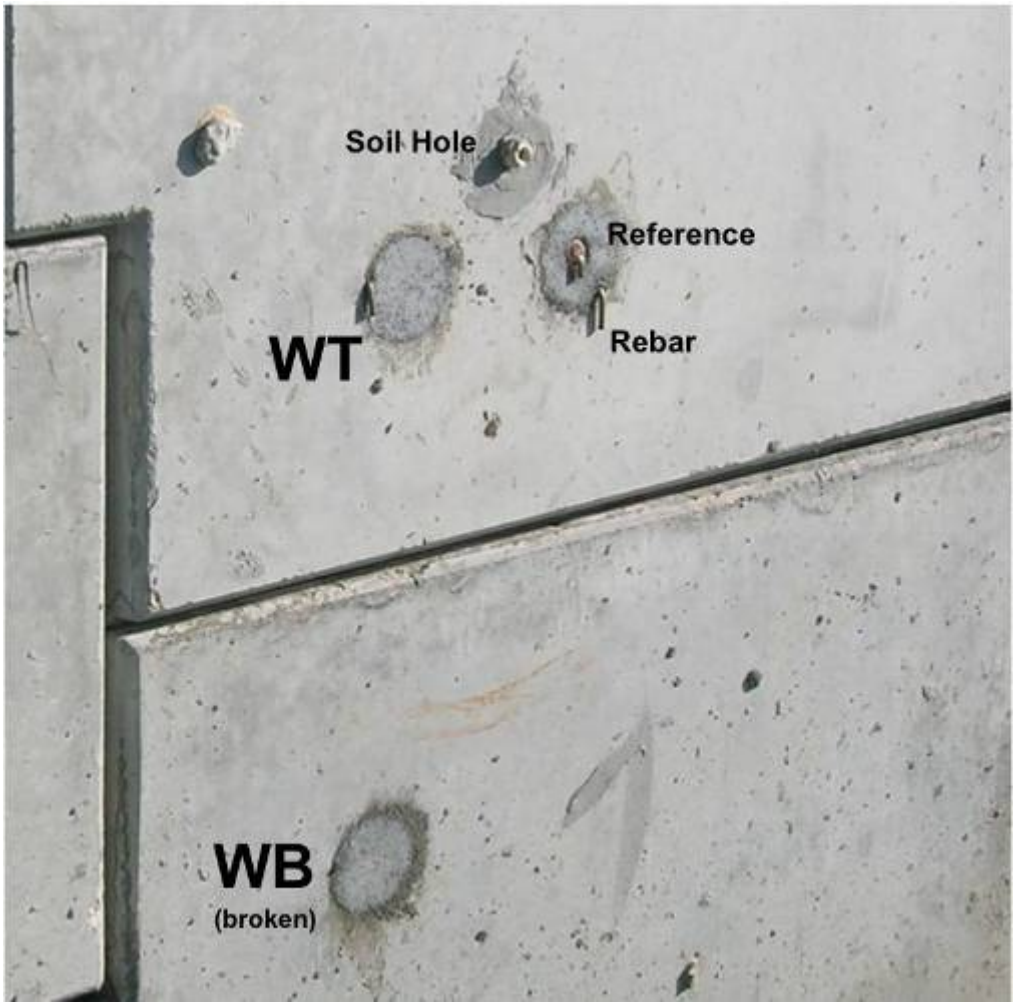

Figure 33 - Panel layout for panel R1 at PCE. WT and WB refer to the top and bottom strip connectors respectively.

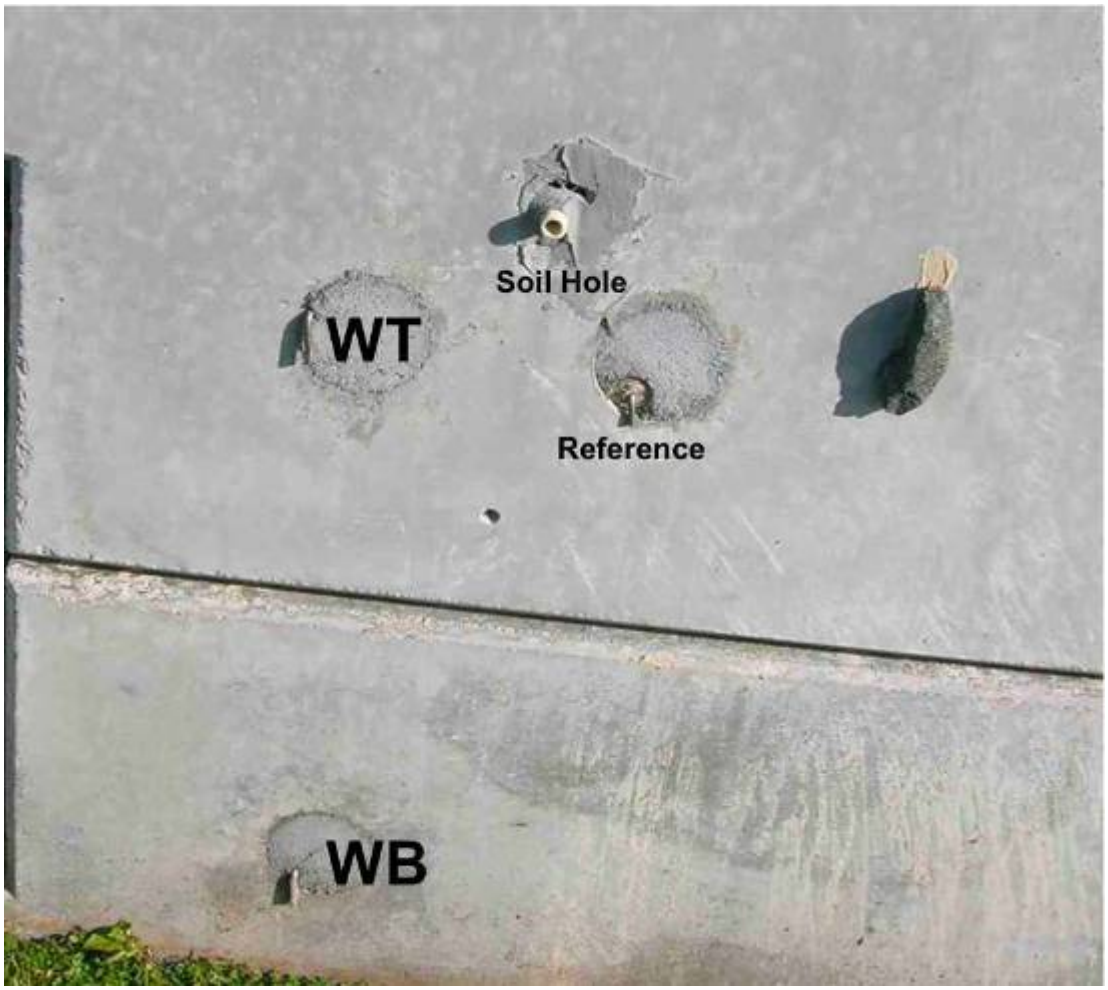

Figure 34 - Panel layout for panel R5 at PCE. WT and WB refer to the top and bottom strip connectors respectively.

Appendix 1: Site Instrumentation Diagrams (Continued)

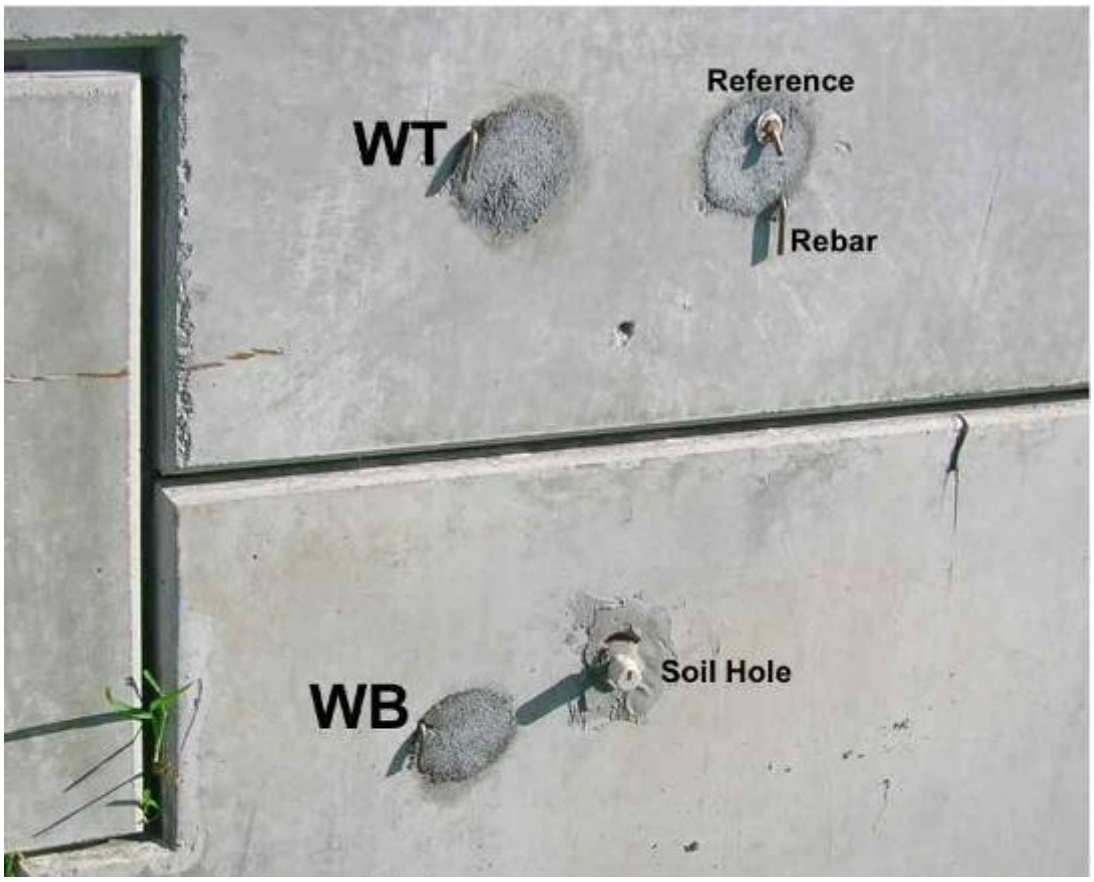

Figure 35 - Panel layout for panel R14 at PCE. WT and WB refer to the top and bottom strip connectors respectively.

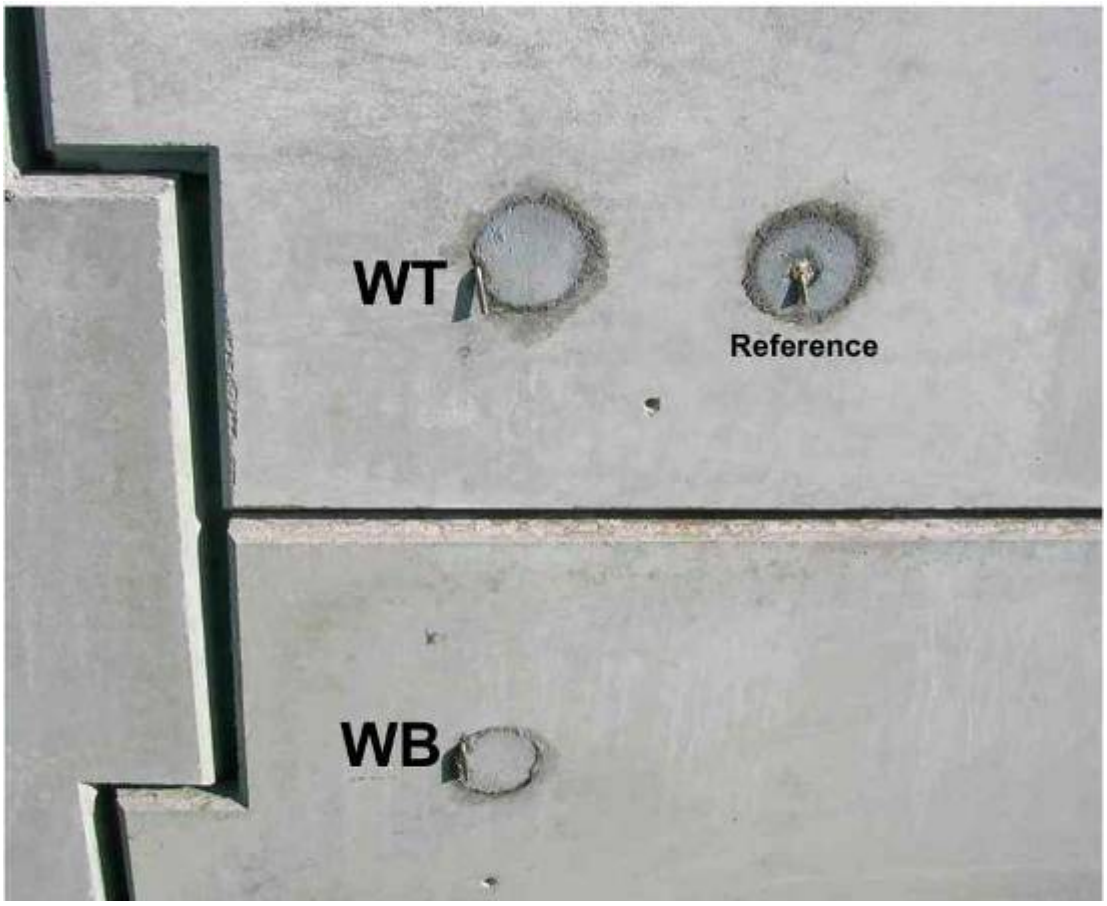

Figure 36 - Panel layout for panel R28 at the Stuart NE site. WT and WB refer to the top and bottom strip connectors respectively.

Appendix 1: Site Instrumentation Diagrams (Continued)

PCW Wall

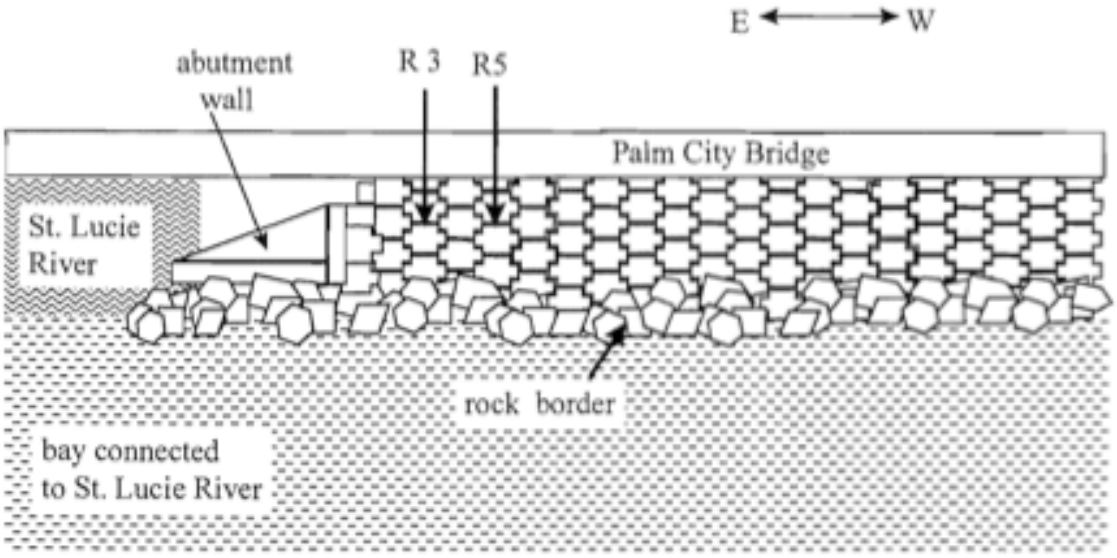

Figure 37 - Diagram indicating the location of the panels R3W and R5W PCW [15].

Appendix 1: Site Instrumentation Diagrams (Continued)

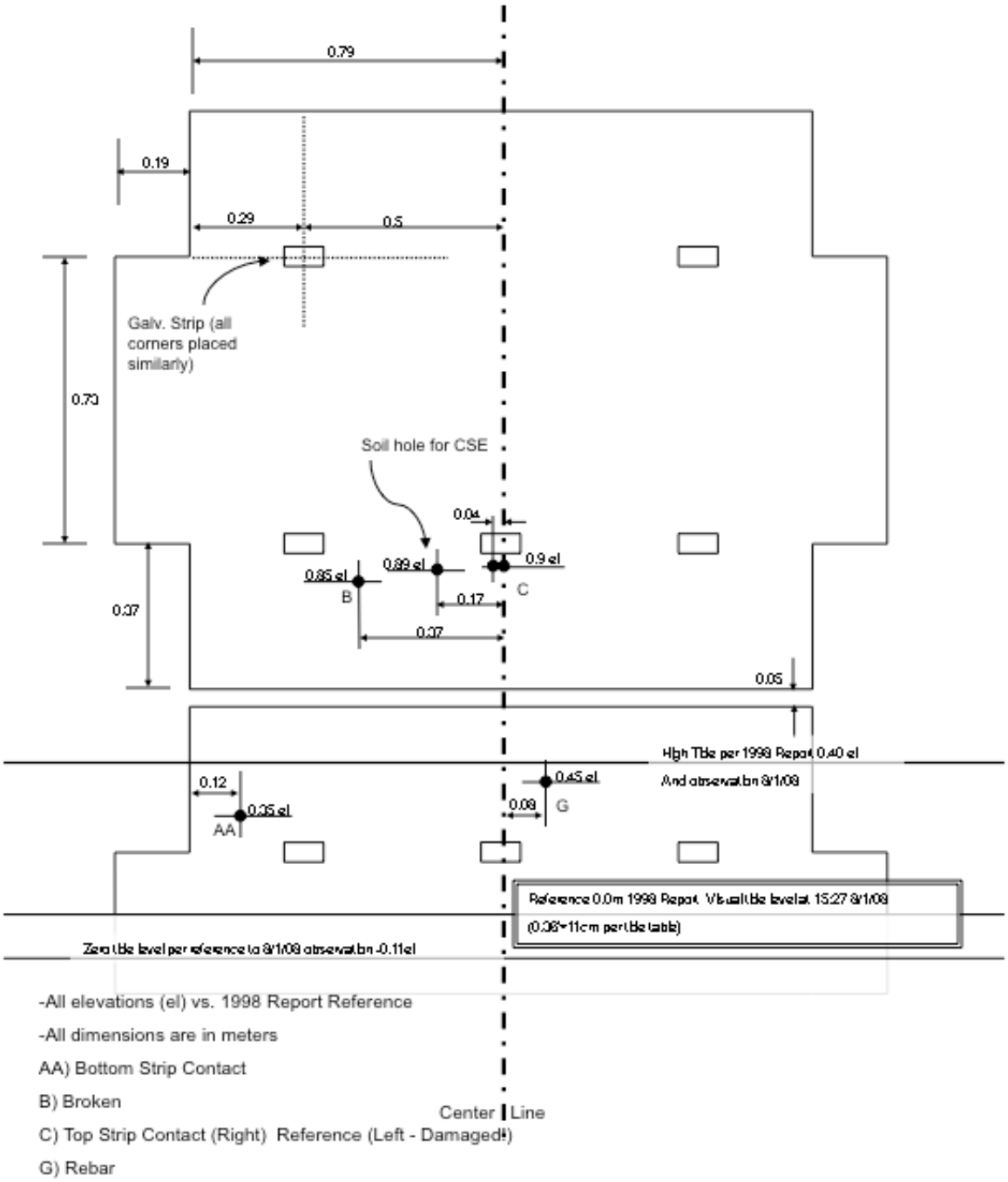

Figure 38 - Detailed panel information for panel R3W at PCW.

Appendix 1: Site Instrumentation Diagrams (Continued)

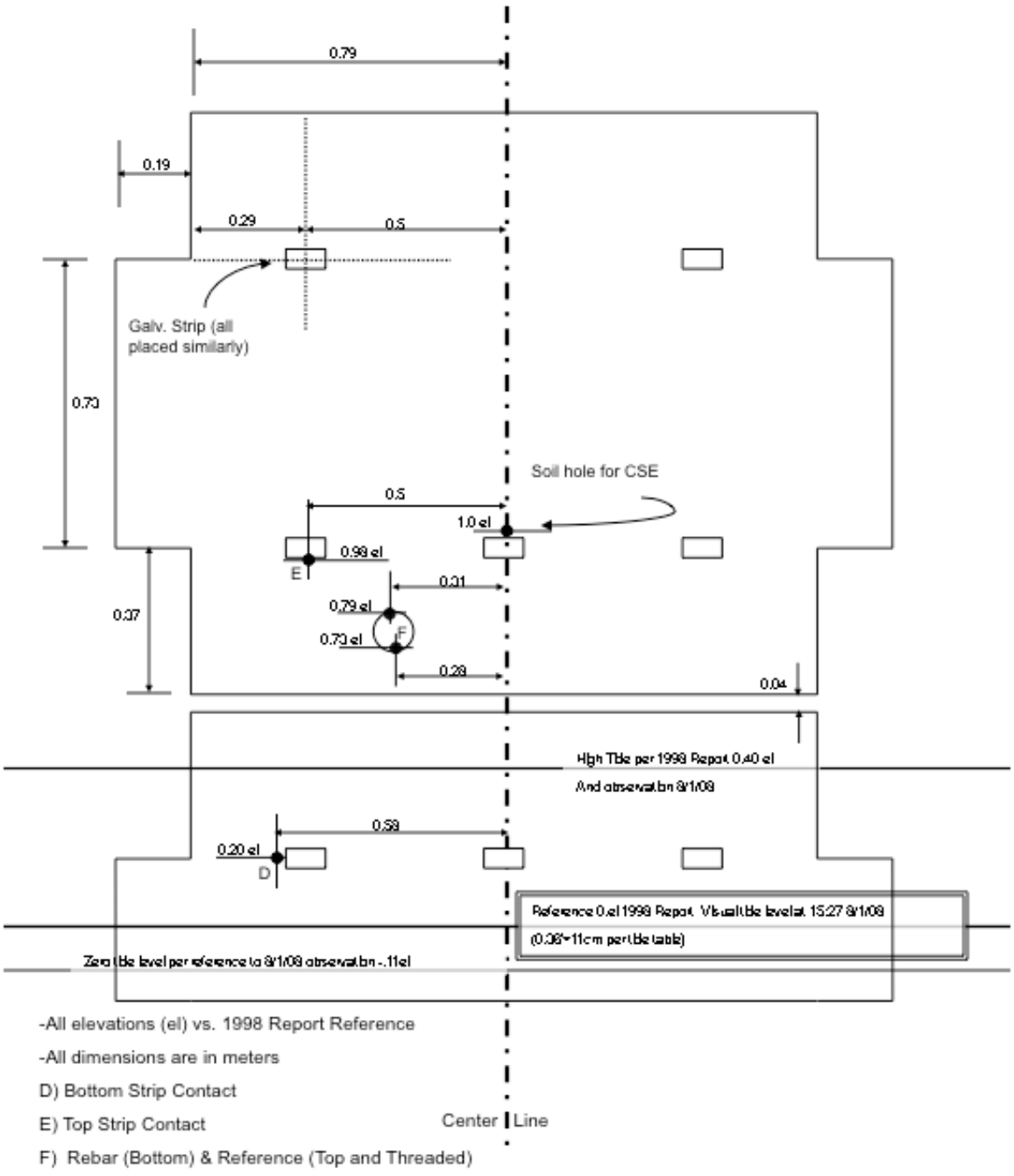

Figure 39 - Detailed panel information for panel R5W at PCW.

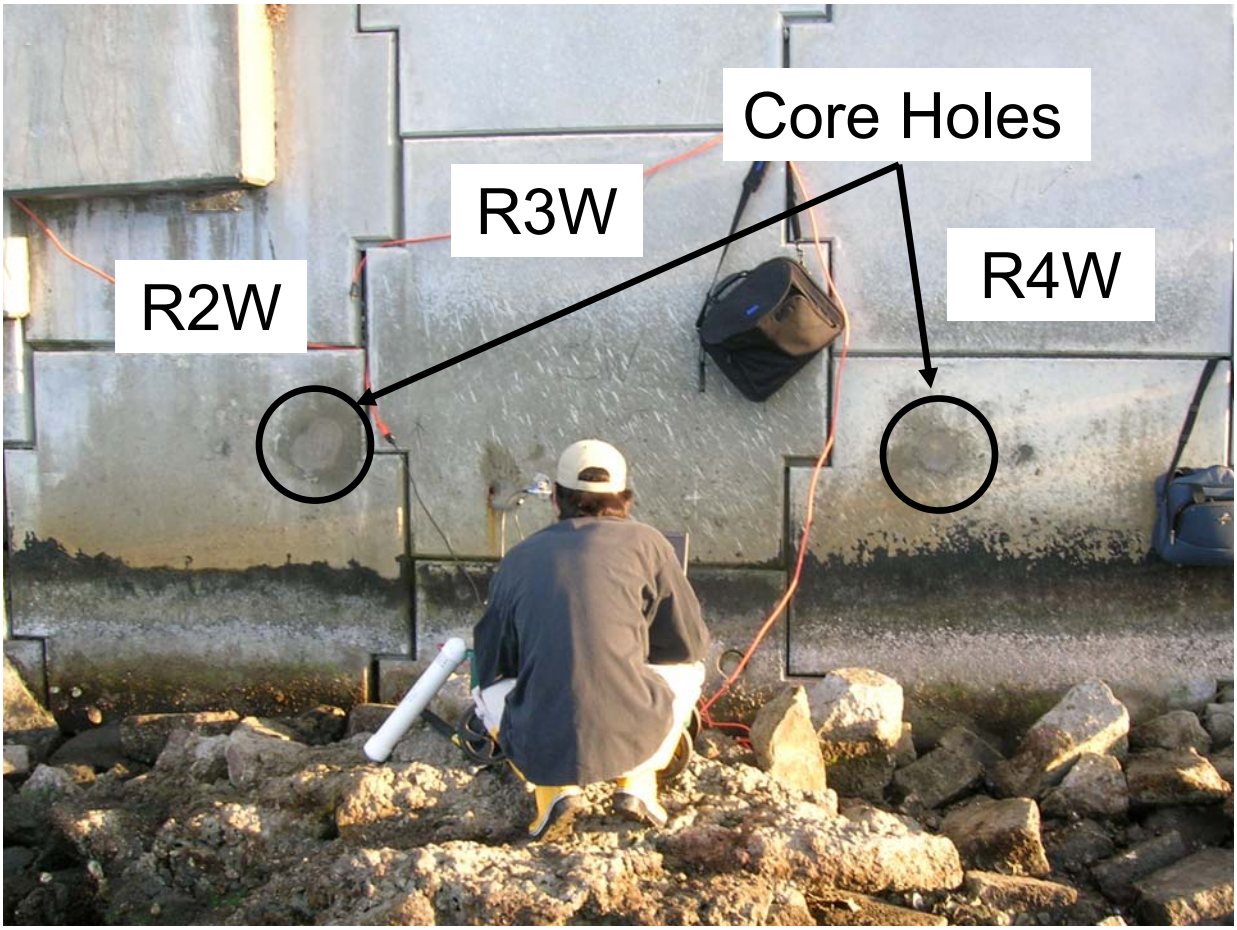

Figure 40 - Location of additional core holes at PCW. Soil samples and metal reinforcement coupons were removed from each hole in panels R2W and R4W.

Site: PSL

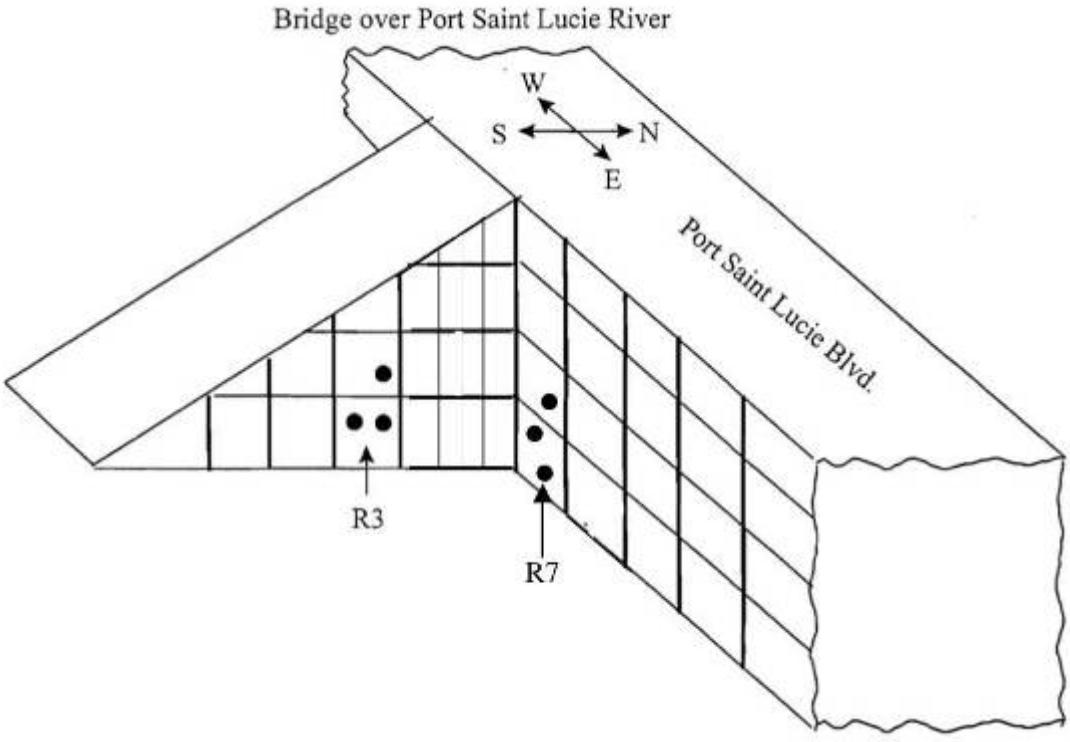

Figure 41 - View of relative panel locations at PSL. This figure is revised from the report for the 1994-98 survey to show correct cluster locations [15].

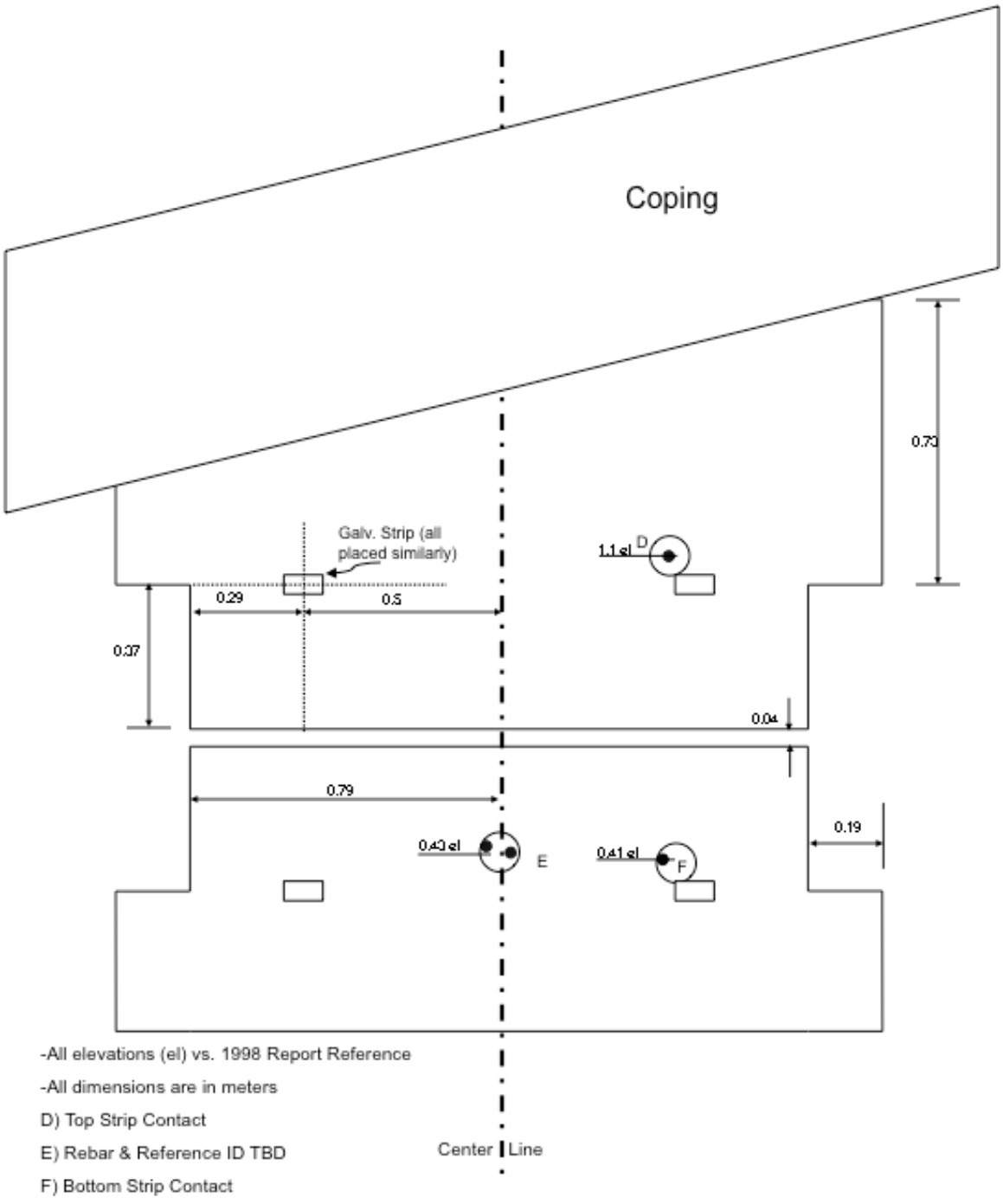

Figure 42 - Detailed panel information for panel 3 at PSL.

Appendix 1: Site Instrumentation Diagrams (Continued)

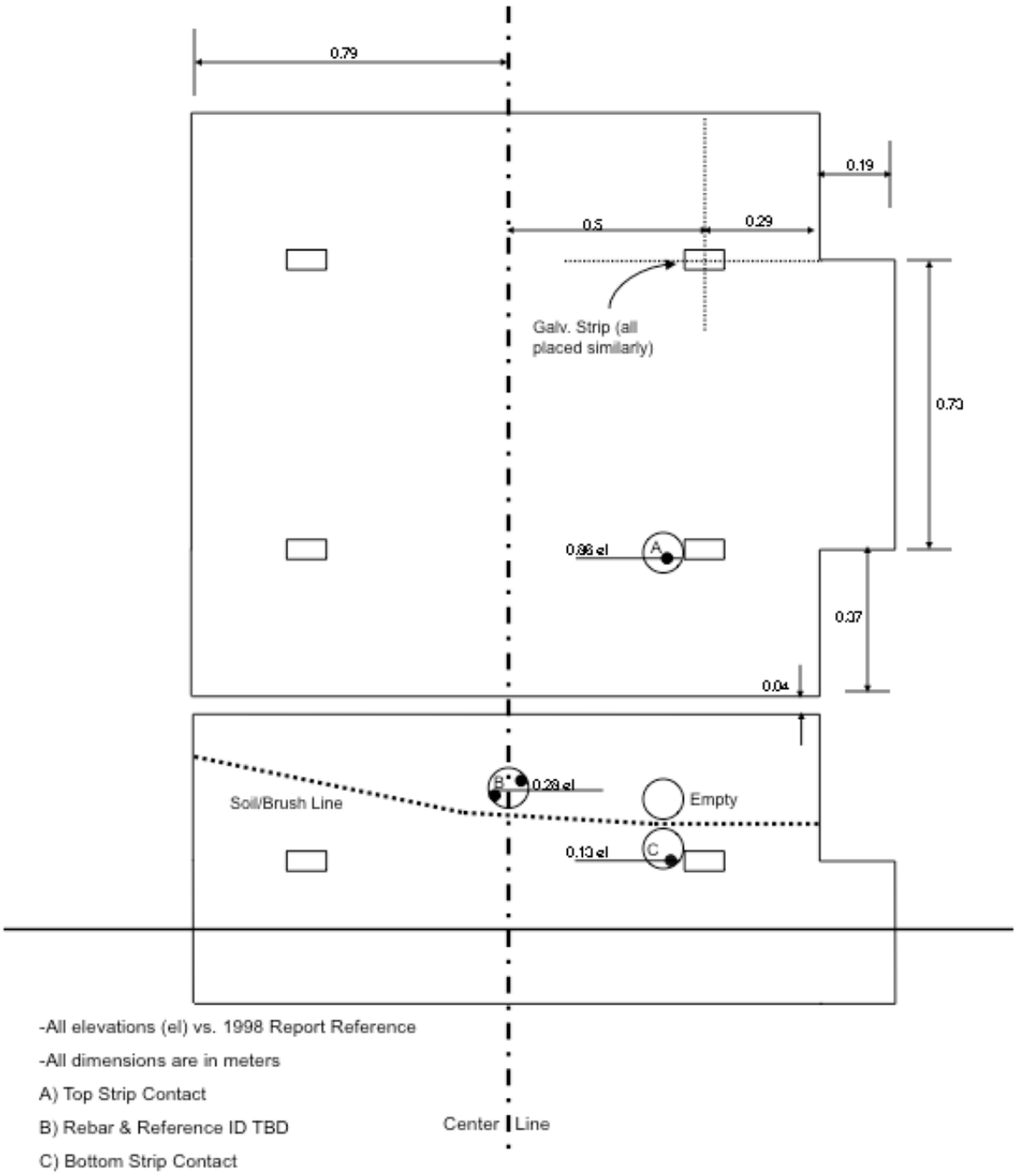

Figure 43 - Detailed panel information for panel 7 at PSL.

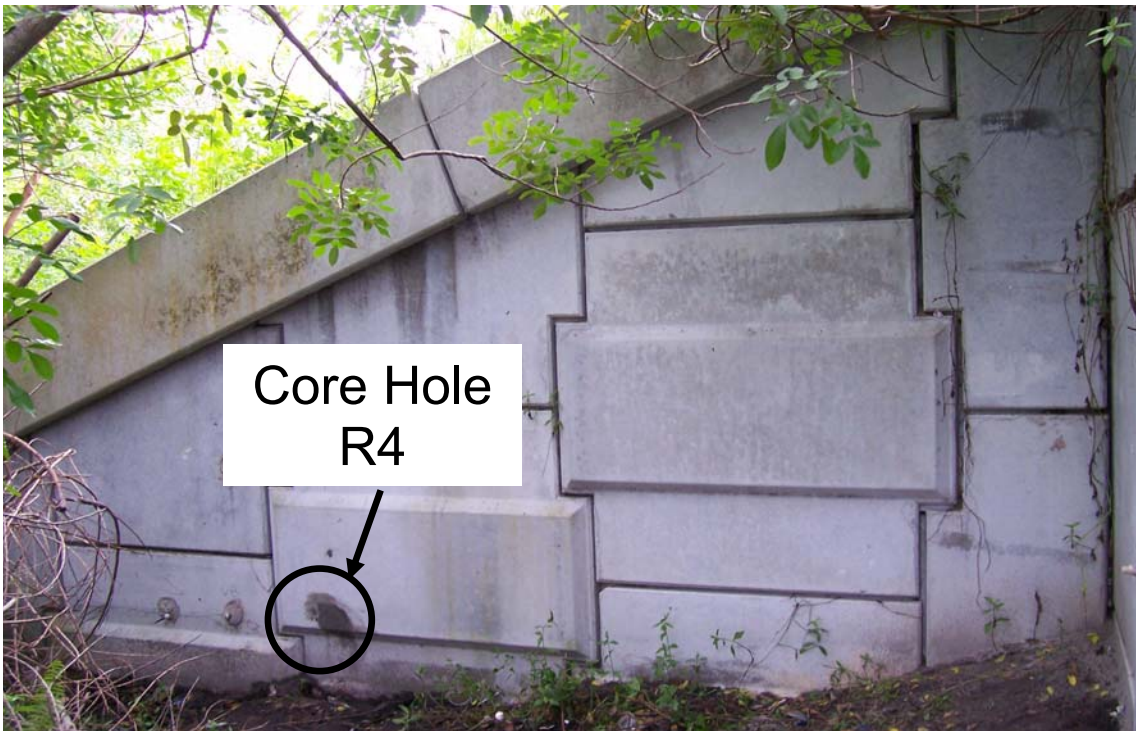

Figure 44 - Additional core hole at PSL panel R4, from which a soil sample was extracted.

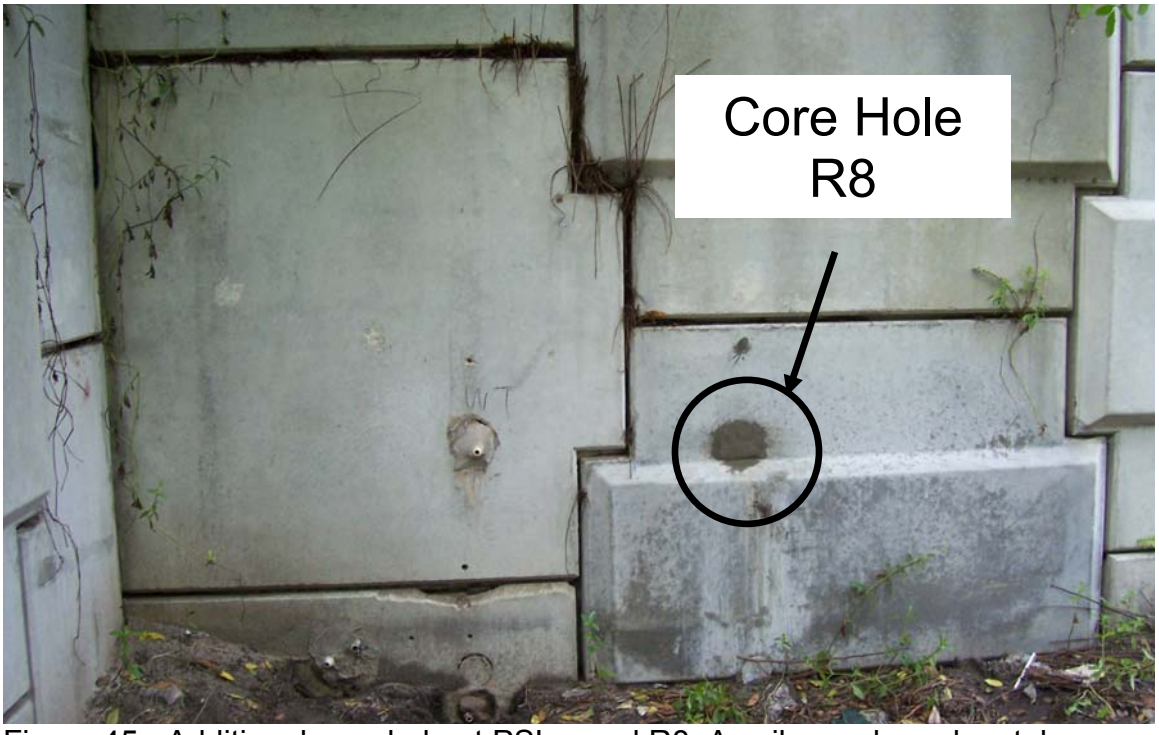

Figure 45 - Additional core hole at PSL panel R8. A soil sample and metal reinforcement coupon were removed.

Site: OCA

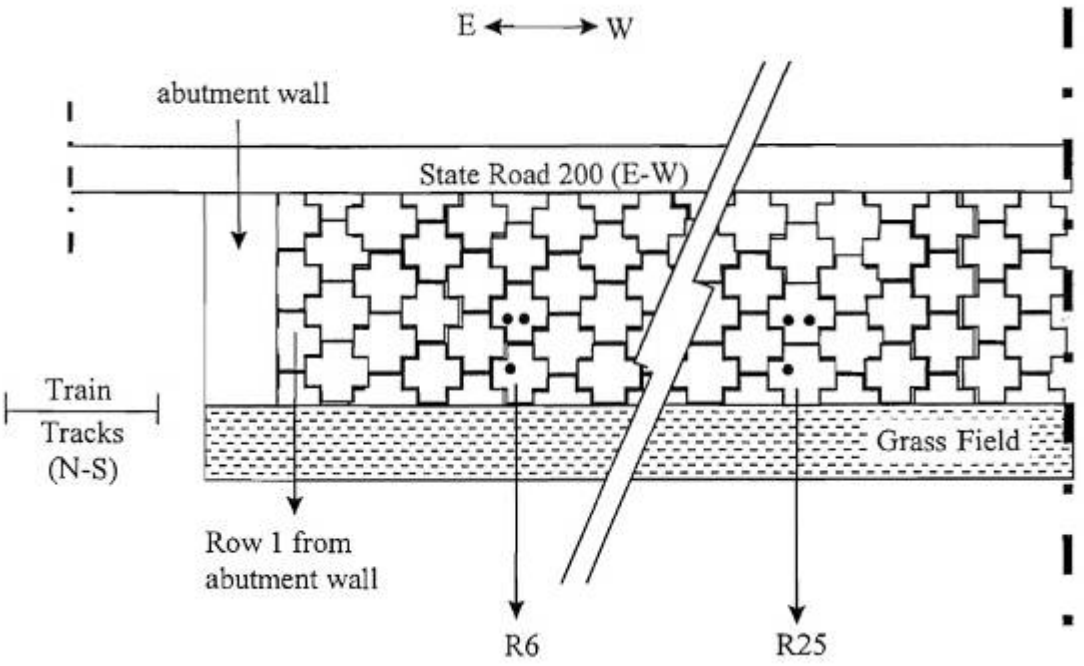

Figure 46 - Diagram indicating the location of the panels R6 and R25 at OCA [15].

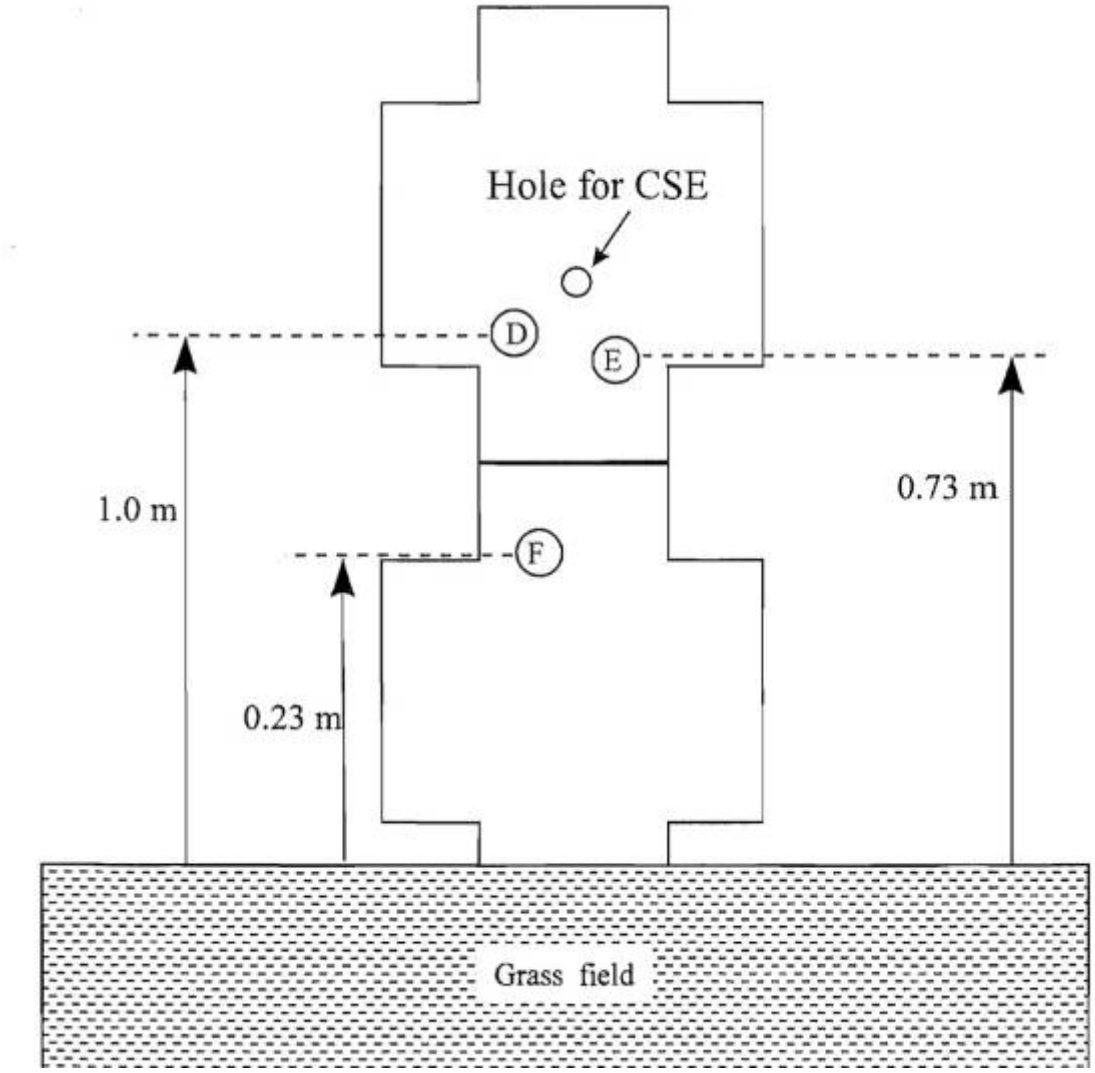

Figure 47 - Panel layout for Panel 6 at OCA. D corresponds to the top galvanized strip, E to the steel rebar and reference electrode (the reference electrode is identified on site by a green cable) and F corresponds to the bottom galvanized strip [15].

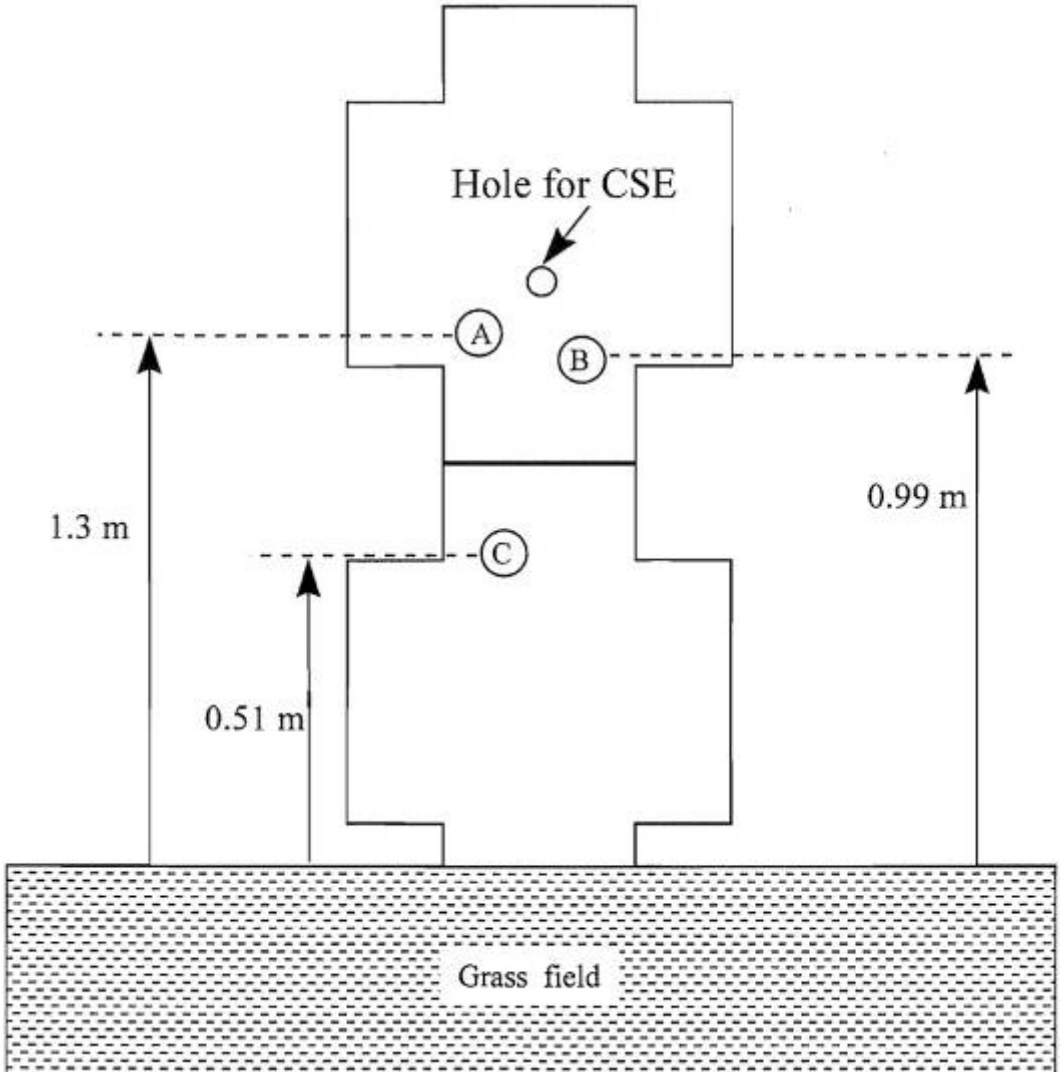

Figure 48 - Panel layout for Panel 25 at OCA. A corresponds to the top galvanized strip, B to the rebar and reference electrode (the reference electrode is identified on site by a green cable) and C corresponds to the bottom galvanized strip [15].

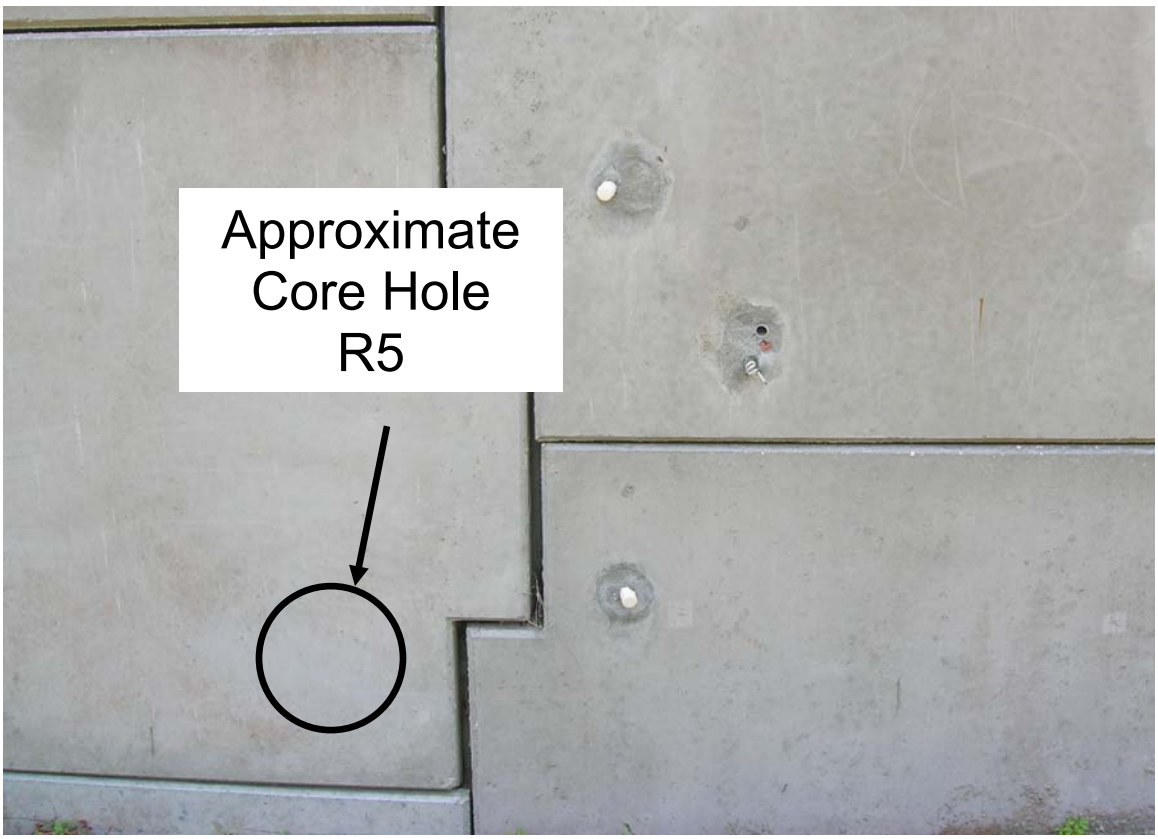

Figure 49 - Approximate location of an additional core hole at OCA panel R5. A soil sample and two metal reinforcement coupons were extracted from that hole.

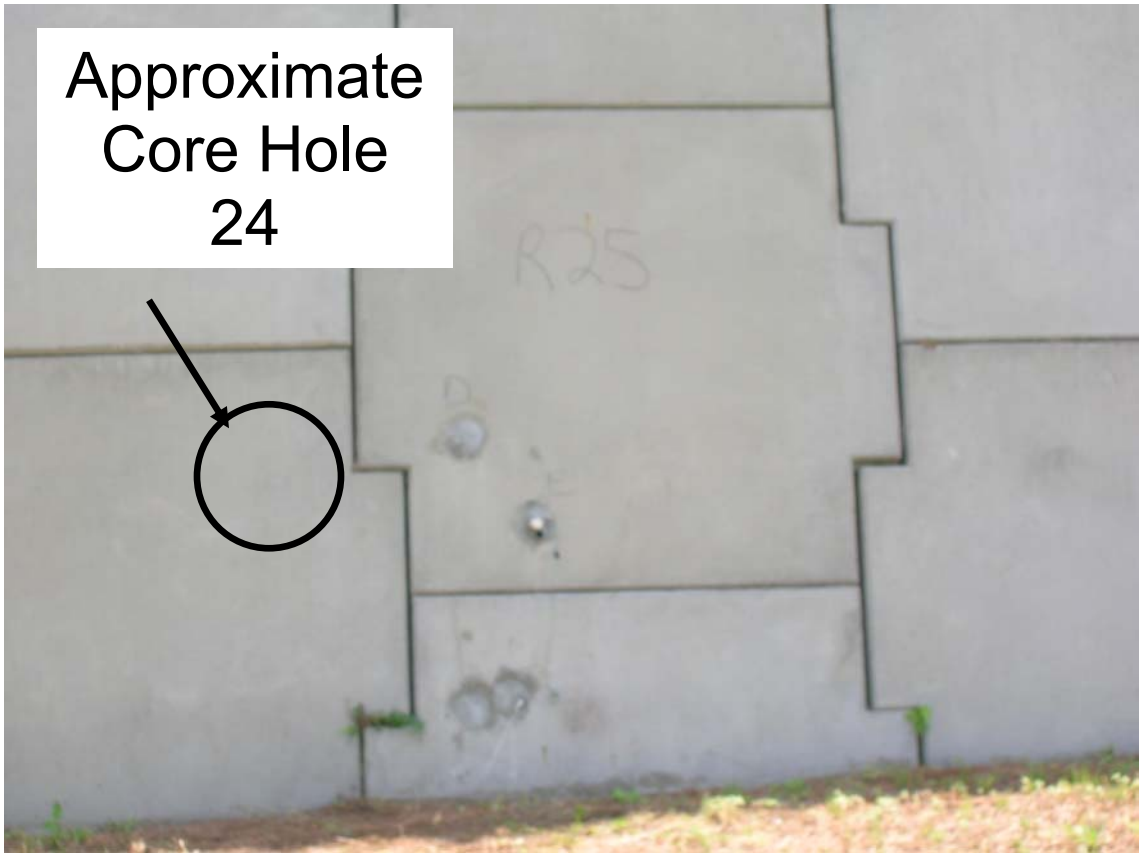

Figure 50 - Approximate location of an additional core hole at OCA panel R24. A soil sample and one metal reinforcement coupon were extracted from that hole.

Appendix 1: Site Instrumentation Diagrams (Continued)

Site: ABJ

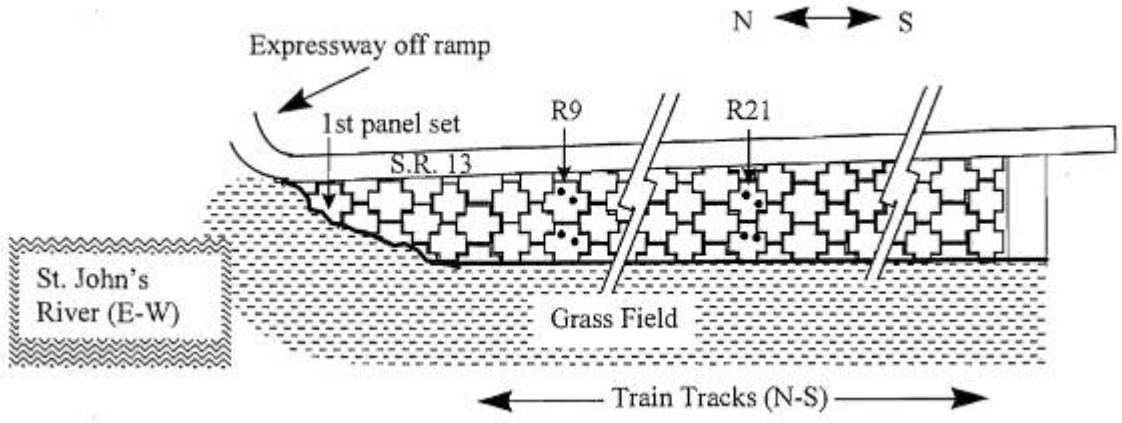

Figure 51 - Diagram indicating the location of the panels R9 and R21 of ABJ [15].

Appendix 1: Site Instrumentation Diagrams (Continued)

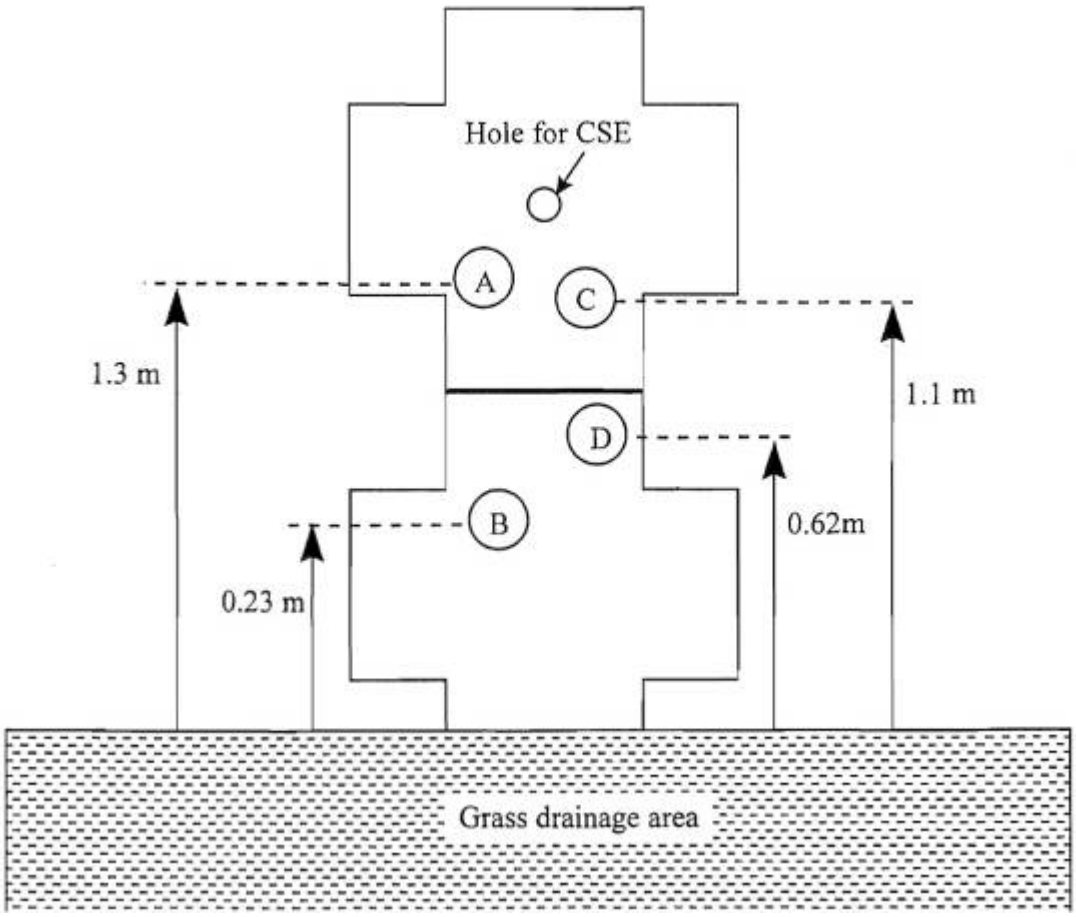

Figure 52 - Panel layout for Panel 9 at ABJ. A represents corresponds to the top galvanized strip, B represents to the bottom galvanized strip, C represents to an added Zn-Al strip, and D represents to the rebar and reference electrode (the reference electrode has is identified on site by a green cable) [15].

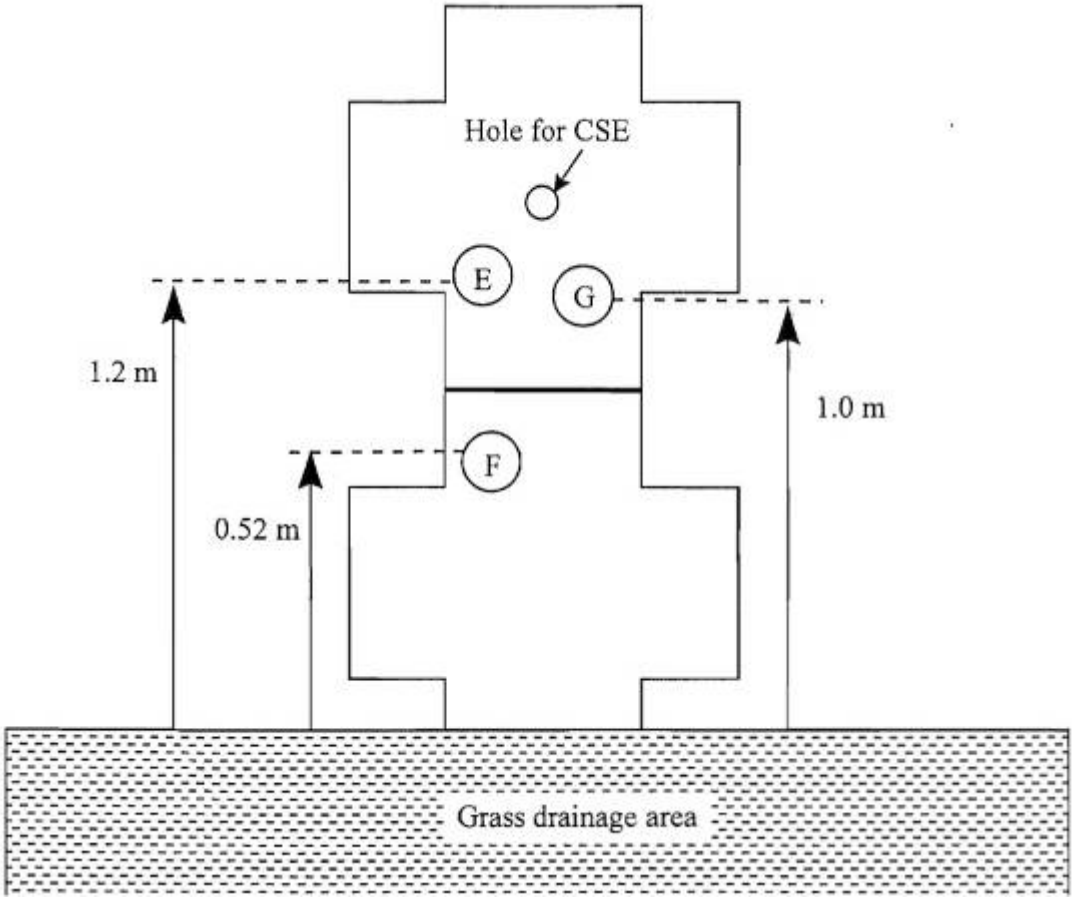

Figure 53 - Panel layout for Panel 21 at ABJ. E represents corresponds to the top galvanized strip, F represents to the bottom galvanized strip, and G represents to the rebar and reference electrode (the reference electrode is identified on site by a green cable) [15].

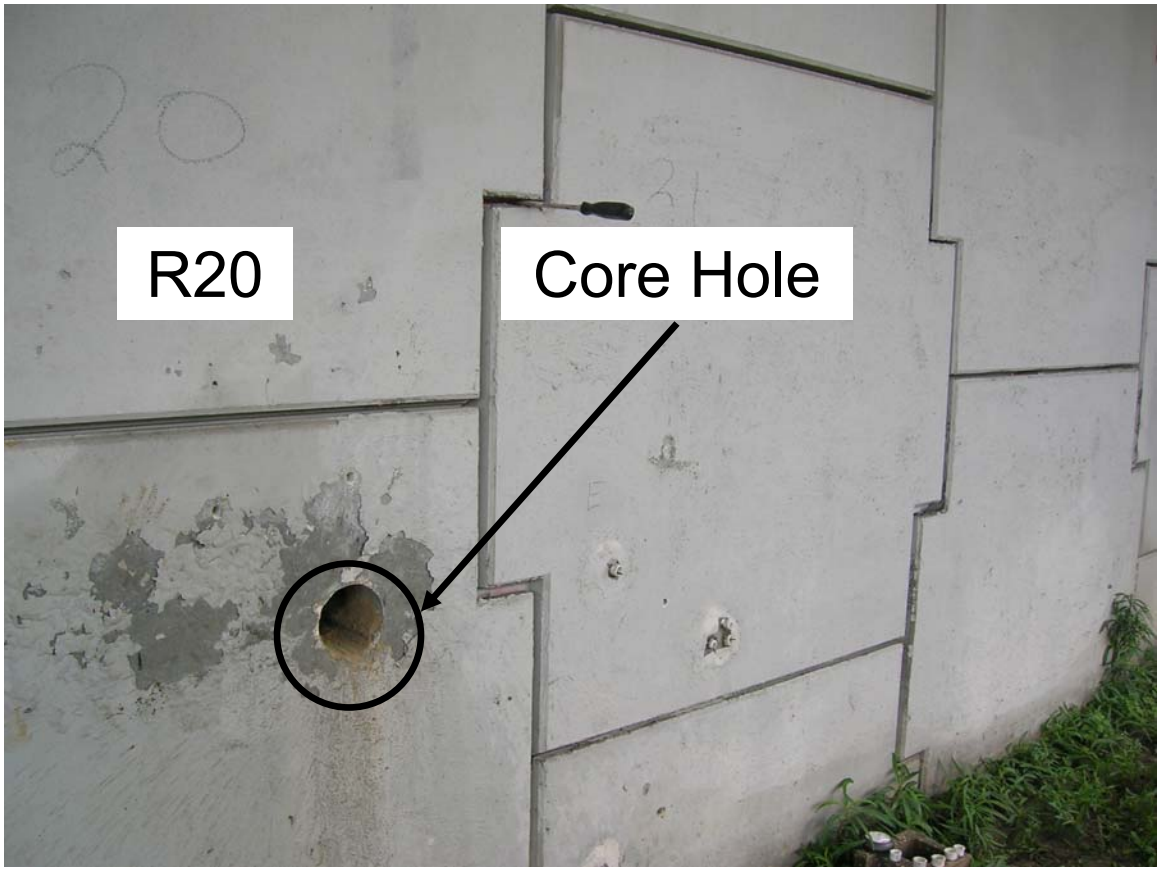

Figure 54 - Additional core hole at ABJ panel R20. A soil sample and metal reinforcement coupon were removed from that hole.

Appendix 1: Site Instrumentation Diagrams (Continued)

Site: VET

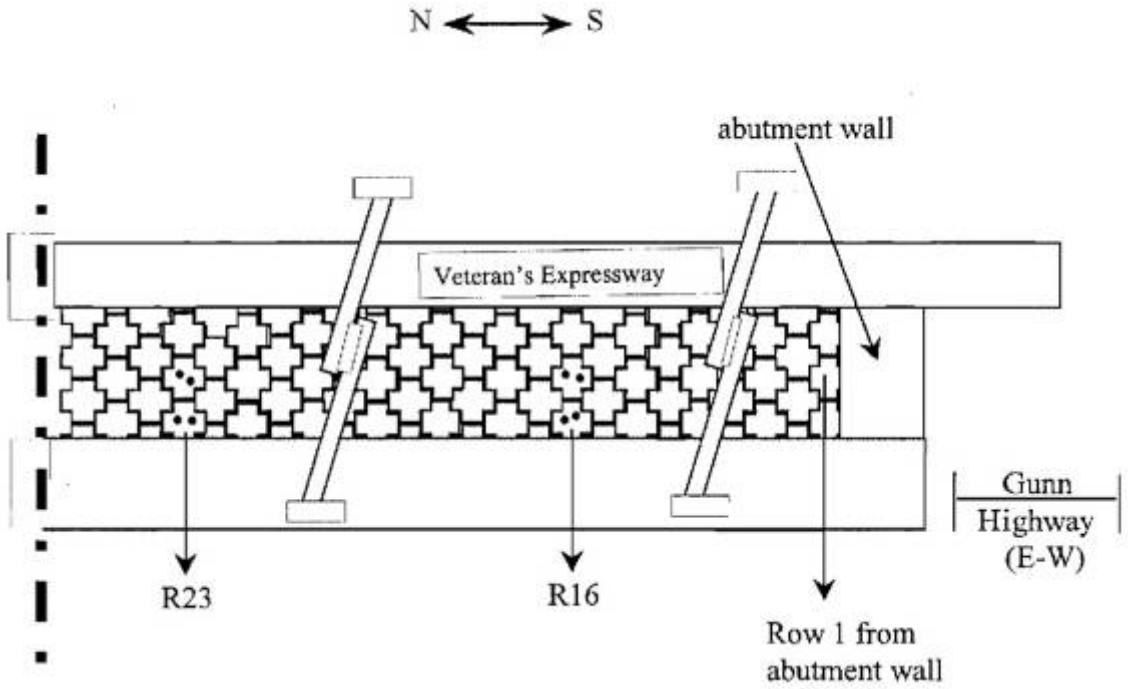

Figure 55 - Diagram indicating the location of the panels R16 and R23 of VET [15].

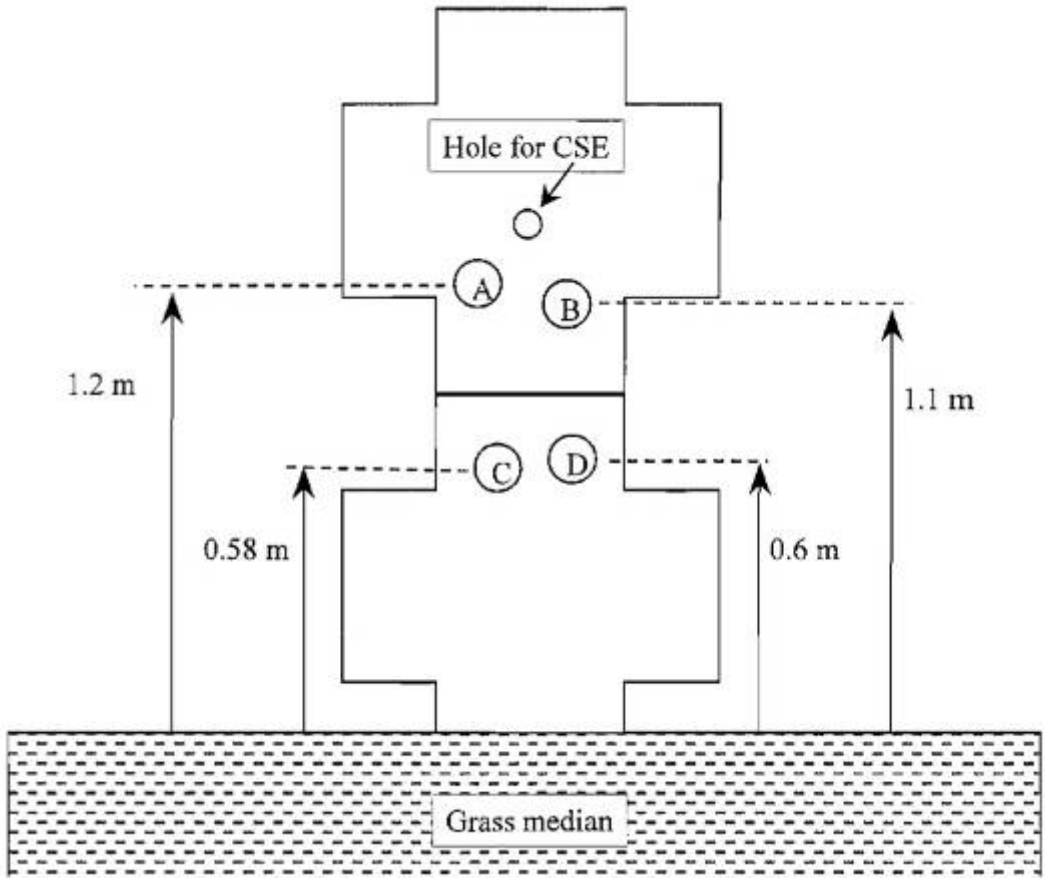

Figure 56 - Panel layout for Panel 16 at VET. A corresponds to the top galvanized strip, B to the rebar and reference electrode (the reference electrode is identified on site by a green cable), C to the bottom galvanized strip, and D to the added Zn-Al strip [15].

Appendix 1: Site Instrumentation Diagrams (Continued)

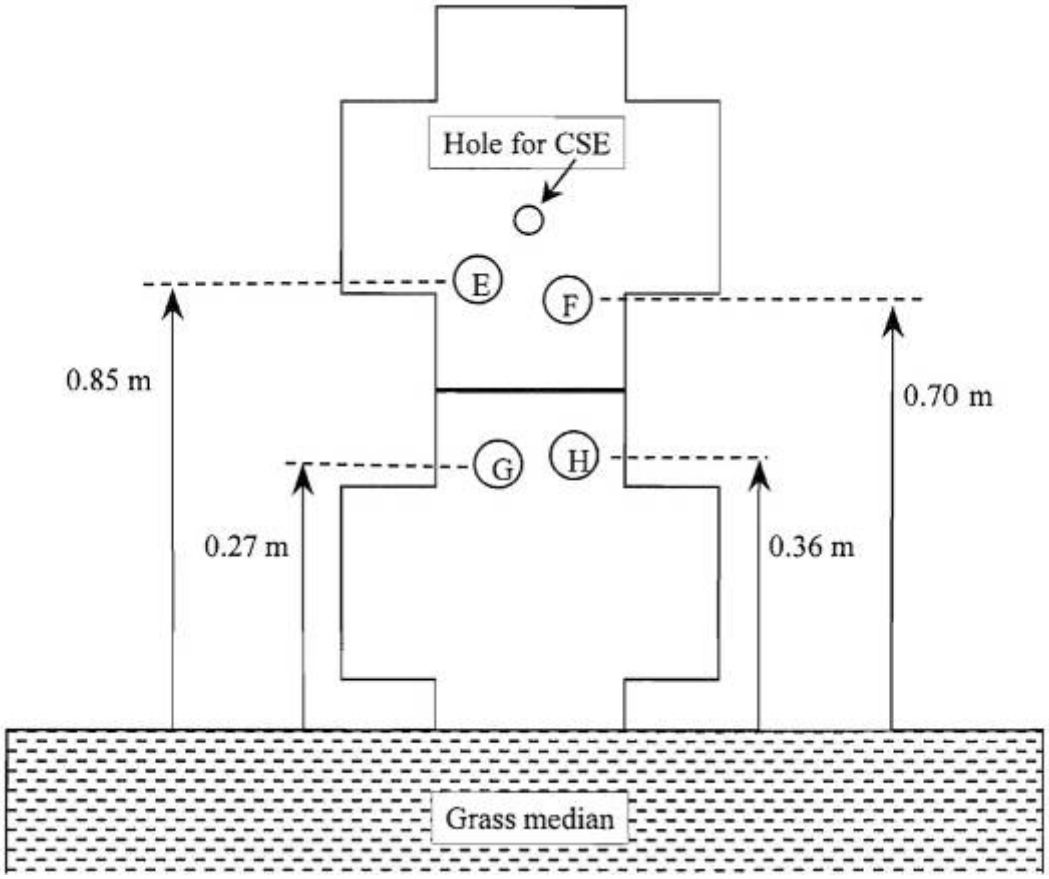

Figure 57 - Panel layout for Panel 23 at VET. E corresponds to the top galvanized strip, F to the reference G to the bottom galvanized strip, and H to the added Zn-Al strip. Note: This location does not have rebar steel inserted [15].

Appendix 1: Site Instrumentation Diagrams (Continued)

Table A1.1 Dimensions of test elements.

Site	Reinforcing Strips: Position or Panel Set		Length (m)	Width (cm)	Thickness (cm)	Area Exposed to Soil (cm^2)
Brickell Ave., Miami SE + NW	Regular Strips	Top	4.6	5.0	0.4	4938
		Bottom	6.1	7.5	1.5	10970
	Extra Strips	Top	3.1	5.0	0.4	3348
		Bottom	3.1	7.5	1.5	5580
Pensacola Ave., Tallahassee	R17		6.1	8.0	0.3	10120
	R23		6.1	8.0	0.3	10120
	R44		6.1	8.0	0.3	10120
	R62		6.1	8.0	0.3	10120
Palm City Bridge, Northeast Wall, Stuart	R1		6.7	5.0	0.4	7242
	R5		6.7	5.0	0.4	7242
	R14		6.7	5.0	0.4	7242
	R28		6.7	5.0	0.4	7242
Palm City Bridge, Northwest Wall, Stuart	R3W		5.5	5.0	0.4	5929
	R5W		5.5	5.0	0.4	5929
Port St. Lucie Blvd., Port Saint Lucie	R3		4.3	5.0	0.4	4613
	R7		4.9	5.0	0.4	5271
State Rd. 200, Ocala	R6		4.3	6.0	0.5	5553
	R25		5.2	4.0	0.5	4667
Acosta Bridge, Jacksonville*	R9		5.0	5.0	0.4	5404
	R21		5.0	5.0	0.4	5404
Veterans Expressway, Tampa	R16		6.0	5.0	0.4	6484
	R23		6.0	5.0	0.4	6484
Howard Frankland Bridge, Tampa	Longitudinal Wires			Transverse Wires		Mesh
	Length (m)	Dia. (cm)	Area (cm^2)	Length (m)	Dia. (cm)	Area (cm^2)	Total Area Exposed to Soil (cm^2)
	3.7	0.95	5458	0.91	0.95	3002	8460
Steel Bars							
	Length (m)		Dia. (cm)		Area Exposed to Soil (cm^2)		
Port St. Lucie	2.5		1.3		993		
Frankland†	2.4		1.3		973		
All Other Sites	3.1		1.3		1216		

* Length was estimated based on the height of the reinforcement compared to other structures
† New rebars were inserted in to panels R7, R9, R15, and R21

APPENDIX 2: DETAILED ACR DATA

This Appendix contains detailed electrochemical data. Tables A2.1 to A2.7 tabulate Nilsson meter solution resistance measurements, number ("Disc") identifying the Gamry™ data file for LPR tests, calculated LPR Rp value and corresponding ACR values for each test run in the field in both the first and second surveys.

Tables A2.8 to A2.14 list, for the second survey only, all the electrochemical impedance spectroscopy (EIS) test results together with the corresponding LPR results of tests conducted for the same element during the same visit.

In all tables the first column refers to the element tested and its paired counter electrode. The abbreviations are as follows:

GT:	galvanized top element,
GB:	galvanized bottom element,
S:	buried plain steel rebar
Z	buried Zn-Al strips.
Comb.:	(Combination) test arrangement measured.

In BR various combinations are not repeated as there are 6 reference electrodes used at BRN and 4 reference electrodes used at BRS for each elevation. Values of 'X' denote discarded tests where the calculated Rp values numbers were near 0 or over 1,000Ω, except for Zn-Al Rp > 1,000Ω.

Figures 58 to 65 are cumulative distributions of ACR for galvanized steel elements, grouped by site. Figure 66 shows the corrosion rate behavior of the inserted plain steel rebars grouped by age.

Appendix 2: Detailed ACR Data (Continued)

Table A2.1 LPR data for BR.

Note: Differences in combinations based upon different reference electrodes used.

		February 8, 1991				September 24, 1991				January 25, 1992				March 17, 1992			
			LPR				LPR				LPR				LPR		
	Comb.	Rs (Ω)	Disc	Rp (Ω)	ACR (µm/y)	Rs (Ω)	Disc	Rp (Ω)	ACR (µm/y)	Rs (Ω)	Disc	Rp (Ω)	ACR (µm/y)	Rs (Ω)	Disc	Rp (Ω)	ACR (µm/y)
NW Top																	
AG/GL	1					62	0001	162	0.36								
AG/GL	2					43	0002	160	0.36								
AG/GR	3					42	0003	159	0.37								
AG/GL	4					38	0004	152	0.38								
AG/GL	5					62	0005	176	0.33								
AG/GR	6					44	0006	159	0.37								
S/GL	7					41	0007	50	2.5								
S/GL	8					33	0008	44	2.8								
S/GR	9					61	0009	75	1.7								
S/GL	10					34	0010	44	2.8								
S/GL	11					47	0011	58	2.1								
S/GR	12					61	0012	71	1.7								
GL/GR	13					23	0013	129	0.61								
GL/GR	14					41	0014	146	0.54								
GR/GL	15					31	0015	139	0.57								
GR/GL	16					32	0016	132	0.60								
NW Bottom																	
AG/GL	1					14	0017	65	0.54					23	0033	98	0.36
AG/GL	2					15	0018	65	0.54					16	0034	83	0.42
AG/GR	3					25	0019	74	0.47					23			
AG/GL	4					18	0020	65	0.54					18	0035	84	0.42
AG/GL	5					12	0021	61	0.57					20			
AG/GR	6					18	0022	65	0.54					30			
S/GL	7					25	0023	33	3.8					31	0036	43	2.9
S/GL	8					37	0024	47	2.6					42	0037	52	2.4
S/GR	9					24	0025	31	4.0					27			
S/GL	10					26	0026	34	3.6					30	0038	40	3.1
S/GL	11					35	0027	44	2.8					44			
S/GR	12					22	0028	30	4.1					29			
GL/GR	13					23	0029	71	0.50					34	0039	98	0.36
GL/GR	14					26	0030	74	0.48					29	0040	92	0.39
GR/GL	15					10	0031	34	1.0					19	0041	53	0.67
GR/GL	16					13	0032	37	0.96					15	0042	47	0.76
SE Top																	
AG/GL	1					22	1007	122	0.48								
AG/GL	2					23	1008	125	0.47								
AG/GR	3					21	1009	126	0.46								
AG/GR	4					24	1010	126	0.46								
GR/GL	5					38	1011	165	0.48								
GR/GL	6					38	1012	154	0.51								
GL/GR	7					35	1013	156	0.51								
GL/GR	8					35	1014	152	0.52								
SE Bottom																	
AG/GL	1	41	1001	88	0.40												
AG/GL	2	43	1002	99	0.35	12	1015	108	0.32					13	1021	49	0.71
AG/GR	3	34				18	1016	108	0.32					10	1022	46	0.76
AG/GR	4	47				20	1017	95	0.37					15	1023	51	0.68
GR/GL	5	21	1003	55	0.65	10	1018	41	0.87					15	1024	51	0.70
GR/GL	6	20	1004	46	0.77	13	1019	41	0.87					14	1025	48	0.74
GL/GR	7	17	1005	41	0.87	21											
GL/GR	8	17	1006	40	0.89	24	1020	27	1.3					11	1026	30	1.2

		August 28, 1992				November 25, 1993				October 15, 2002			
			LPR				LPR				LPR		
	Comb.	Rs (Ω)	Disc	Rp (Ω)	ACR (µm/y)	Rs (Ω)	Disc	Rp (Ω)	ACR (µm/y)	Rs (Ω)	Disc	Rp (Ω)	ACR (µm/y)
NW Top													
AG/GL	1												
AG/GL	2												
AG/GR	3												
AG/GL	4												
AG/GL	5												
AG/GR	6												
S/GL	7												
S/GL	8												
S/GR	9												
S/GL	10												
S/GL	11												
S/GR	12												
GL/GR	13												
GL/GR	14												
GR/GL	15												
GR/GL	16												
NW Bottom													
AG/GL	1												
AG/GL	2	16	0047	85	0.41								
AG/GR	3	24	0048	84	0.42								
AG/GL	4												
AG/GL	5	20	0049	37	0.94								
AG/GR	6	30	0050	11	3.2								
S/GL	7												
S/GL	8												
S/GR	9												
S/GL	10												
S/GL	11												
S/GR	12												
GL/GR	13												
GL/GR	14												
GR/GL	15												
GR/GL	16												
SE Top													
AG/GL	1									45	1201	153	0.38
AG/GL	2									45	1202	106	0.55
AG/GR	3									53	1203	131	0.44
AG/GR	4									61	1204	87	0.67
GR/GL	5									66	1205	142.9	0.55
GR/GL	6									69	1206	151.5	0.52
GL/GR	7									84	1207	155	0.51
GL/GR	8									84	1208	149.6	0.53
SE Bottom													
AG/GL	1									13	1209	91	0.38
AG/GL	2	13	1035	50.1	0.70					14	1210	82	0.43
AG/GR	3	11	1036	37.5	0.93					11	1211	90	0.39
AG/GR	4	14	1037	43.3	0.81					15	1212	83	0.42
GR/GL	5	15	1038	44	0.81					17	1213	59	0.60
GR/GL	6	14	1039	41.7	0.85					16	1214	56	0.64
GL/GR	7									14	1215	54	0.66
GL/GR	8	10	1040	20.6	1.7					14	1216	51	0.70

		December 25, 2002				April 4, 2003				June 2, 2004			
			LPR				LPR				LPR		
	Comb.	Rs (Ω)	Disc	Rp (Ω)	ACR (µm/y)	Rs (Ω)	Disc	Rp (Ω)	ACR (µm/y)	Rs (Ω)	Disc	Rp (Ω)	ACR (µm/y)
NW Top													
AG/GL	1	X	0201	X						89	0245	346	0.17
AG/GL	2	X	0202	X						62	0246	356	0.16
AG/GR	3	70	0203	161	0.36					61	0247	349	0.17
AG/GL	4	X	0204	X						57	0248	338	0.17
AG/GL	5	X	0205	X						87	0249	339	0.17
AG/GR	6	66	0206	158	0.37					62	0250	339	0.17
S/GL	7									65	0251	8	16
S/GL	8									55	0252	6	20
S/GR	9									94	0253	11	12
S/GL	10									57	0254	13	9.6
S/GL	11									73	0255	10	12
S/GR	12									91	0256	18	6.8
GL/GR	13	102	0207	180	0.44					33	0257	163	0.48
GL/GR	14	56	0208	169	0.47					56	0258	161	0.49
GR/GL	15	X	0209	X						52	0259	379	0.21
GR/GL	16	X	0210	X						55	0260	366	0.22
NW Bottom													
AG/GL	1	34	0211	112	0.31	37	0229	121	0.29	30	0261	80	0.43
AG/GL	2	25	0212	114	0.31	27	0230	122	0.29	22	0262	88	0.40
AG/GR	3	33	0213	113	0.31	37	0231	120	0.29	20	0263	93	0.38
AG/GL	4	28	0214	125	0.28	30	0232	120	0.29	24	0264	85	0.41
AG/GL	5	35	0215	99	0.35	32	0233	122	0.29	25	0265	88	0.40
AG/GR	6	44	0216	111	0.31	47	0234	117	0.30	22	0266	104	0.34
S/GL	7	49	0217	8	15	53	0235	14	9.2	43	0267	11	11.6
S/GL	8	62	0218	16	8.0	67	0236	14	8.7	54	0268	11	10.8
S/GR	9	43	0219	13	9.6	47	0237	13	9.9	38	0269	7	18.5
S/GL	10	45	0220	12	9.9	49	0238	12	10.3	40	0270	9	13.1
S/GL	11	65	0221	13	9.3	69	0239	15	8.5	57	0271	11	11.6
S/GR	12	46	0222	15	8.1	49	0240	19	6.5	40	0272	13	9.50
GL/GR	13	44	0223	100	0.36	46	0241	104	0.34	39	0273	80	0.44
GL/GR	14	39	0224	109	0.32	41	0242	104	0.34	35	0274	78	0.46
GR/GL	15	23	0225	18	2.0	25	0243	18	2.0	22	0275	18	1.99
GR/GL	16	19	0226	13	2.7	20	0244	14	2.5	17	0276	15	2.31
SE Top													
AG/GL	1									61	1219	230	0.25
AG/GL	2									62	1220	223	0.26
AG/GR	3									60	1221	225	0.26
AG/GR	4									65	1222	219	0.27
GR/GL	5									79	1223	212	0.37
GR/GL	6									81	1224	203	0.39
GL/GR	7									140	1225	196	0.40
GL/GR	8									140	1226	191	0.41
SE Bottom													
AG/GL	1									14	1227	90	0.39
AG/GL	2									15	1228	88	0.40
AG/GR	3	11	1217	87	0.40					11	1229	90	0.39
AG/GR	4									16	1230	90	0.39
GR/GL	5									18	1231	57	0.62
GR/GL	6									16	1232	63	0.56
GL/GR	7									15	1233	57	0.62
GL/GR	8									15	1234	52	0.68

Appendix 2: Detailed ACR Data (Continued)

Table A2.2 LPR data for HFB.

		November 14, 1991				December 12, 1991				February 7, 1992				April 21, 1992				July 1, 1992				August 15, 2002				February 21, 2003			
			LPR				LPR				LPR				LPR				LPR				LPR				LPR		
	Comb.	Rs (Ω)	Disc	Rp (Ω)	ACR (µm/y)	Rs (Ω)	Disc	Rp (Ω)	ACR (µm/y)	Rs (Ω)	Disc	Rp (Ω)	ACR (µm/y)	Rs (Ω)	Disc	Rp (Ω)	ACR (µm/y)	Rs (Ω)	Disc	Rp (Ω)	ACR (µm/y)	Rs (Ω)	Disc	Rp (Ω)	ACR (µm/y)	Rs (Ω)	Disc	Rp (Ω)	ACR (µm/y)
Panel 7																													
GT/GB	1	18	2001	56	0.82	19	2005	392	0.12	25	2009	74	0.62	20	2029	64	0.72					390	2201	X		570	2225	X	
GB/GT	2	10	2002	65	0.71	9				12	2010	81	0.57	10	2030	77	0.60					220	2202	X		285	2226	X	
NewS/GT	4																					135	2203	48	6.5	220	2227	127	2.44
NewS/GB	3																					130	2204	34	9.0	210			
Panel 9																													
GT/GB	1																					17	2205	66	0.70	25	2228	145	0.32
GB/GT	2																					17	2206	82	0.56	23	2229	93	0.50
NewS/GT	4																					93	2207	24	12.7	120	2230	119	2.60
NewS/GB	3																					92	2208	32	9.6	120	2231	122	2.55
Panel 11																													
GT/GB	1					11	2006	60	0.77	25	2011	39	1.18	13	2031	81	0.57					16	2209	62	0.75	21	2232	117	0.39
GB/GT	2					14	2007	79	0.58	28	2012	65	0.71	15	2032	87	0.53					16	2210	69	0.67	20	2233	114	0.41
OldS/GT	4					60	2008	67	3.7	81	2013	45	5.5	72	2033	119	2.1					86	2211	206	1.2	120	2234	181	1.37
OldS/GB	3					61				82	2014	51	4.9	72	2034	111	2.2					87	2212	133	1.9	120	2235	175	1.42
Panel 15																													
GT/GB	1	14	2003	57	0.81	13				17	2015	61	0.76	15	2035	90	0.51					550	2213	X		1000	2236	X	
GB/GT	2	14	2004	65	0.71	15				20	2016	70	0.66	17	2036	89	0.52					380	2214	X		610			
NewS/GT	4																					200	2215	65	4.8	320	2237	X	
NewS/GB	3																					190	2216	61	5.1	320	2238	X	
Panel 17																													
GT/GB	1					35				35	2017	102	0.45	25	2037	78	0.59					31.5	2217	100	0.46	50	2239	162	0.28
GB/GT	2					35				16	2018	105	0.44	14	2038	92	0.50					12	2218	88	0.52	16	2240	155	0.30
OldS/GT	4					85				60	2019	109	2.3	53	2039	100	2.5					51	2219	107	2.3	74	2241	164	1.51
OldS/GB	3					70				56	2020	95	2.6	50	2040	83	3.0					48	2220	100	2.5	71	2242	148	1.67
Panel 21																													
GT/GB	1																					17	2221	84	0.55	22	2243	155	0.30
GB/GT	2																					14	2222	100	0.46	21	2244	180	0.26
NewS/GT	4																					42	2223	131	2.4	200	2245	264	1.17
NewS/GB	3																					43	2224	134	2.3	200	2246	274	1.13

Appendix 2: Detailed ACR Data (Continued)

Table A2.3 LPR data for PC.

		May 2, 1992				July 29, 1992				September 24, 1992				November 19, 1992				November 13, 1993				August 23, 2003				December 31, 2003				January 25, 2004			
			LPR				LPR				LPR				LPR				LPR				LPR				LPR				LPR		
	Comb.	Rs (Ω)	Disc	Rp (Ω)	ACR (μm/y)	Rs (Ω)	Disc	Rp (Ω)	ACR (μm/y)	Rs (Ω)	Disc	Rp (Ω)	ACR (μm/y)	Rs (Ω)	Disc	Rp (Ω)	ACR (μm/y)	Rs (Ω)	Disc	Rp (Ω)	ACR (μm/y)	Rs (Ω)	Disc	Rp (Ω)	ACR (μm/y)	Rs (Ω)	Disc	Rp (Ω)	ACR (μm/y)	Rs (Ω)	Disc	Rp (Ω)	ACR (μm/y)
NE Wall Panel 1																																	
GT/GB	1	21	4001	183	0.29	23	4017	75.5	0.71	26	4029	110	0.49					32	4033	160	0.34	25											
GB/GT	2	43	4002	168	0.32	40	4018	104.5	0.51	46	4030	110	0.49					60	4034	124	0.43	68											
S/GT	4	70				160	4019	82.4	3.0	200	4031	93	2.7					240	4035	177	1.4	150											
S/GB	3	70	4003	104	2.4	160	4020	82.2	3.0	200	4032	98	2.5					250	4036	158	1.6	145	4201	61	4.1								
GT/S	1a																					50	4202	99	0.54								
Panel 5																																	
GT/GB	1	18	4004	91	0.59	16	4021	55.4	0.29									20	4037	83	0.65	23	4203	57	0.94								
GB/GT	2	43	4005	43	1.3	38	4022	X										42	4038	101	0.53	47	4204	72	0.74								
Panel 14																																	
GT/GB	1	43	4006	148	0.36	38	4023	106.6	0.29													51	4205	180	0.30								
GB/GT	2	57	4007	198	0.27	49	4024	106.8	0.32													60	4206	61	0.88								
S/GT	4					140	4025	106.1	2.3													95	4207	272	0.91								
S/GB	3	120	4008	226	1.1	140	4026	105.8	2.3													93	4208	263	0.94								
Panel 28																																	
GT/GB	1					110	4027	73.4	0.29													55	4209	185	0.29								
GB/GT	2					110	4028	212.5	0.32													76	4210	183	0.29								
NW Wall Panel 3																																	
GT/GB	1					25				35	5001	66	1.0	18	5009	248	0.27	17	5017	99.3	0.66									21	5201	102	0.65
GB/GT	2					0				16	5002	52	1.3	3.9	5010	27.1	2.4	11	5018	37.03	1.8									49	5202	241	0.27
S/GT	4					0				60	5003	43	5.8	38	5011	118.1	2.1	17	5019	35.6	7.0									21	5203	27	9.3
S/GB	3					1				56	5004	8	31	39	5012	2.7	92	6.1	5020	2.21	112									37	5204	X	
Panel 5																																	
GT/GB	1					19				28	5005	105	0.63	4.2	5013	135.8	0.48	24	5021	109.2	0.60					33				41	5205	142	0.46
GB/GT	2					46				29	5006	24	2.7	23	5014	X		8.7	5022	30.33	2.2					21				27	5206	47	1.4
S/GT	4					37				130	5007	98	2.5	38	5015	15	17	88	5023	36.6	6.8									87	5207	33	7.4
S/GB	3					37				120	5008	8	31	39	5016	14	18	89	5024	49.8	5.0									85	5208	32	7.7

Appendix 2: Detailed ACR Data (Continued)

Table A2.4 LPR data for PSL.

		November 18, 1992				November 13, 1993				January 2, 2004				September 9, 2004			
			LPR				LPR				LPR				LPR		
	Comb.	Rs (Ω)	Disc	Rp (Ω)	ACR (μm/y)	Rs (Ω)	Disc	Rp (Ω)	ACR (μm/y)	Rs (Ω)	Disc	Rp (Ω)	ACR (μm/y)	Rs (Ω)	Disc	Rp (Ω)	ACR (μm/y)
Panel 3																	
GT/GB	1	10	6001	60	1.4	12	6009	43	2.0	15	6201	X		14	6211	369	0.20
GB/GT	2	7	6002	42	2.0	8	6010	44	1.9	10	6202	X		9	6212	250	0.30
S/GT	4	16	6003	20	15	15	6011	33	2.5	17	6203	9	9.0	16	6213	13	6.4
S/GB	3	15	6004	19	16	14	6012	28	3.1	17	6204	13	6.3	14	6214	13	6.5
GB/GT	X													7	6219	150	0.49
Panel 7																	
GT/GB	1	6	6005	32	2.3	7	6013	58	1.3					9	6215	89	0.83
GB/GT	2	7	6006	25	3.0	6	6014	34	2.2					7	6216	116	0.64
S/GT	4	23	6007	29	10	25	6015	144	0.51	20	6205	77	1.1	19	6218	58	1.5
S/GB	3	24	6008	30	10	26	6016	133	0.56					20	6217	67	1.3
GT/S	5									12	6206	115	0.65				

Table A2.5 LPR data for OCA.

		January 14, 1993				April 8, 1993				September 25, 1993				June 5, 2003				December 27, 2003			
			LPR				LPR				LPR				LPR				LPR		
	Comb.	Rs (Ω)	Disc	Rp (Ω)	ACR (μm/y)	Rs (Ω)	Disc	Rp (Ω)	ACR (μm/y)	Rs (Ω)	Disc	Rp (Ω)	ACR (μm/y)	Rs (Ω)	Disc	Rp (Ω)	ACR (μm/y)	Rs (Ω)	Disc	Rp (Ω)	ACR (μm/y)
Panel 6																					
GT/GB	1	57	7001	333	0.20	63	7009	301	0.23	63	7017	274	0.26	62	7201	270	0.26	66	7215	369	0.19
GB/GT	2	64	7002	247	0.28	61	7010	234	0.30	63	7018	194	0.36	53	7202	80	0.88	57	7216	64	1.1
S/GT	4	67	7003	22	8.3	78	7011	59	4.2	95	7019	87	2.8	130	7203	59	4.3	140	7217	78	3.2
S/GB	3	67	7004	30	11	77	7012	53	4.8	95	7020	66	3.8	130	7204	76	3.3	140	7218	87	2.9
Panel 25																					
GT/GB	1	75	7005	148	0.56	70	7013	128	0.64					90	7205	115	0.72	86	7219	120	0.7
GB/GT	2	150	7006	305	0.27	140	7014	99	0.84					160	7206	45	1.8	140	7220	X	
S/GT	4	210	7007	52	4.3	260	7015	187	4.3					230	7207	X		210	7221	151	1.7
S/GB	3	210	7008	57	4.8	265	7016	183	4.3					220	7208	846	0.30	220	7222	140	1.8

Appendix 2: Detailed ACR Data (Continued)

Table A2.6 LPR data for ABJ.

		April 7, 1993				September 24, 1993				August 14, 2003				December 26, 2003			
			LPR				LPR				LPR				LPR		
	Comb.	Rs (Ω)	Disc	Rp (Ω)	ACR (μm/y)	Rs (Ω)	Disc	Rp (Ω)	ACR (μm/y)	Rs (Ω)	Disc	Rp (Ω)	ACR (μm/y)	Rs (Ω)	Disc	Rp (Ω)	ACR (μm/y)
Panel 9																	
GT/GB	1	51	8001	251	0.29	44	8010	132	0.58	46	8201	119	0.61	61	8215	276	0.26
GB/GT	2	48	8002	247	0.29	37	8011	116	0.66	40	8202	74	0.98	57	8216	210	0.34
S/GT	4					75	8012	X		15	8203	14	18	20	8217	45	5.5
S/GB	3	13	8003	30	8.3	77	8013	X		15	8204	13	19	20	8218	10	24
Z/GT	6	750	8004	635	1.9	810	8014	1394	0.86								
Z/GB	5	770	8005	483	2.6	820	8015	1134	1.1	800	8205	592	2.1				
Panel 21																	
GT/GB	1	34	8006	118	0.61	32	8016	11	0.69	33	8206	92	0.78	41	8219	233	0.31
GB/GT	2	44	8007	121	0.60	39	8017	84	0.91	36	8207	79	0.92	48	8220	144	0.50
S/GT	4	59	8008	51	4.9	89	8018	83	2.8	210	8208	171	1.5				
S/GB	3	58	8009	54	4.6	95	8019	95	2.6	210	8209	181	1.4				

Table A2.7 LPR data for VET.

		August 3, 1993				January 15, 1994				May 30, 2003				July 18, 2003				January 21, 2005			
			LPR				LPR				LPR				LPR				LPR		
	Comb.	Rs (Ω)	Disc	Rp (Ω)	ACR (μm/y)	Rs (Ω)	Disc	Rp (Ω)	ACR (μm/y)	Rs (Ω)	Disc	Rp (Ω)	ACR (μm/y)	Rs (Ω)	Disc	Rp (Ω)	ACR (μm/y)	Rs (Ω)	Disc	Rp (Ω)	ACR (μm/y)
Panel 16																					
GT/GB	1	30	9001	56	1.1	29	9011	78	0.77	15	9201	59	1.0					18	9219	68	0.89
GB/GT	2	41	9002	52	1.1	40	9012	76	0.79	21	9202	72	0.83					23	9220	75	0.80
S/GT	4	92	9003	36	6.9	71				54	9203	X		51	9217	43	5.8	59	9221	42	5.9
S/GB	3	90	9004	37	6.8	69	9013	45	5.5	52	9204	X		50	9218	50	5.0	58	9222	45	5.6
Z/GT	6	160	9005	107	4.0	170	9014	367	1.2												
Z/GB	5	150	9006	112	3.8	160	9015	294	1.5	90	9205	X									
Panel 23																					
GT/GB	1	36	9007	59	1.0	36	9016	95	0.63	13	9206	30	2.0					16	9223	73	0.82
GB/GT	2	40	9008	58	1.0	39	9017	80	0.75	18	9207	73	0.8					21	9224	68	0.88
Z/GT	4	110	9009	73	5.3	140	9018	294	1.3	14	9208	224	1.7								
Z/GB	3	130	9010	38	10	120	9019	311	1.2	15	9209	192	2.0					71	9225	212	1.8

Appendix 2: Detailed ACR Data (Continued)

Table A2.8 EIS-LPR data for BR.

Note: Differences in combinations based upon different reference electrodes used.

		October 15, 2002									December 25, 2002									April 4, 2003									June 2, 2004								
			LPR			EIS						LPR			EIS						LPR			EIS						LPR			EIS				
	Comb.	Rs (Ω)	Disc	Rp (Ω)	ACR (µm/y)	Disc	Rp (Ω)	n	Y_o ($S \cdot s^n$)	ACR (µm/y)	Rs (Ω)	Disc	Rp (Ω)	ACR (µm/y)	Disc	Rp (Ω)	n	Y_o ($S \cdot s^n$)	ACR (µm/y)	Rs (Ω)	Disc	Rp (Ω)	ACR (µm/y)	Disc	Rp (Ω)	n	Y_o ($S \cdot s^n$)	ACR (µm/y)	Rs (Ω)	Disc	Rp (Ω)	ACR (µm/y)	Disc	Rp (Ω)	n	Y_o ($S \cdot s^n$)	ACR (µm/y)
NW Top																																					
AG/GL	1										X	0201	X																89	0245	346	0.17					
AG/GL	2										X	0202	X																62	0246	356	0.16					
AG/GR	3										70	0203	161	0.36															61	0247	349	0.17	0277	467	0.4	4E-01	0.12
AG/GL	4										X	0204	X																57	0248	338	0.17					
AG/GL	5										X	0205	X																87	0249	339	0.17					
AG/GR	6										66	0206	158	0.37															62	0250	339	0.17					
S/GL	7																												65	0251	8	16					
S/GL	8																												55	0252	6	20.0					
S/GR	9																												94	0253	11	12					
S/GL	10																												57	0254	13	9.6	0278	X			
S/GL	11																												73	0255	10	12					
S/GR	12																												91	0256	18	6.8					
GL/GR	13										102	0207	180	0.44															33	0257	163	0.48					
GL/GR	14										56	0208	169	0.47															56	0258	161	0.49	0279	305	0.4	4E-01	0.26
GR/GL	15										X	0209	X																52	0259	379	0.21					
GR/GL	16										X	0210	X																55	0260	366	0.22	0280	654	0.3	8E-03	0.12
NW Bottom																																					
AG/GL	1										34	0211	112	0.31						37	0229	121	0.29						30	0261	80.3	0.43					
AG/GL	2										25	0212	114	0.31						27	0230	122	0.29						22	0262	87.8	0.40					
AG/GR	3										33	0213	113	0.31	0227	X				37	0231	120	0.29						20	0263	92.8	0.38	0281	X			
AG/GL	4										28	0214	125	0.28						30	0232	120	0.29						24	0264	84.9	0.41					
AG/GL	5										35	0215	99	0.35						32	0233	122	0.29						25	0265	87.6	0.40					
AG/GR	6										44	0216	111	0.31						47	0234	117	0.30						22	0266	104	0.34					
S/GL	7										49	0217	8	15						53	0235	14	9.2						43	0267	11	11.6	0282	X			
S/GL	8										62	0218	16	8.0						67	0236	14	8.7						54	0268	11	10.8					
S/GR	9										43	0219	13	9.6	0228	X				47	0237	13	9.9						38	0269	7	18.5	0283	X			
S/GL	10										45	0220	12	9.9						49	0238	12	10.3						40	0270	9	13.1					
S/GL	11										65	0221	13	9.3						69	0239	15	8.5						57	0271	11	11.6	0284	X			
S/GR	12										46	0222	15	8.1						49	0240	19	6.5						40	0272	13	9.50					
GL/GR	13										44	0223	100	0.36						46	0241	104	0.34						39	0273	79.9	0.44					
GL/GR	14										39	0224	109	0.32						41	0242	104	0.34						35	0274	78	0.46	0285	88	0.3	2E-02	0.41
GR/GL	15										23	0225	18	2.0						25	0243	18	2.0						22	0275	18	1.99	0286	33	0.3	2E-03	1.1
GR/GL	16										19	0226	13	2.7						20	0244	14	2.5						17	0276	15	2.31					
SE Top																																					
AG/GL	1	45	1201	153	0.38																								61	1219	230	0.25					
AG/GL	2	45	1202	106	0.55																								62	1220	223	0.26					
AG/GR	3	53	1203	131	0.44																								60	1221	225	0.26	1235	X			
AG/GR	4	61	1204	87	0.67																								65	1222	219	0.27					
GR/GL	5	66	1205	143	0.55																								79	1223	212	0.37					
GR/GL	6	69	1206	151	0.52																								81	1224	203	0.39					
GL/GR	7	84	1207	155	0.51																								140	1225	196	0.40					
GL/GR	8	84	1208	150	0.53																								140	1226	191	0.41					
SE Bottom																																					
AG/GL	1	13	1209	91	0.38																								14	1227	90	0.39					
AG/GL	2	14	1210	82	0.43																								15	1228	88	0.40					
AG/GR	3	11	1211	90	0.39						11	1217	87	0.40	1218	211	0.4	5E-02	0.00										11	1229	90	0.39	1236	148	0.4	5E-02	0.02
AG/GR	4	15	1212	83	0.42																								16	1230	90	0.39					
GR/GL	5	17	1213	59	0.60																								18	1231	57	0.62					
GR/GL	6	16	1214	56	0.64																								16	1232	63	0.56					
GL/GR	7	14	1215	54	0.66																								15	1233	57	0.62					
GL/GR	8	14	1216	51	0.70																								15	1234	52	0.68					

Appendix 2: Detailed ACR Data (Continued)

Table A2.9 EIS-LPR data for HFB.

		August 15, 2002									February 21, 2003								
			LPR			EIS						LPR			EIS				
	Comb.	Rs (Ω)	Disc	Rp (Ω)	ACR (μm/y)	Disc	Rp (Ω)	n	Y_o ($S \cdot s^n$)	ACR (μm/y)	Rs (Ω)	Disc	Rp (Ω)	ACR (μm/y)	Disc	Rp (Ω)	n	Y_o ($S \cdot s^n$)	ACR (μm/y)
Panel 7																			
GT/GB	1	390	2201	X							570	2225	X						
GB/GT	2	220	2202	X							285	2226	1k						
S/GT	4	135	2203	48	6.5						220	2227	127	2.44					
S/GB	3	130	2204	34	9.0						210								
Panel 9																			
GT/GB	1	17	2205	66	0.70						25	2228	145	0.32					
GB/GT	2	17	2206	82	0.56						23	2229	93	0.50					
S/GT	4	93	2207	24	12.7						120	2230	119	2.60					
S/GB	3	92	2208	32	9.6						120	2231	122	2.55					
Panel 11																			
GT/GB	1	16	2209	62	0.75						21	2232	117	0.39	2247	194	0.3	2E-02	0.2
GB/GT	2	16	2210	69	0.67						20	2233	114	0.41	2248	148	0.4	2E-02	0.3
S/GT	4	86	2211	206	1.2						120	2234	181	1.37	2249	X			
S/GB	3	87	2212	133	1.9						120	2235	175	1.42					
Panel 15																			
GT/GB	1	550	2213	X							1000	2236	X						
GB/GT	2	380	2214	X							610								
S/GT	4	200	2215	65	4.8						320	2237	X						
S/GB	3	190	2216	61	5.1						320	2238	X						
Panel 17																			
GT/GB	1	31.5	2217	100	0.46						50	2239	162	0.28	2250	159	0.5	2E-02	0.3
GB/GT	2	12	2218	88	0.52						16	2240	155	0.30	2251	221	0.4	3E-02	0.2
S/GT	4	51	2219	107	2.3						74	2241	164	1.51	2252	X			
S/GB	3	48	2220	100	2.5						71	2242	148	1.67					
Panel 21																			
GT/GB	1	17	2221	84	0.55						22	2243	155	0.30	2253	236	0.4	2E-02	0.2
GB/GT	2	14	2222	100	0.46						21	2244	180	0.26	2254	253	0.5	4E-02	0.2
S/GT	4	42	2223	131	2.4						200	2245	264	1.17					
S/GB	3	43	2224	134	2.3						200	2246	274	1.13	2255	281	0.5	6E-03	1.1

Appendix 2: Detailed ACR Data (Continued)

Table A2.10 EIS-LPR data for PC.

		August 23, 2003									December 31, 2003									January 25, 2005								
			LPR			EIS						LPR			EIS						LPR			EIS				
	Comb.	Rs (Ω)	Disc	Rp (Ω)	ACR (μm/y)	Disc	Rp (Ω)	n	Y_o ($S \cdot s^n$)	ACR (μm/y)	Rs (Ω)	Disc	Rp (Ω)	ACR (μm/y)	Disc	Rp (Ω)	n	Y_o ($S \cdot s^n$)	ACR (μm/y)	Rs (Ω)	Disc	Rp (Ω)	ACR (μm/y)	Disc	Rp (Ω)	n	Y_o ($S \cdot s^n$)	ACR (μm/y)
NE Wall																												
Panel 1																												
GT/GB	1	25																										
GB/GT	2	68																										
S/GT	4	150																										
S/GB	3	145	4201	61	4.1	4211	114	0.2	1E-02	2.2																		
GT/S	1a	50	4202	99	0.54																							
Panel 5																												
GT/GB	1	23	4203	57	0.94																							
GB/GT	2	47	4204	72	0.74	4212	170	0.3	3E-02	0.32																		
Panel 14																												
GT/GB	1	51	4205	180	0.30																							
GB/GT	2	60	4206	61	0.88	4213	113	0.4	4E-02	0.48																		
S/GT	4	95	4207	272	0.91	4214	258	0.3	5E-03	1.0																		
S/GB	3	93	4208	263	0.94																							
Panel 28																												
GT/GB	1	55	4209	185	0.29	4215	644	0.3	2E-02	0.08																		
GB/GT	2	76	4210	183	0.29																							
NW Wall																												
Panel 3																												
GT/GB	1																			21	5201	102	0.65	5209	X			
GB/GT	2																			49	5202	241	0.27					
S/GT	4																			21	5203	27	9.3					
S/GB	3																			37	5204	X		5210	X			
Panel 5																												
GT/GB	1										33									41	5205	142	0.46	5211	339	0.3	3E-02	0.19
GB/GT	2										21									27	5206	47	1.4	5212	X			
S/GT	4																			87	5207	33	7.4	5213	X			
S/GB	3																			85	5208	32	7.7	5214	X			

Appendix 2: Detailed ACR Data (Continued)

Table A2.11 EIS-LPR data for PSL.

		January 2, 2004									September 9, 2004								
			LPR			EIS						LPR			EIS				
	Comb.	Rs (Ω)	Disc	Rp (Ω)	ACR (µm/y)	Disc	Rp (Ω)	n	Y_o ($S \cdot s^n$)	ACR (µm/y)	Rs (Ω)	Disc	Rp (Ω)	ACR (µm/y)	Disc	Rp (Ω)	n	Y_o ($S \cdot s^n$)	ACR (µm/y)
Panel 3																			
GT/GB	1	15	6201	X		6207	223	0.5	5E-02	0.38	14	6211	369	0.20	6221	189	0.5	6E-02	0.45
GB/GT	2	9.5	6202	X		6208	171	0.6	5E-02	0.49	8.7	6212	250	0.30	6220	166	0.6	6E-02	0.51
S/GT	4	17	6203	9.4	9.0	6209	X				16	6213	13	6.4					
S/GB	3	17	6204	13	6.3						14	6214	13	6.5	6224	25	0.3	2E-01	12
GB/GT	X										7.2	6219	150	0.49					
Panel 7																			
GT/GB	1										8.9	6215	89	0.83	6223	110	0.5	1E-01	0.67
GB/GT	2										6.95	6216	116	0.64	6222	159	0.6	1E-02	0.47
S/GT	4	20	6205	77	1.1						19	6218	58	1.5					
S/GB	3										20	6217	67	1.3	6225	108	0.5	1E-01	2.8
GT/S	5	12	6206	115	0.65	6210	170	0.5	7E-02	0.43									

Table A2.12 EIS-LPR data for OCA.

		June 5, 2003									December 27, 2003								
			LPR			EIS						LPR			EIS				
	Comb.	Rs (Ω)	Disc	Rp (Ω)	ACR (µm/y)	Disc	Rp (Ω)	n	Y_o ($S \cdot s^n$)	ACR (µm/y)	Rs (Ω)	Disc	Rp (Ω)	ACR (µm/y)	Disc	Rp (Ω)	n	Y_o ($S \cdot s^n$)	ACR (µm/y)
Panel 6																			
GT/GB	1	62	7201	270	0.26	7209	220	0.4	9E-02	0.32	66	7215	369	0.19					
GB/GT	2	53	7202	80	0.88	7210	161	0.5	1E-02	0.44	57	7216	64	1.1	7223	X			
S/GT	4	130	7203	59	4.3	7211	X				140	7217	78	3.2	7224	X			
S/GB	3	130	7204	76	3.3	7212	X				140	7218	87	2.9					
Panel 25																			
GT/GB	1	90	7205	115	0.72	7213	277	0.3	2E-02	0.25	86	7219	120	0.7	7225	382	0.2	9E-03	0.18
GB/GT	2	160	7206	45	1.8	7214	141	0.3	2E-02	0.50	140	7220	X						
S/GT	4	230	7207	2546	0.10						210	7221	151	1.7	7226	226	0.3	2E-02	1.1
S/GB	3	220	7208	846	0.30						220	7222	140	1.8					

Appendix 2: Detailed ACR Data (Continued)

Table A2.13 EIS-LPR data for ABJ.

		August 14, 2003									December 26, 2003								
			LPR			EIS						LPR			EIS				
	Comb.	Rs (Ω)	Disc	Rp (Ω)	ACR (µm/y)	Disc	Rp (Ω)	n	Y_o ($S \bullet s^n$)	ACR (µm/y)	Rs (Ω)	Disc	Rp (Ω)	ACR (µm/y)	Disc	Rp (Ω)	n	Y_o ($S \bullet s^n$)	ACR (µm/y)
Panel 9																			
GT/GB	1	46	8201	119	0.61	8210	214	0.3	2E-02	0.34	61	8215	276	0.26					
GB/GT	2	40	8202	74	0.98						57	8216	210	0.34	8221	202	0.2	1E-02	0.36
S/GT	4	15	8203	14	18						20	8217	45	5.5					
S/GB	3	15	8204	13	19	8211	21	0.4	2E-01	12	20	8218	10	24	8222	492	0.3	1E-02	0.51
Z/GT	6																		
Z/GB	5	800	8205	592	2.1	8212	517	0.5	1E-02	2.4									
Panel 21																			
GT/GB	1	33	8206	92	0.78	8213	213	0.3	3E-02	0.34	41	8219	233	0.31	8223	1370	0.3	2E-02	0.05
GB/GT	2	36	8207	79	0.92						48	8220	144	0.50					
S/GT	4	210	8208	171	1.5														
S/GB	3	210	8209	181	1.4	8214	1720	0.2	1E-02	0.15									

Table A2.14 EIS-LPR data for VET.

		May 30, 2003									July 18, 2003									January 21, 2005								
			LPR			EIS						LPR			EIS						LPR			EIS				
	Comb.	Rs (Ω)	Disc	Rp (Ω)	ACR (µm/y)	Disc	Rp (Ω)	n	Y_o ($S \bullet s^n$)	ACR (µm/y)	Rs (Ω)	Disc	Rp (Ω)	ACR (µm/y)	Disc	Rp (Ω)	n	Y_o ($S \bullet s^n$)	ACR (µm/y)	Rs (Ω)	Disc	Rp (Ω)	ACR (µm/y)	Disc	Rp (Ω)	n	Y_o ($S \bullet s^n$)	ACR (µm/y)
Panel 16																												
GT/GB	1	15	9201	59	1.0	9210	110	0.4	7E-02	0.55										18	9219	68	0.89	9226	121	0.4	5E-02	0.50
GB/GT	2	21	9202	72	0.83	9211	872	0.3	6E-02	0.07										23	9220	75	0.80					
S/GT	4	54	9203	X		9212	X				51	9217	43	5.8	9219	X				59	9221	42	5.9					
S/GB	3	52	9204	X							50	9218	50	5.0	9220	X				58	9222	45	5.6	9227	195	0.3	9E-02	1.3
Z/GT	6																											
Z/GB	5	90	9205	X																								
Panel 23																												
GT/GB	1	13	9206	30	2.0	9213	142	0.3	8E-02	0.42										16	9223	73	0.82	9228	137	0.4	7E-02	0.44
GB/GT	2	18	9207	73	0.8	9214	143	0.4	8E-02	0.42										21	9224	68	0.88					
Z/GT	4	14	9208	224	1.7	9215	X																					
Z/GB	3	15	9209	192	2.0	9216	X													71	9225	212	1.8					

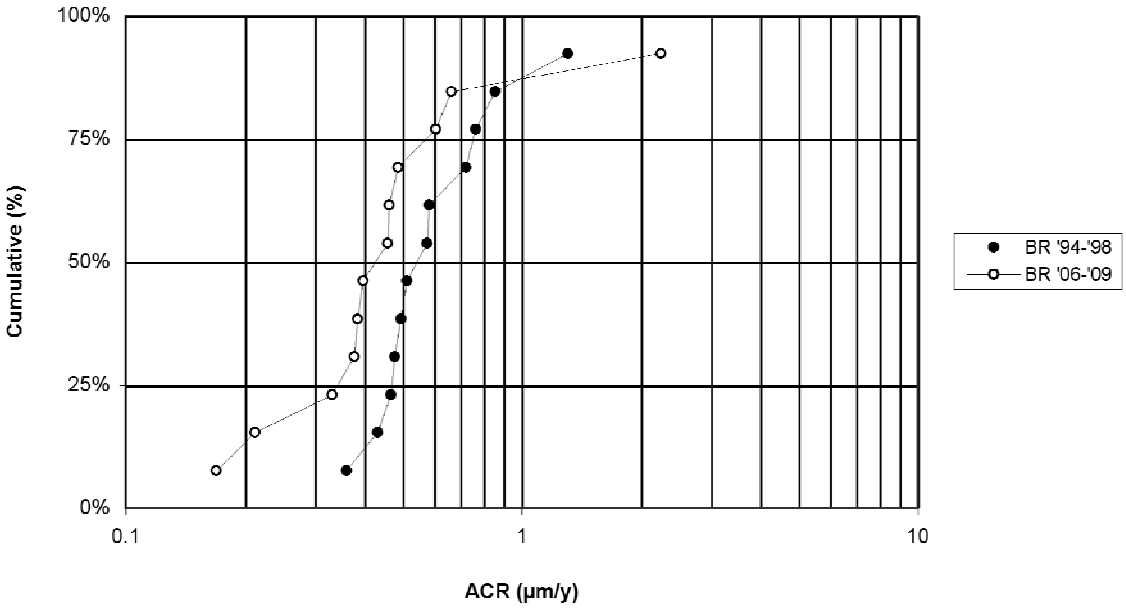

Figure 58 - Cumulative distribution of ACR from BRN and BRS.

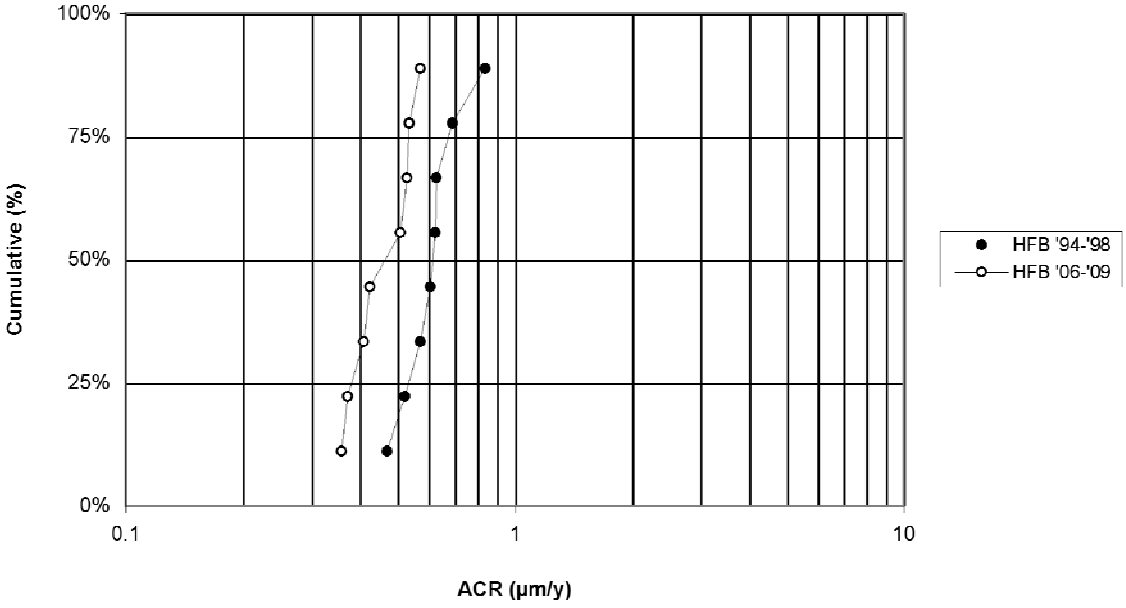

Figure 59 - Cumulative distribution of ACR from HFB.

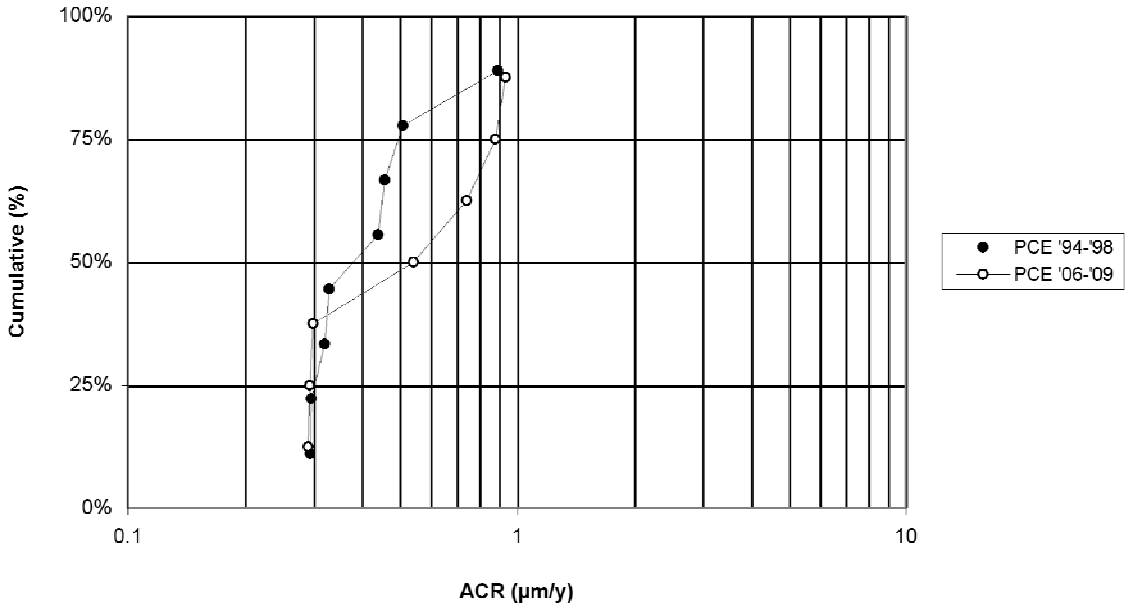

Figure 60 - Cumulative distribution of ACR from PCE.

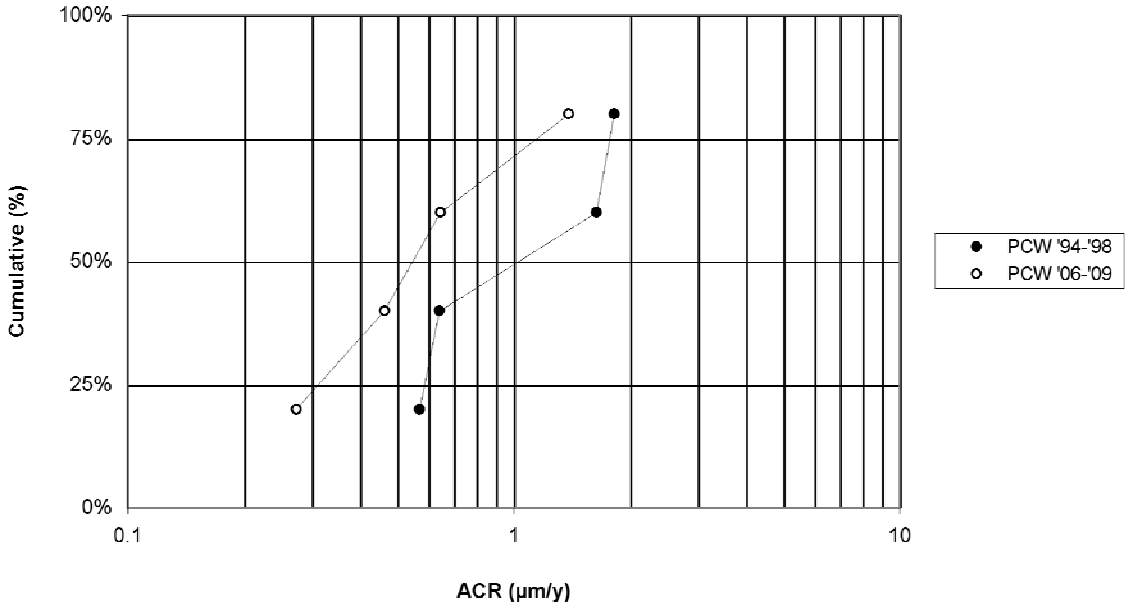

Figure 61 - Cumulative distribution of ACR from PCW.

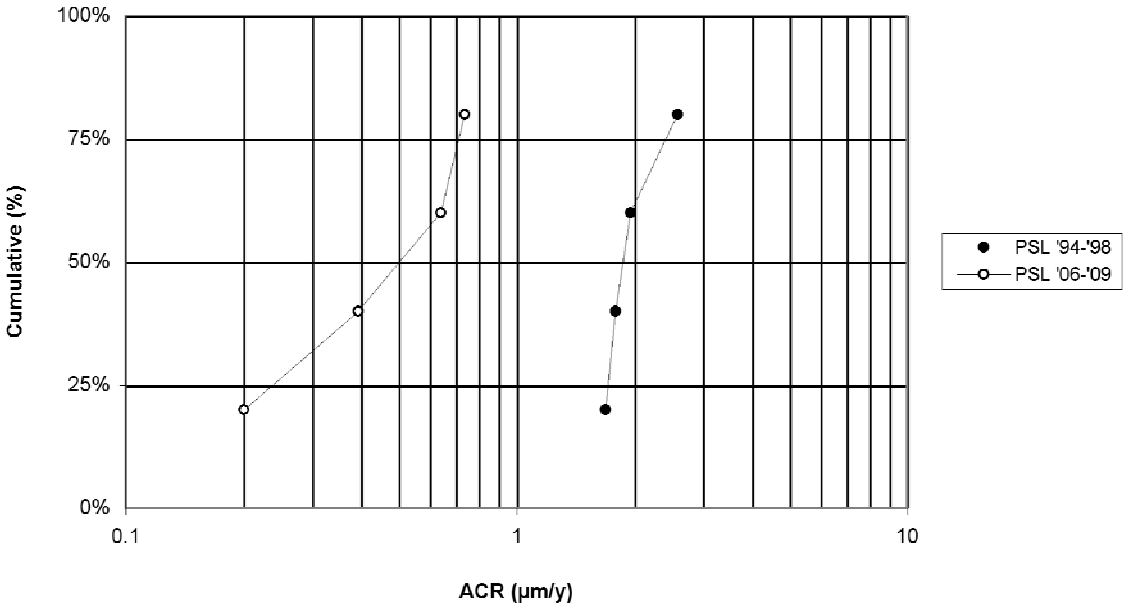

Figure 62 - Cumulative distribution of ACR from PSL.

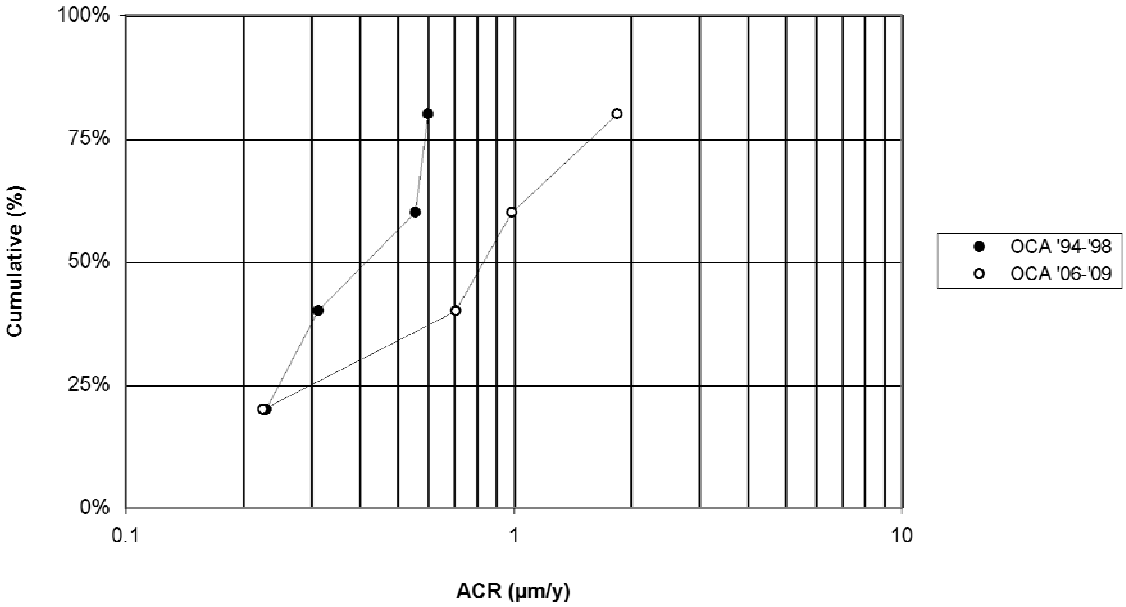

Figure 63 - Cumulative distribution of ACR from OCA.

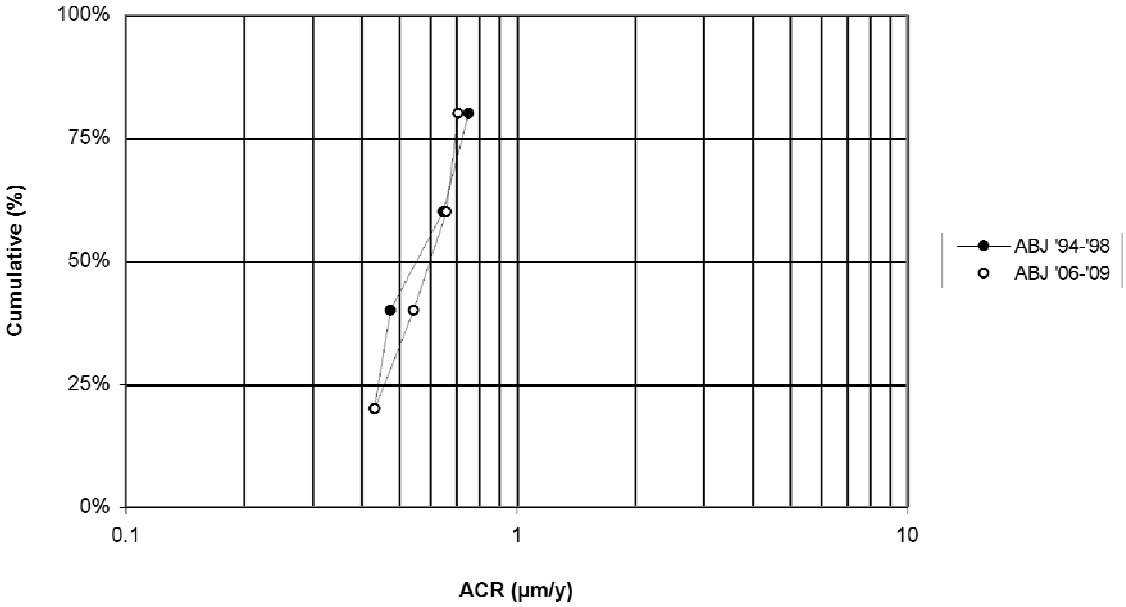

Figure 64 - Cumulative distribution of ACR from ABJ.

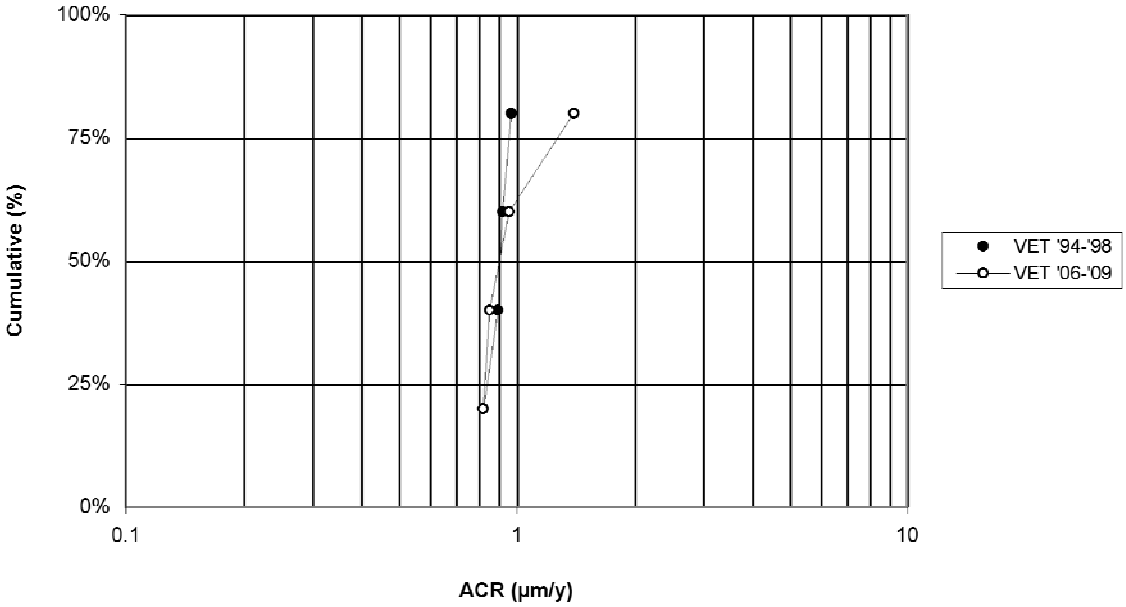

Figure 65 - Cumulative distribution of ACR from VET.

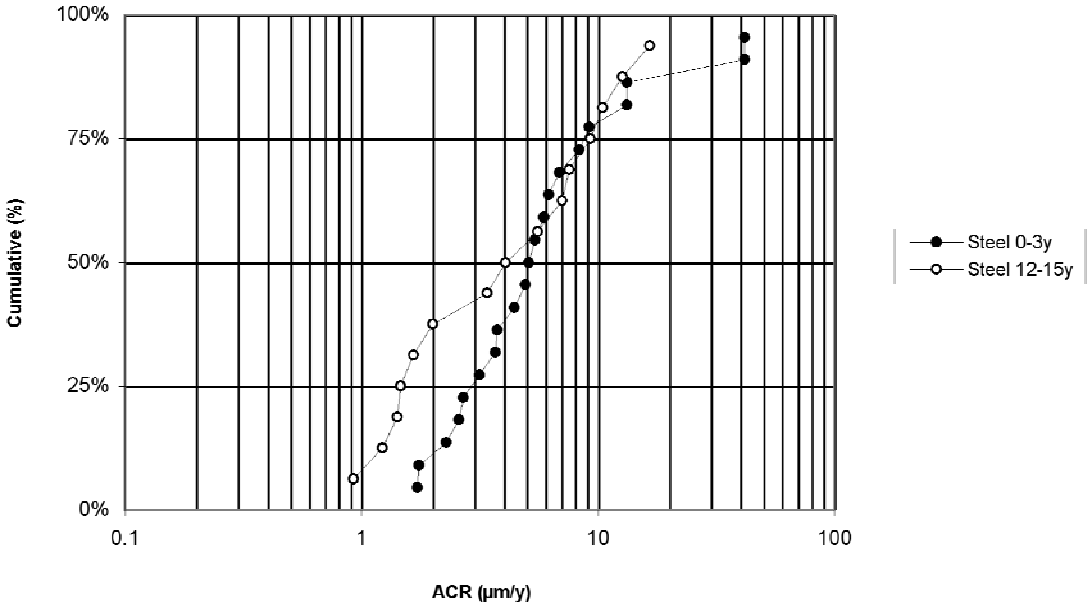

Figure 66 - Cumulative distribution of ACR from all plain steel elements in all walls grouped by years since insertion.

APPENDIX 3: METALLOGRAPHY

This appendix contains detailed information of the Metallographic examinations conducted on the structural element coupons collected from the field sites. Table A3.1 is a more detailed version of the concise Table 3.1 presented earlier. Table A3.2 lists all of the details regarding the extracted metal coupons including how many metallographic mounted samples were made. Figure 67 presents a summary of average percentage of coupon surface showing rust for all coupons from each site, as function of age of the wall at the time of coupon extraction. Figure 68 shows the distribution of galvanized and corrosion product thicknesses from metallographic examinations, averaged per site. Figures 69 to 75 show views of the as-extracted metal coupons after light cleaning to remove loosely adhering soil. Dashed lines indicate where the specimens where cut to prepare the metallographic cross sections (only-post-sectioning pictures are available for HFB). In all cases, "Top Side" indicates the face of the strip that was facing upwards in the structure. Figures 76 to 81 contain pictures of post sectioned HFB coupons.

Appendix 3: Metallography (Continued)

Table A3.1 Detailed direct observation of metal coupons.

Site	Location - Panel	Side[1]	Coating Condition[3]	Red Rust
BRN		-	-	-
BRS		-	-	-
HFB	9 Hook	All[2]	VG	NP
	9 Top	All[2]	VG	NP
	21 Top	All[2]	VG	NP
	21 Bottom	All[2]	VG	NP
PCE		-	-	-
PCW	2W	Top	VG	<5%
		Bottom		<5%
		Side		<5%
	4W	Top	VG	NP
		Bottom		NP
		Side		NP
PSL	8	Top	VG	<5%
		Bottom		<5%
		Side		<5%
OCA	5A	Top	G	<10%
		Bottom		<10%
		Side		<50%
	5B	Top		<10%
		Bottom		<5%
		Side		<50%
	24	Top	VG	<5%
		Bottom		<5%
		Side		NP
ABJ	20	Top	VG	<20%
		Bottom		NP
		Side		<5%
VET		-	-	-

1. Refers to face of the strip in contact with the soil.
2. In HFB the mesh are cylindrical, so the entire surface was examined uniformly.
3. VG=very good (<5% red rust on entire surface), G=good (5-20% red rust on entire surface)

Table A3.2 Listing of all mounted samples and respective measurement information.

Site	Panel	Length of Coupon (cm)	Mounted Samples	Pictures Used	Readings	Galv		Corr Prod		Galv	Corr Prod	Galv	Corr Prod	Galv	Corr Prod	sum
						Average (µm)	St. Dev. (µm)	Average (µm)	St. Dev. (µm)	Met Sample Average (µm)	Met Sample Average (µm)	Coupon avg (µm)	Coupon avg (µm)	Structure avg (µm)	Structure avg (µm)	sum (µm)
HFB	9 Top	19	HF9T-1							96	44	99	42	107	55	161
			HF9T-2	3	4	108	7	40	8							
					3	86	19	66	21							
					5	92	16	33	9							
			HF9T-3	3	3	105	19	43	31	102	40					
					4	102	26	56	20							
					5	100	12	26	5							
			HF9T-4													
	9 Hook	9.5	HF 9 Hook-0													
			HF 9 Hook-1													
			HF 9 Hook-2													
			HF 9 Hook-3													
			HF 9 Hook-4													
	21 Top	24	HFR21T1-Epoxy	3	5	98	13	30	13	119	26	114	66			
					5	138	15	39	23							
					4	123	5	5	8							
			HFR21T2-Epoxy													
			HFR21T3-Epoxy													
			HF-21-T-4	3	3	83	6	33	8	77	125					
					0											
					4	72	9	194	17							
			HFR21-0-T													
			HFR21-1-T	3	4	154	40	29	7	145	48					
					5	134	15	29	16							
					3	149	13	105	16							
			HFR21-2-T													
	21 Bottom	20	HFR21B-A									107	56			
			HFR21B-B													
			HFR21B-1	3	4	116	17	32	10	118	43					
					4	98	17	40	15							
					4	139	19	56	3							
			HF21B-MC-1													
			HF21B-MC-2	3	4	71	14	32	19	97	69					
					4	124	12	53	11							
					3	97	8	141	27							
			HF21B-MC-3													
OCA	5A	4	Ocala5A	7	6	72	7	10	5	103	21	103	21	119	15	135
					6	129	2	21	7							
					5	39	16	22	6							
					5	127	8	28	12							
					5	118	14	23	7							
					6	111	6	28	6							
					7	120	7	17	5							
	5B	4	Ocala5B													
	24	5.5	Ocala24	5	5	139	6	12	6	135	10	135	10			
					5	144	10	12	12							
					6	131	7	0	0							
					6	143	4	17	6							
					4	113	12	9	2							
ABJ	20	8	Jax-A	5	6	80	6	5	1	75	15	75	15	75	15	90
					7	73	6	6	4							
					6	82	6	28	6							
					5	71	15	18	13							
					6	68	11	18	8							
PCW	2W	3	Stu2W	7	3	53	14	91	18	66	62	66	62	56	50	106
					4	52	21	92	17							
					5	65	17	42	16							
					5	82	24	38	25							
					5	85	17	44	18							
					4	53	17	70	23							
					4	60	11	78	16							
	4W	4	Stu4W	13	4	40	9	31	10	45	39	45	39			
					6	45	9	26	13							
					6	45	8	40	8							
					5	48	7	32	11							
					7	49	13	32	10							
					5	57	17	33	18							
					5	38	4	54	8							
					4	39	9	66	24							
					4	37	3	57	12							
					4	42	11	62	23							
					4	47	15	29	5							
					3	53	11	28	9							
					4	49	11	29	9							
PSL	8	4	PSL-A	5	5	124	7	18	6	139	22	139	22	139	22	161
					5	138	9	13	4							
					8	150	3	14	4							
					4	130	6	32	14							
					6	146	7	36	2							
Galvanized Control	N/A	N/A	Galv Control	10	3	158	2			151	0	151	0	151	0	151
					4	173	17									
					5	148	3									
					6	152	5									
					7	162	4									
					4	165	5									
					4	165	4									
					4	155	3									
					5	128	4									
					6	119	8									

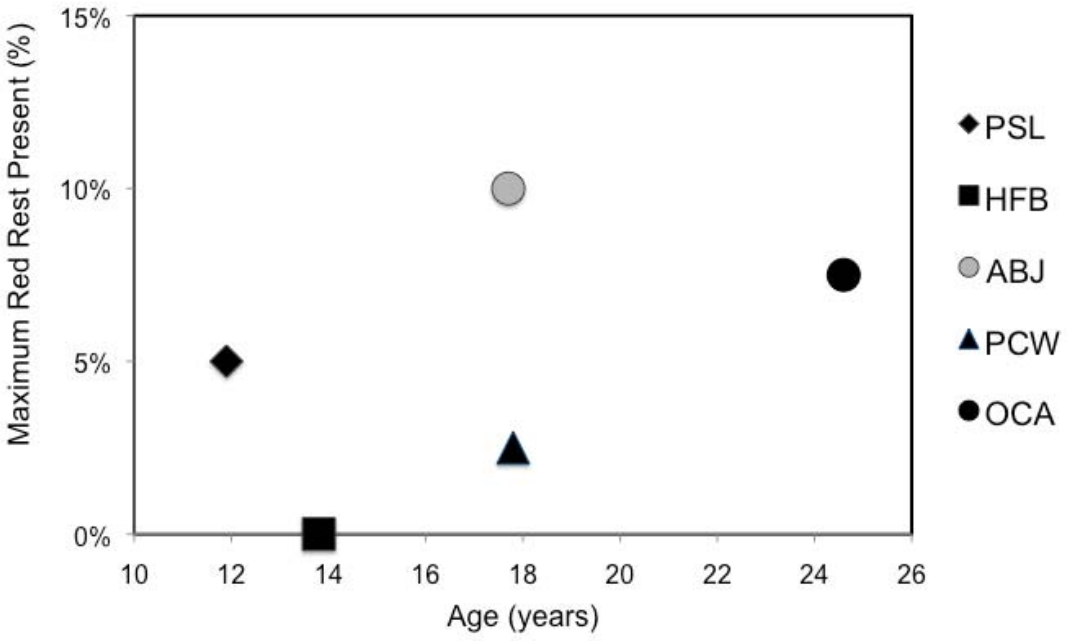

Figure 67 - Plot of percentage of red rust observed by age by site.

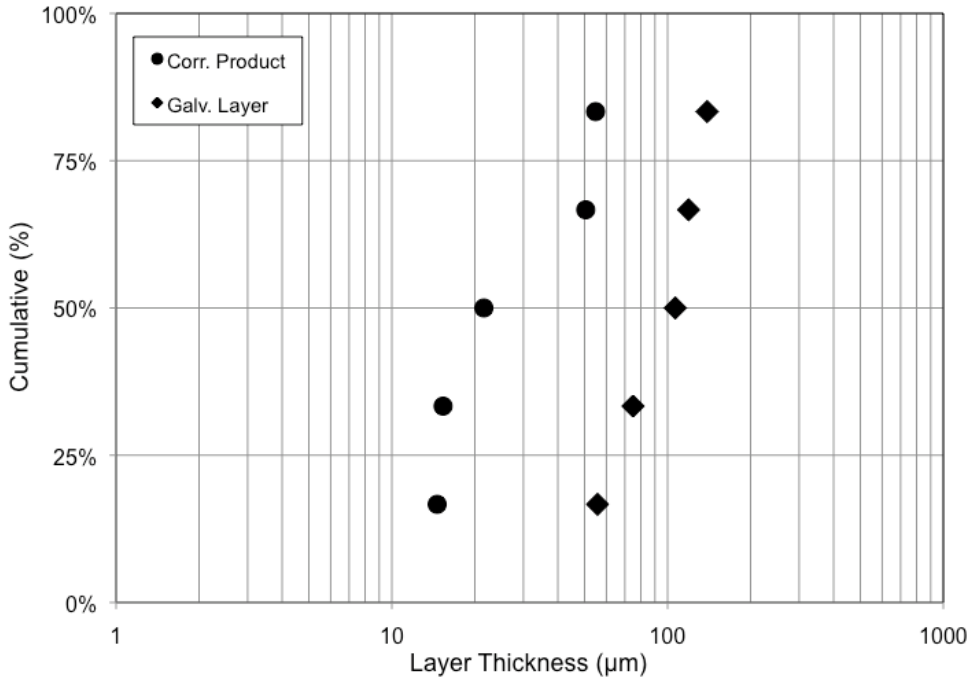

Figure 68 - Cumulative lognormal distribution of coating thickness measurements from coupons collected from the field.

Appendix 3: Metallography (Continued)

Note: in Figures 69 to 75 the dashed lines represent the cross section examined using the microscope.

Figure 69 - The top side of the coupon from PCW panel 2W.

Figure 70 - The top side of the coupon from PCW panel 4W.

Figure 71 - The top side of the coupon from PSL panel 8.

Figure 72 - The top side of coupon ‘A’ from OCA panel 5.

Figure 73 - The top side of coupon ‘B’ from OCA panel 5.

Figure 74 - The top side of the coupon from OCA panel 24.

Figure 75 - The top side of the coupon from ABJ panel 20.

Figure 76 - Elevation views of the coupon from HFB panel 9 top mesh. A: Top is up. B: Opposite side, top is down. The wall panel connection is to the left in both pictures.

Figure 77 - The bottom side of the coupon from HFB panel 9 top mesh. The wall panel connection is to the left.

Figure 78 - Elevation views of the coupon from HFB panel 22 top mesh. A: Top is up. B: Opposite side, top is down. The wall panel connection is to the left in both pictures.

Figure 79 - View from above (A) and below (B) of part of the coupon from HFB panel 22 top mesh.

Figure 80 - View from top (A), side (B), and bottom (C) of part of the coupon from HFB panel 22 bottom mesh.

Figure 81 - Pictures of segments cut from a hook in HFB panel 9 in the top layer mesh. The hook was heavily deformed during the coring of the hole to make an electrical contact to the mesh causing much of the disbanding of the galvanizing and later the rusting (B).

APPENDIX 4: SOIL PROPERTIES

Table A4.1 Soil measurement properties measured in the 2006-09 survey in detail.

Wall	Panel Location*	Cl^- (ppm)		SO_4^{2-} (ppm) †	Resistivity (kΩ•cm)	pH
		FDOT†	USF◊			
BRN	-	-	-	-	-	-
BRS	-	-	-	-	-	-
HFB	R9 Top	ND‡	ND	3.5	15.5	-
	R9 Mid.	ND	-	6.4	21.5	-
	R9 Bot.	-	ND	-	14.0	-
PCE	-	-	-	-	-	-
PCW	R2W	ND	ND	10.7	13.5	8
	R4W	ND	ND	12.2	13.2	8
PSL	R4	ND	ND	14.0	11.6	8
	R8	ND	ND	16.3	7.8	7.5
OCA	R5	ND	ND	4.6	21.4	6
	R24	ND	ND	3.5	27.9	7
ABJ	R20	ND	1.5	3.5	16.4	7
VET	-	-	-	-	-	-

* Refer to figures in Appendix 1: Site Instrumentation Diagrams for details.
† Test performed by the FDOT Materials Office Received April 1, 2008.
‡ ND – Not Detected, samples registering less than 1ppm.
◊ Test performed to verify FDOT readings.